IN THE UNITED STATES PATENT AND TRADEMARK OFFICE	*Application Number*	09/297,092
	Filing Date	May 18, 1999
	Inventor	PAULISTA et al.
	Group Art Unit	1636
	Examiner Name	S. Kaushal
	Attorney Docket Number	2923-0115
Title of the Invention: COMPOUNDS WITH IMPROVED CARTILAGE-INDUCING AND/OR BONE INDUCING ACTIVITY		

DECLARATION UNDER 37 C.F.R. 1.132

Commissioner for Patents
Washington, D.C. 20231

Sir:

I,Gertrud Hötten, hereby state and declare as follows:

I am very familiar with the present invention, the above-identified application, and the Office Action dated October 23, 2002.

Experiments were conducted under my direction and control which show that MP52 has cartilage and bone inducing activity. The experiments which were conducted are as follows.

I hereby declare that all statements made herein of my own knowledge are true and that all statements made on information and belief are believed to be true; and further that these statements were made with the knowledge that willful false statements and the like so made are punishable by fine or imprisonment, or both, under Section 1001 of Title 18 of the United States Code and that such willful false statements may jeopardize the validity of the application or any patent issued thereon.

Signed this ___ day of March 2003

_____

Dr. Gertrud Hötten

Expression of MP52 in E.coli

A part of MP52 containing additional Histidine residues at its N-terminus (HisMP52) was expressed in E.coli. The His-tag simplifies the purification by binding to metal chelat columns.

A C-terminal part of MP52 (119 amino acids) containing the amino acids 383-501 in SEQ ID NO. 1 and additional 10 amino acids at the N-terminus (MHHHHHHHKLI) was expressed using the prokaryotic vector pBP2. The vector pBP2 is a derivative of the pBR322 plasmid containing an ampicillin resistance gene. The T7-promoter is followed by a ribosome binding site, a start codon, 6 Histidine codons, a multiple cloning site for insertion of the target gene, stop codons in each reading frame and a terminator. The plasmid containing the above mentioned part of MP52 was deposited at the DSM (DSM 10028, 2. Juni 1995). The expression of HisMP52 is induced by providing a source of T7 RNA polymerase. The expression host BL21(DE3)pLysS (Novagen #69451-1) contains a chromosomal copy of the T7 RNA polymerase gene under lacUV5 control and expression of HisMP52 was induced by IPTG according to the instructions of the manufacturer. Monomeric HisMP52 is expressed in inclusion bodies which can be isolated according to standard procedures. Purification of HisMP52 was performed using a Nickel chelat column as described by Hochuli et al. (BIO/Technology 6, 1988, 1321-1325). Further purification was done by a reversed phase column (Nucleosil 300-7C4, Machery-Nagel, 715023) with a 0 to 90% acetonitril gradient containing 0.1% TFA in 100 minutes (flow rate: 2 ml/min). The elution of HisMP52 starts at about 35% acetonitril. The lyophilized HisMP52 was solubilized in a denaturing buffer (6M guanidinium chlorid, 150 mM NaCl, 3 mM DTT, 10 mM Tris pH 8; 2,6 mg/ml) and refolded to the dimeric HisMP52 at a final concentration of 160 µg/ml in a common Tris-buffer system (pH 9.5) containing EDTA (2-10 mM), CHAPS (15-50 mM), NaCl (1-2 M) and a redox-system (1 mM GSSG, 2 mM GSH) for 48 hours at 23°C. Residual monomeric HisMP52 was separated from the dimer by reversed phase HPLC. For this purpose HisMP52 was loaded on the column (Aquapore Octyl 20 micron, Applied Biosystems) at 35% buffer B (buffer A: 0.1% TFA in water, buffer B: 90% acetonitril, 0.1 % TFA). With a 35-60% buffer B gradient in 50 minutes (flow rate 3 ml/min) the

dimeric HisMP52 starts to elute at about 40% buffer B followed by the monomeric form starting at about 43% buffer B. The purified dimeric HisMP52 was lyophilized, stored at -70°C and used for the biological activity studies.

Additionally a C-terminal part of MP52 (119 amino acids) containing the amino acids 383-501 in SEQ ID NO. 1 were expressed and purified essentially as described in detail in the WO 96/33215. This protein, starting with a Proline at its N-terminus was named rhMP52 (recombinant human MP52).

Biological activity of MP52

***In vivo* parietal bone assay**

HisMP52 (1, 3 and 10 µg/20µl/site) was dissolved in phosphate-buffered saline (PBS; pH 3.4) containing 0.01 % human serum albumin and repeatedly injected onto the periosteum of neonatal rat parietal bone once a day. The injection of HisMP52 was started one day after birth and finished after 12 days of injection for histopathological examination (hematoxyline-eosin stain).
As shown in FIGURE 1, HisMP52 stimulates in a dose dependent manner the increase of bone thickness by newly formed bone.

***In vivo* segmental bone defect model**

A five millimeter segmental bone defect was created in a middle region of the femur of 13-week-old male Sprague-Dawley rats using a fine toothed saw blade. Physiological saline was dropped for avoiding tissue damage. A polyethylene plate was fixed along the lateral cortex with 2 millimeter diameter stainless screws. A solution containing 0.5% porcine type I collagen (200 µl) was mixed with HisMP52 (20µg), lyophilized and implanted into the defects. A solution of 0.5% porcine type I collagen alone was treated in the same manner and used as a control. The rats were sacrificed 12 weeks after the implantation and the femora were removed.

The time course of healing of the segmental bone defects was evaluated by soft X-ray radiography after 4, 8 and 12 weeks of implantation. As shown in FIGURE 2 the defect treated with HisMP52 was filled with mineralized tissue after 8 and 12 weeks whereas the control caused no radiographical changes in the defect even after 12 weeks.

The bone mineral content in the defects of the femurs was measured after the 12-week treatment by dual energy X-ray absorptiometry (DEXA). The HisMP52 group has a significantly elevated level compared to the control group as shown in FIGURE 3.

One rat of both groups was subjected to histological analysis after 12 weeks. Staining (hematoxyline and eosin, alcian blue) of decalcified sections of the femur defects treated with HisMP52 revealed an accomplished osseous union across the defect containing bone marrow cells (data not shown). In the control, muscle, adipose and fibrous tissues showed only a delayed or non-union defect.

For measuring the torsional strength the polyethylene plates and stainless screws were removed and the diaphyses of the femurs of the remaining rats were fixed by burying up both ends with resin and attaching them to the bone strain system (MZ-500D, Maruto Testing Machine Co.). The lower resin was rotated at a speed of 180 degrees/min. The torsional strength was determined by measuring the maximum force required to break the bone. As shown in FIGURE 4, the torsional strength of the femurs treated with HisMP52 is significantly higher then the control value.

Full-thickness defect model of rabbit articular cartilage

A two millimeter-diameter defect was created in the medial femoral condyle through the subchondral plate in rabbits (about 2 kg) with an orthopedic hand drill. After that, the drill hole was reamed with a biopsy needle. The hyaluronic acid gel (10µl, 1%) mixed with or without HisMP52 (3 µg) was introduced into the cartilage

defect. Six weeks after operation, decalcified transections of the articular cartilage were stained with alcian blue.
FIGURE 5 shows that a zonal structure appears after treatment with the HisMP52/ hyaluronic acid (HA) mixture which resembles the intact cartilage. The HA-treated control defects show the generation of chondrocytes but miss the zonal structure of articular cartilage.

Ectopic bone formation assay in mice

The ectopic bone formation assay is a well known method to determine the cartilage and bone inducing potential of BMPs or related proteins. Cerasorb® is a crystallographically pure ß-TCP matrix and was used with a granule size of 50-150 µm and 150-500 µm. Cerasorb® was coated with 200 µg rhMP52 and was implanted subcutaneously in the mice (male ICR, 8 weeks) backs. 200 µg rhMP52/ß-TCP (50-150 µm) were implanted in 5 mice and 200 µg rhMP52/ß-TCP (150-500 µm) were implanted likewise in 5 mice. The administration sites were dissected two weeks after implantation and submitted to histological examination. FIGURE 6 shows that both rhMP52/ß-TCP combinations with different granule sizes were able to induce new bone.

The above described experiments clearly demonstrate, that MP52 is very useful for treating bone damage or defects as well as diseases which can be diminished or healed by bone and cartilage growth. These could be for example treating of bone fractures and non unions, bone reconstruction, applications in the jaw, dental or facial region and spinal fusions.

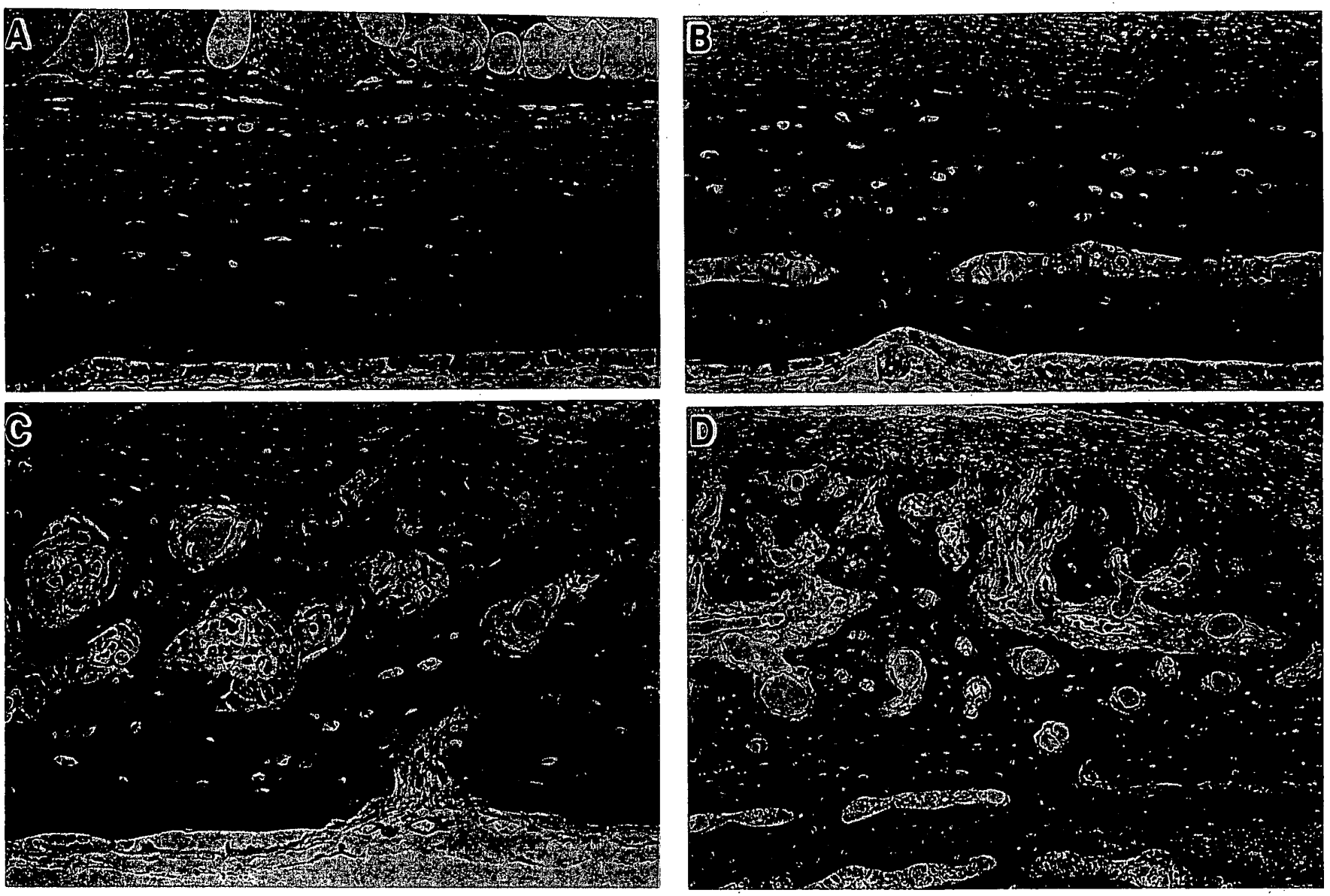

FIGURE 1: Calvaria from neonatal rats treated with HisMP52 (B: 1 µg; C: 3 µg; D: 10 µg). The control is shown in A.

Magnification x 66 (A, B, C), x33 (D).

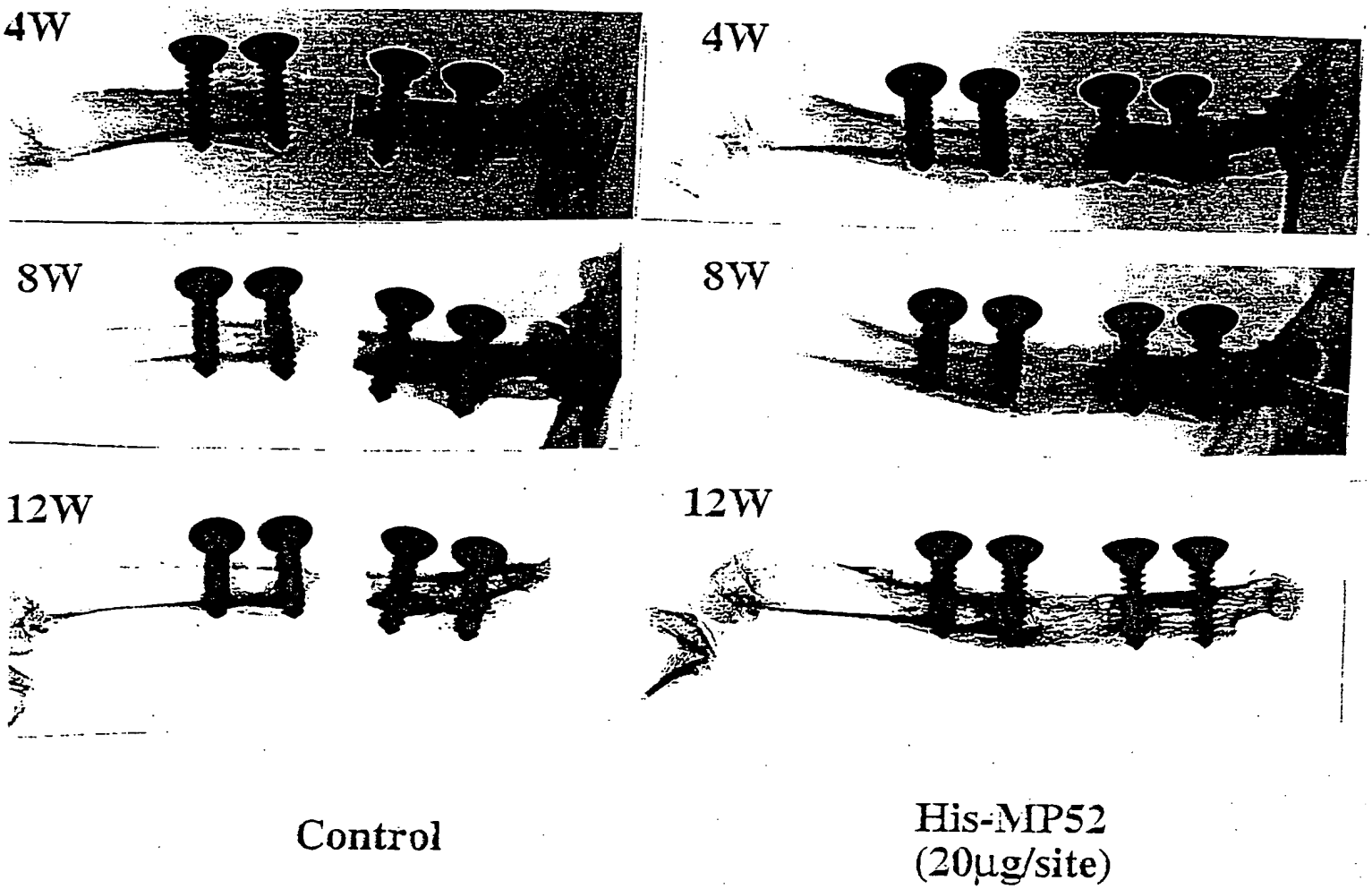

FIGURE 2: Radiographic changes in segmental bone defects (5 mm) in rat femurs 4, 8 and 12 weeks (w) after implantation of HisMP52 (20 μg/site) with type I collagen fibers or collagen fibers alone as a control.

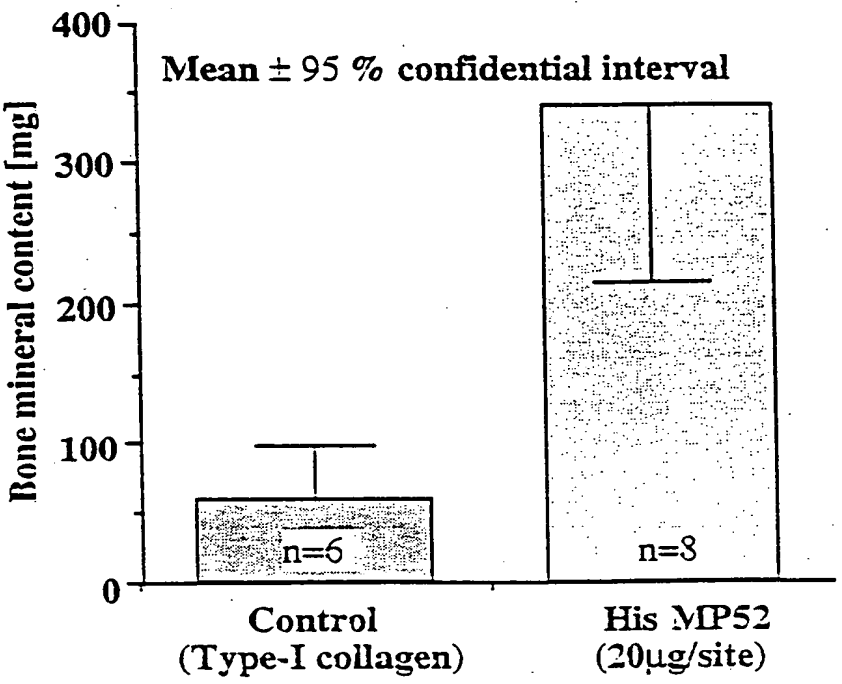

FIGURE 3: Bone mineral content of segmental bone defects (5 mm) in rat femurs 12 weeks after implantation of HisMP52 (20 µg/site) with type I collagen fibers or collagen fibers alone as a control.

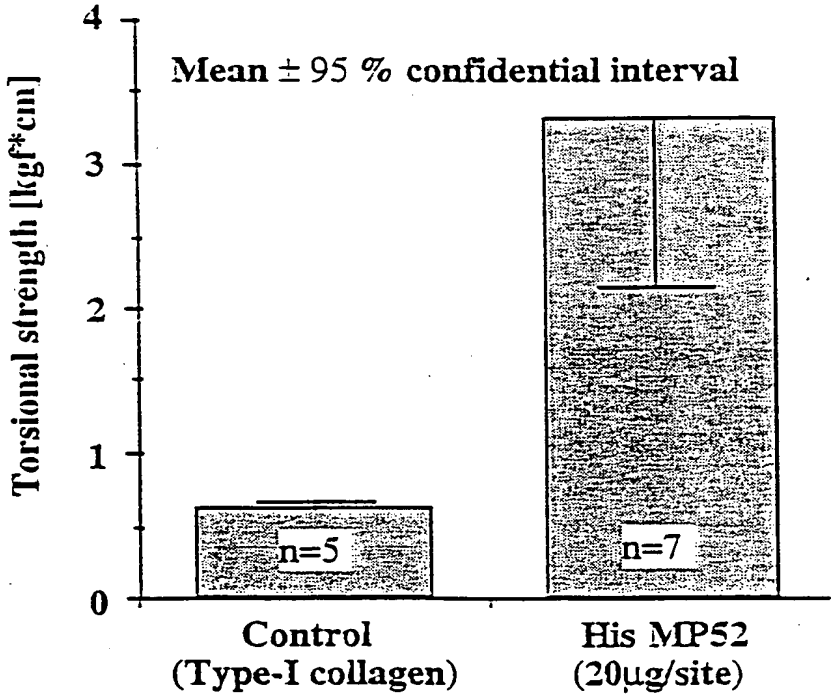

FIGURE 4: Torsional strength of rat femurs with segmental bone defects (5 mm) 12 weeks after implantation of HisMP52 (20 µg/site) with type I

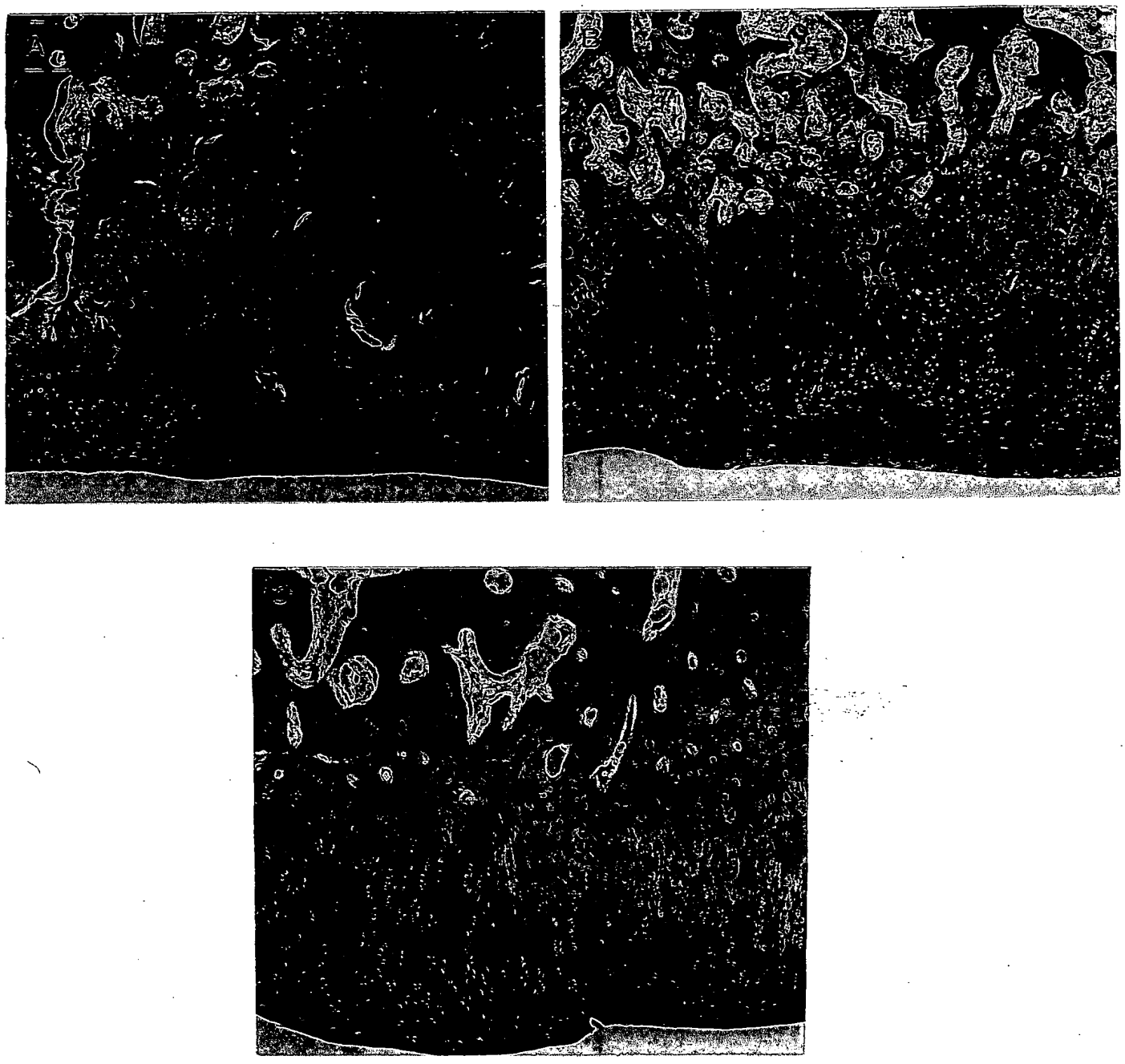

FIGURE 5: Full-thickness defect of articular cartilage in rabbits six weeks after treatment with hyaluronic acid (A) or treatment with a HisMP52/Hyaluronic acid (B) mixture. Intact articular cartilage is shown for comparison (C).

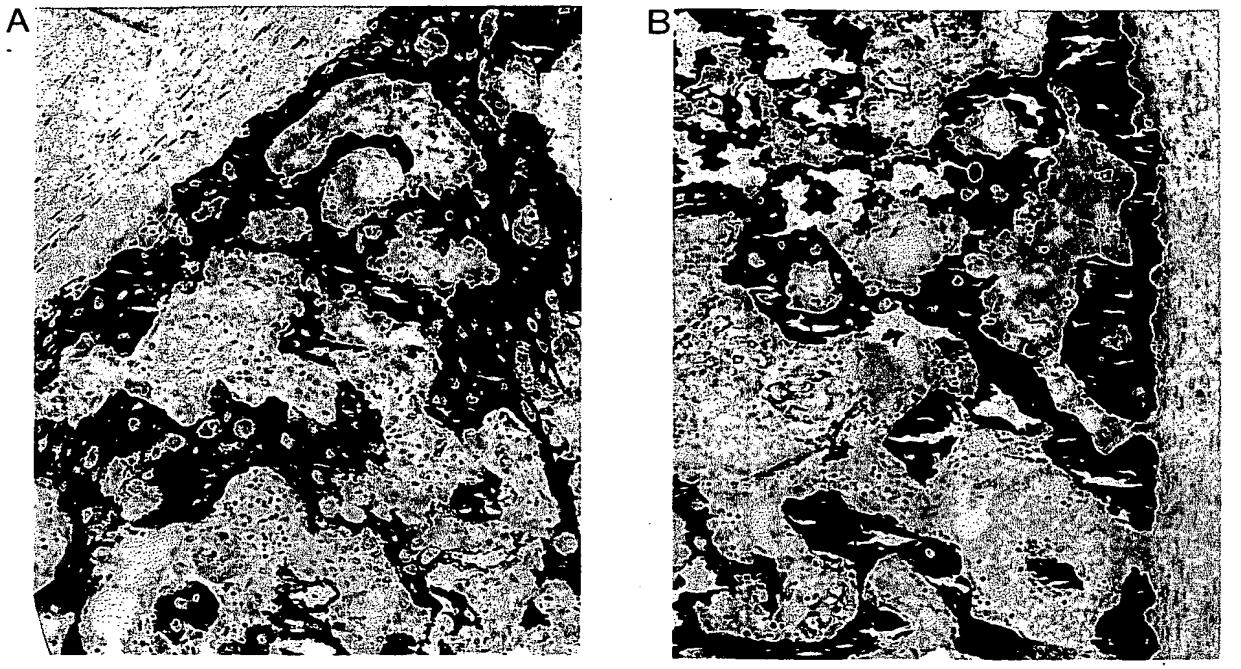

Figure 6: Ectopic bone formation (von Kossa stain) in mice two weeks after implantation of
A: 200 µg rhMP52/ß-TCP (50-150 µm) or
B: 200 µg rhMP52/ß-TCP (150-500 µm).

#26

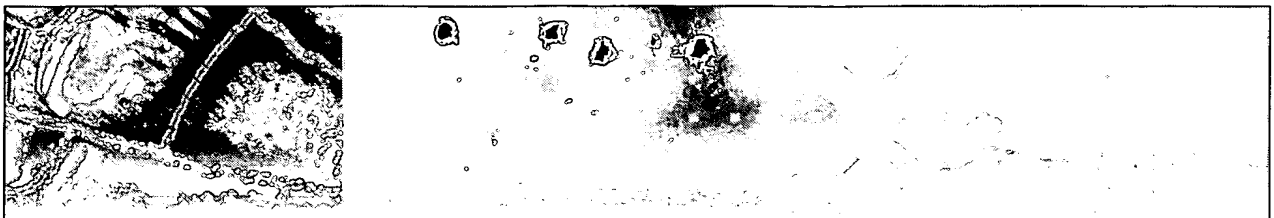

Enhancement of bone growth by coating of osteoconductive beta-TCP with recombinant human growth/differentiation factor-5 (rhGDF-5)

Authors: Poehling, Sylke; Jochims, Karin; Happersberger, Peter; Hellerbrand, Klaus; Bolz, Wolfgang; Kohnert, Ulrich

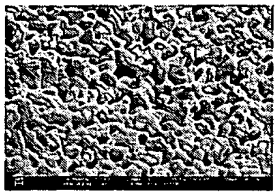

Fig 1:
Scanning electron microscopy (SEM) of beta-TCP (Magnification x5000). Scanning electron microscopy (SEM) by Prof M Epple, Department of Anorganic Chemistry, University of Bochum, Germany.

Introduction

Autogenous bone is considered the "gold standard" graft material for reconstruction of defects in the dental and maxillofacial area. A major disadvantage of autogenous bone grafts is the need for a second surgical procedure. Therefore, alternative materials are being evaluated. The combination of bone substitutes and osteoinductive proteins is a major focus of research in this area.
Scil Biomedicals is developing an innovative bone regeneration material (MD05) based on a synthetic osteoconductive bone substitute beta-tricalcium phoshate, (Fig. 1) coated with rhGDF-5, a member of the TGF-beta family of proteins. Effectiveness of MD05 was tested in the rat full-thickness calvarial defect model, which has been widely used for the evaluation of bone substitutes.

Results

Histological and histomorphometric analysis

Performance of beta-TCP coated with 12.5 or 50 µg rhGDF-5 was significantly superior to the performance of beta-TCP alone regarding new bone formation and bone marrow formation (Fig. 2, 3, Tables 1, 2). Degradation of beta-TCP was significantly enhanced by coating with rhGDF-5. A linear concentration/effect relationship between rhGDF-5 concentration and the measured parameters was demonstrated. No excessive bone growth was noted in any animal. All materials were well tolerated.

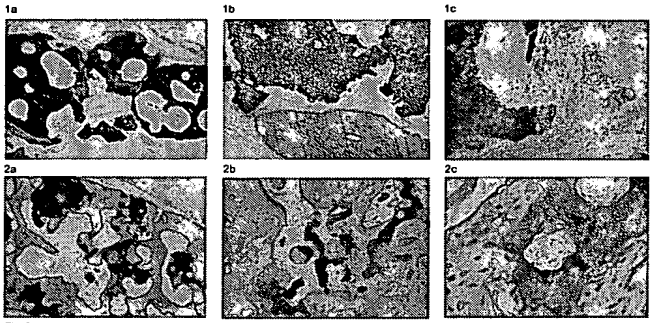

Fig 2:
Representative sections of 6 mm calvarial defects 6 weeks after implantation of 25 mg beta-TCP (1) or of 25 mg beta-TCP coated with 50 µg rhGDF-5 (2) (Donath & Brunner 1982). Sections were stained with modified Paragon; magnifications x4 (a), x10 (b), x25 (c).

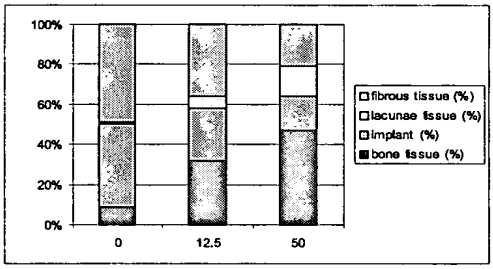

Fig 3:
Histogram of 6 mm calvarial defects 6 weeks after implantation with 25 mg beta-TCP coated with 0, 12.5 or 50 µg rhGDF-5.

Table 1: Histomorphometric analyses

	µg rhGDF-5/25 mg of material		
	0	12.5	50
Bone tissue (%)	8.9	31.7	46.9
Implant (%)	41.3	26.4	17.1
Lacunae tissue (%)	0.9	5.7	15.4
Fibrous tissue (%)	48.8	36.1	20.5

Table 2: One-sided p-values - non-parametric comparison of group difference (Steel 1959)

Comparison	Bone tissue %	Implant %	Lacunae tissue %	Fibrous tissue %
12.5 vs. 0	0.007*	0.007*	0.017*	0.105
50 vs. 0	0.0002*	0.0002*	0.0003*	0.0046*
50 vs. 12.5	0.046*	0.046*	0.026*	0.081

*statistically significant

Coating technology

A coating procedure that results in homogeneous distribution of rhGDF-5 was established (Fig. 4, Method A). Inhomogenous coating of the granules (Fig. 4, Method B) lead to impaired performance of the material in the rat calvarial defect model (data not shown).

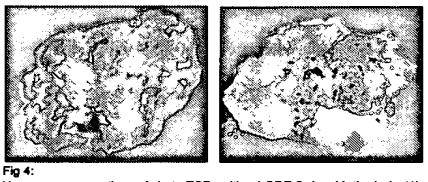

Fig 4:
Homogenous coating of beta-TCP with rhGDF-5 by Method A (1). Inhomogeneous coating of beta-TCP with rhGDF-5 by Method B (2).

In vitro release kinetic

It was shown by *in vitro* analyses that rhGDF-5 is almost completely released from beta-TCP within 7 days (Fig. 5).

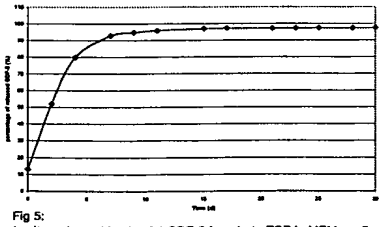

Fig 5:
In vitro release kinetic of rhGDF-5 from beta-TCP in MEM medium containing FCS. Medium was exchanged every 48 h. Release was determined by ELISA.

Conclusion

- Beta-TCP coated with rhGDF-5 induced significantly more bone formation than beta-TCP alone.
- No excessive bone growth was induced by coating with rhGDF-5.
- Beta-TCP coated with rhGDF-5 was well tolerated.
- Homogenous coating of the granules resulted in improved performance of the material.
- RhGDF-5 was completely released from beta-TCP within 7 days.

Materials and Methods

Rats were implanted with 25 mg beta-TCP coated with 0, 12.5 or 50 µg of rhGDF-5. The implant materials were placed onto two 6 mm full-thickness defects created in the parietal bone (Bosch et al. 1998). After 6 weeks the rats were sacrificed and the implanted sites were subjected to histological and histomorphometric analyses.

References:

Bosch C, Melsen B, Vargervik K. Importance of the critical-size bone defect in testing bone-regenerating materials. J. Craniofac Surg 1998; 9, 310-6.
Donath K, Brunner G. A method for the study of undecalcified bone and teeth with attached soft tissues. J Oral Pathol 1982; 11: 318-326.

Acknowledgement:

The authors would like to thank Sandra Lang and Stephanie Wank for excellent technical assistance.

scil

THE JOURNAL OF BIOLOGICAL CHEMISTRY
Vol. 271, No. 35, Issue of August 30, pp. 21345–21352, 1996
Printed in U.S.A.

Identification of Type I and Type II Serine/Threonine Kinase Receptors for Growth/Differentiation Factor-5*

(Received for publication, April 22, 1996)

Hideki Nishitoh‡§, Hidenori Ichijo‡¶, Michio Kimura‖, Tomoaki Matsumoto‖, Fusao Makishima‖, Akira Yamaguchi, Hidetoshi Yamashita‡ ‡‡, Shoji Enomoto§, and Kohei Miyazono‡§§**

*From the ‡Department of Biochemistry, the Cancer Institute, Tokyo, Japanese Foundation for Cancer Research, 1-37-1 Kami-Ikebukuro, Toshima-ku, Tokyo 170, Japan, the §Second Department of Oral and Maxillofacial Surgery, Tokyo Medical and Dental University, 1-5-45 Yushima, Bunkyo-ku, Tokyo 113, Japan, ‖Drug Discovery Research Laboratories, Pharma Research & Development Division, Hoechst Japan Limited, 1-3-2 Minamidai, Kawagoe 350-11, Japan, the **Department of Oral Pathology, School of Dentistry, Showa University, 1-5-8 Hatanodai, Shinagawa-ku, Tokyo 142, Japan, and the ‡‡Department of Ophthalmology, Faculty of Medicine, University of Tokyo, 7-3-1 Hongo, Bunkyo-ku, Tokyo 113, Japan*

Growth/differentiation factor-5 (GDF-5) is a member of the bone morphogenetic protein (BMP) family, which plays an important role in bone development *in vivo*. Mutations in the GDF-5 gene result in *brachypodism* in mice and Hunter-Thompson type chondrodysplasia in human. BMPs transduce their effects through binding to two different types of serine/threonine kinase receptors, type I and type II. However, binding abilities appear to be different among the members of the BMP family. BMP-4 binds to two different type I receptors, BMP receptors type IA (BMPR-IA) and type IB (BMPR-IB), and a type II receptor, BMP receptor type II (BMPR-II). In addition to these receptors, osteogenic protein-1 (OP-1, also known as BMP-7) binds to activin type I receptor (ActR-I) as well as activin type II receptors (ActR-II and ActR-IIB). Here we investigate the binding and signaling properties of GDF-5 through type I and type II receptors. GDF-5 induced alkaline phosphatase activity in a rat osteoprogenitor-like cell line, ROB-C26. ^{125}I-GDF-5 bound to BMPR-IB and BMPR-II but not to BMPR-IA in ROB-C26 cells and other nontransfected cell lines. Analysis using COS-1 cells transfected with the receptor cDNAs revealed that GDF-5 bound to BMPR-IB but not to the other type I receptors when expressed alone. When COS-1 cells were transfected with type II receptor cDNAs, GDF-5 bound to ActR-II, ActR-IIB, and BMPR-II but not to transforming growth factor-β type II receptor. In the presence of type II receptors, GDF-5 bound to different sets of type I receptors, but the binding was most efficient to BMPR-IB compared with the other type I receptors. Moreover, a transcriptional activation signal was efficiently transduced by BMPR-IB in the presence of BMPR-II or ActR-II after stimulation by GDF-5. These results suggest that BMPR-IB mediates certain signals for GDF-5 after forming the heteromeric complex with BMPR-II or ActR-II.

Growth/differentiation factor-5 (GDF-5),[1] also termed cartilage-derived morphogenetic protein-1 or CDMP-1; Refs. 1–3) is a member of the bone morphogenetic protein (BMP) family that constitutes a part of the transforming growth factor-β (TGF-β) superfamily. Several proteins belong to the BMP family, which can be divided into three subgroups based on their structural similarities; *i.e. Drosophila* decapentaplegic gene product (DPP), BMP-2 and BMP-4 form one subgroup; *Drosophila* 60A, BMP-5, BMP-6/Vgr1, osteogenic protein (OP)-1/BMP-7, and OP-2/BMP-8 form one subgroup; and GDF-5, -6, and -7 form another subgroup (4–6).

BMPs were originally identified as proteins that induce ectopic bone and cartilage formation *in vivo* (7, 8). *In vitro* studies have revealed that BMPs have various biological effects on different cell types, *e.g.* stimulation of proteoglycan synthesis in chondroblasts (9), synthesis of collagen and alkaline phosphatase during chondrogenic and osteogenic differentiation (9–11), and induction of differentiation in neural cells (12, 13). GDF-5 also stimulates chondrogenic phenotype expression *in vitro* and induces cartilage and bone formation *in vivo* (14).

BMPs are widely distributed not only in bone and cartilage but in other tissues; *e.g.* BMP-3, -4, -5, and -6 are found in lung and liver, and OP-1/BMP-7 is expressed in kidney (15). BMPs play important roles in the embryonal development. Null mutation in the BMP-4 gene leads to defects in mesoderm formation during the early embryonic stage (16). OP-1/BMP-7-deficient mice die shortly after birth because of poor kidney development and have eye defects and skeletal abnormalities (17, 18). GDF-5/CDMP-1 is predominantly expressed in the precartilaginous mesenchymal condensation and the cartilaginous cores of the developing long bone (1, 3). Mutations in the murine GDF-5 gene result in abnormal skeletal development, known as *brachypodism* (1). In a recent study, a mutation in the human GDF-5 gene was shown to be associated with a recessive human chondrodysplasia (Hunter-Thompson type) (19). The resulting phenotype of this disorder is similar to murine *brachypodism*.

Members of the TGF-β superfamily transduce their signals through the formation of heteromeric complexes of two different types of serine/threonine kinase receptors, *i.e.* type I recep-

* This work was supported in part by grants-in-aid for scientific research from the Ministry of Education, Science and Culture of Japan. The costs of publication of this article were defrayed in part by the payment of page charges. This article must therefore be hereby marked "*advertisement*" in accordance with 18 U.S.C. Section 1734 solely to indicate this fact.

¶ To whom correspondence should be addressed. Tel./Fax: 81-3-3918-0342.

§§ Supported by the Japan Research Foundation for Clinical Pharmacology.

[1] The abbreviations used are: GDF, growth/differentiation factor; CDMP, cartilage-derived morphogenetic protein; BMP, bone morphogenetic protein; TGF-β, transforming growth factor-β; DPP, decapentaplegic gene product; OP, osteogenic protein; ALK, activin receptor-like kinase; TβR, TGF-β receptor; ActR, activin receptor; BMPR, BMP receptor; FBS, fetal bovine serum; ALP, alkaline phosphatase; NTA, nitrilotriacetic acid.

tors of about 50–55 kDa and type II receptors of more than 70 kDa (20–22). A series of receptor serine/threonine kinases, termed activin receptor-like kinase (ALK)-1 to -6, was previously identified to constitute a type I receptor family, including a TGF-β type I receptor (TβR-I/ALK-5), two activin type I receptors (ActR-I/ALK-2 and ActR-IB/ALK-4), and two BMP type I receptors (BMPR-IA/ALK-3 and BMPR-IB/ALK-6) (23–29). Type II receptors for activin (ActR-II and ActR-IIB) (30–32), for TGF-β (TβR-II) (33), and for BMPs (BMPR-II) (34–37) have been identified in mammals. In the TGF-β and activin receptor systems, ligand binds first to its specific type II receptor, and the complex of ligand and type II receptor is then recognized by type I receptor. Upon formation of the heteromeric receptor complex, type I receptor is phosphorylated by type II receptor, and subsequent activation of the catalytic activity of type I receptor kinase is essential for signaling (38, 39).

BMP-4 binds to BMPR-IA and BMPR-IB efficiently (27, 28, 40, 41) in the presence of DAF-4, a type II receptor in *Caenorhabditis elegans* (42), whereas OP-1/BMP-7 binds to BMPR-IB and less efficiently to BMPR-IA (27). OP-1/BMP-7, but not BMP-4, can also bind to one of the activin type I receptors, ActR-I, in the presence of DAF-4 (27). In addition, OP-1/BMP-7 was recently shown to bind ActR-II and ActR-IIB and mediate certain activin-like effects through the ActR-II·ActR-I complex (43). We have recently shown that ALK-1 (also termed TGF-β superfamily receptor type I or R3) mediates certain signals after stimulation by OP-1/BMP-7.[2] Human BMPR-II was recently cloned, and it was shown that BMP-2, BMP-4, and OP-1/BMP-7 bound to BMPR-II and transduced signals in combination with certain type I receptors after forming heteromeric complexes (35–37). In contrast to the TGF-β and activin receptors, BMP type I and type II receptors bind ligands independently, but binding affinity is up-regulated in the presence of both receptor types. The ligand-receptor interactions of BMPs in mammals are remarkably similar to those observed with the DPP receptor system in *Drosophila* (44, 45). However, the precise signaling mechanism of the BMP/DPP receptor systems remains unknown.

We investigated the biological effect of GDF-5 on osteoprogenitor-like cell lines and identified type I and type II receptors for GDF-5; BMPR-IB and BMPR-II, but not BMPR-IA, bound GDF-5 in ROB-C26 cells and other cell types. Moreover, we show here that GDF-5 transduces its signal through heteromeric complexes of BMPR-IB and various type II receptors.

EXPERIMENTAL PROCEDURES

Cell Culture—Mink lung epithelial cells (Mv1Lu) and COS-1 cells were obtained from American Type Culture Collection (Rockville, MD). Chemically mutagenized Mv1Lu cell line (R mutant, clone 4-2) (46) and U-1240 MG human glioblastoma cells (47) were obtained from M. Laiho (University of Helsinki, Finland) and J. Massagué (Memorial Sloan-Kettering Cancer Center, New York), and Bengt Westermark (University of Uppsala, Sweden), respectively. A rat osteoprogenitor-like cell line, ROB-C26 (10), was cultured in α-minimal essential medium (Life Technologies, Inc.) containing 10% fetal bovine serum (FBS) and antibiotics (100 units/ml penicillin). The other cells were cultured in Dulbecco's modified Eagle's medium containing 10% FBS and antibiotics in 5% CO_2 atmosphere at 37 °C.

Alkaline Phosphatase (ALP) Activity—For a histochemical analysis of ALP activity, cells were fixed for 10 min with 3.7% formaldehyde at room temperature. After washing with phosphate-buffered saline, the cells were incubated for 20 min with a mixture of 0.1 mg/ml of naphthol AS-MX phosphate (Sigma), 0.5% *N,N*-dimethylformamide, 2 mM $MgCl_2$, and 0.6 mg/ml of fast blue BB salt (Sigma) in 0.1 M Tris-HCl, pH 8.5, at room temperature.

For a quantitative analysis of ALP activity, cells were washed with 20 mM Tris-HCl, pH 7.5, and 150 mM NaCl and extracted with lysis buffer (20 mM Tris-HCl, pH 7.5, 150 mM NaCl, and 1% Triton X-100). ALP activity was determined by an established technique using *p*-nitrophenyl phosphate (Sigma) as a substrate (48). Protein concentration in each extract was measured by *DC* protein assay (Bio-Rad) using bovine serum albumin as a standard.

Preparation of Polyclonal Antibodies—Antisera to the type I receptors were made against synthetic peptides corresponding to the intracellular juxtamembrane parts of the type I receptors (26, 49). An antiserum against ActR-II (ARC-2), which detects only ActR-II, was generated against a peptide corresponding to the C-terminal tail of ActR-II (50). An antiserum against the intracellular part of ActR-II (mARII) (51), which cross-reacts with ActR-IIB, was a gift from K. Verschueren (University of Leuven, Belgium). Antisera against TGF-β receptor type II (DRL) and BMPR-II (SMN and NRR) were generated against peptides corresponding to the C-terminal tails of the receptors, as previously reported (26, 36).

Transient Transfection of cDNAs—Transient transfection plasmids encoding the type I receptors were previously described (26, 27). ActR-II cDNA was a gift from L. S. Mathews and W. W. Vale (Salk Institute, San Diego, CA). ActR-IIB1 cDNA, BMPR-II^{His} construct and p3TP-Lux promoter-reporter construct were obtained from J. Massagué. For transient transfection, cDNAs for type I or type II receptors subcloned into pSV7d (52), pcDNA1, pcDNA3 (Invitrogen), or pCMV5 (53) expression vectors were used. These plasmids and p3TP-Lux promoter-reporter construct (1 μg of each) were transfected into COS-1 or R mutant Mv1Lu cells by the transfection kit of eukaryotic cells (Tfx™-50, Promega), following the manufacturer's protocol. One or two days after, the cells were used for affinity cross-linking and immunoprecipitation studies or transcriptional response assay.

Binding, Affinity Cross-linking, and Isolation of the Cross-linked Complexes—Recombinant human BMP-2 and GDF-5[3] were iodinated according to the chloramine-T method as described (26). Cells were incubated on ice for 2–3 h with 0.2–0.5 nM of ^{125}I-labeled ligands in the presence or absence of unlabeled ligands in a binding buffer (phosphate-buffered saline containing 0.9 mM $CaCl_2$, 0.49 mM $MgCl_2$, and 1 mg/ml bovine serum albumin). After incubation, the cells were washed with the binding buffer without bovine serum albumin, and cross-linking was done in the same buffer containing 0.27 mM of disuccinimidyl suberate (Pierce) and 1 mM of *bis*(sulfosuccinimidyl) suberate (Pierce) for 15 min on ice. The cells were washed once with a buffer containing 10 mM Tris-HCl, pH 7.4, 1 mM EDTA, 10% glycerol, and 0.3 mM phenylmethylsulfonyl fluoride (Sigma) and lysed for 20 min in lysis buffer (20 mM Tris-HCl, pH 7.5, 150 mM NaCl, 10 mM EDTA, 1% Triton X-100, 1% sodium deoxycholate) containing 1.5% Trasylol (Bayer) and 1 mM phenylmethylsulfonyl fluoride and clarified by centrifugation. Cross-linked materials were then incubated with antisera for 45 min at 4 °C. Immune complexes were bound to protein A-Sepharose (Kabi-Pharmacia) for 30 min at 4 °C, washed once with a buffer containing 20 mM Tris-HCl, pH 7.5, 500 mM NaCl, 1% Triton X-100, 1% sodium deoxycholate, 0.2% SDS, followed by one wash in distilled water. For isolation of BMPR-II^{His} complexes, cells were extracted with a buffer containing 50 mM Tris-HCl, pH 7.5, 150 mM NaCl, 0.5% Triton X-100, and protease inhibitors. Cell extracts were clarified by centrifugation and incubated with Ni^{2+}-NTA-agarose (Qiagen) for 1 h at 4 °C in the presence of 20 mM imidazole. Beads were rinsed briefly once with the same buffer. The immune complexes or complexes isolated by Ni^{2+}-NTA-agarose were eluted by boiling for 3 min in SDS sample buffer (100 mM Tris-HCl, pH 8.8, 0.01% bromphenol blue, 36% glycerol, 4% SDS) containing 10 mM dithiothreitol and analyzed by SDS-7% polyacrylamide gel electrophoresis. The gels were fixed, dried, and subjected to the analysis using a Fuji BAS 2000 Bio-Imaging Analyzer (Fuji Photo Film).

Transcriptional Response Assay—R mutant Mv1Lu cells were co-transfected with p3TP-Lux promoter-reporter construct (25, 54) with plasmids containing the type I or type II receptor cDNAs as described above. One day after transfection, cells were starved in Dulbecco's modified Eagle's medium containing 0.2% FBS for 6 h and then exposed to 300 ng/ml of GDF-5 for 24 h. Luciferase activity in the cell lysate was measured using the luciferase assay system (Toyo Ink) according to the manufacturer's protocol and a luminometer (AutoLumat LB953; EG&G Berthold).

[2] H. Nishitoh, M. Saitoh, I. Asahina, S. Enomoto, T. K. Sampath, M. Takagi, and H. Ichijo, submitted for publication.

[3] M. Takahashi, H. Tanaka, S. Kawai, H. Pan, K. Osawa, H. Miki, Y. Muraki, Y. Konno, T. Itoh, H. Takamatsu, K. Enomoto, M. Katsuura, and M. Kimura, manuscript in preparation.

RESULTS

ALP Activity—GDF-5 stimulated mesenchyme aggregation and chondrogenesis in rat limb bud cells *in vitro* and induced ectopic cartilage and bone formation in mice tissues of rodents *in vivo* (14). However, several osteoblastic cell lines, such as MC3T3-E1 cells, did not efficiently respond to GDF-5 as measured by ALP activity in contrast to the effects of other BMPs. To identify the signaling receptors for GDF-5, we first attempted to find cell lines that respond to GDF-5 using the enzyme histochemical study of ALP activity. In ROB-C26 rat osteoprogenitor-like cell line, GDF-5 increased the number of ALP-positive cells at 300 ng/ml (Fig. 1*A*). However, most cell lines, including MC3T3-E1 mouse osteoblastic cells, ROS17/2.8 rat osteosarcoma cells, and C2C12 mouse myoblastic cells, had no significant increase in ALP activity by the treatment with GDF-5 (data not shown). Fig. 1*B* shows the dose-dependent effect of GDF-5 on ROB-C26 cells treated for 6 days. ALP activity was induced by GDF-5 in a dose-dependent manner.

Identification of GDF-5 Receptors in Nontransfected Cell Lines—In order to investigate which serine/threonine kinase receptors act as type I and type II receptors for GDF-5, the ROB-C26 cells were tested for the binding of GDF-5. The cells were affinity-labeled using ^{125}I-GDF-5, and the cross-linked complexes were analyzed by immunoprecipitation using the antiserum against each of type I and type II receptors, followed by SDS-gel electrophoresis under reducing conditions. Cross-linked complexes of 80–90 kDa could be immunoprecipitated by the antiserum to BMPR-IB (Fig. 2*A*). A high molecular mass complex of 150–200 kDa, which may represent a type II receptor complex, was co-immunoprecipitated by the BMPR-IB antiserum. The type II receptor complex could be immunoprecipitated by the BMPR-II antiserum, and co-immunoprecipitation of the type I receptor complex was also seen (Fig. 2*A*). Immunoprecipitation by the BMPR-II antiserum was less efficient than that by the BMPR-IB antiserum, which may be due to a poor affinity of the BMPR-II antiserum (36). Weak bands could be seen after immunoprecipitation by the antisera against ALK-1, BMPR-IA, and TβR-II (Fig. 2*A*), but these were not reproducible.

Binding of ^{125}I-BMP-2 was also tested in the ROB-C26 cells (Fig. 2*B*). Although ^{125}I-BMP-2 is known to bind BMPR-IA and BMPR-IB as well as BMPR-II in other systems, binding to only BMPR-IB and BMPR-II could be seen in this cell type, suggesting that this cell line predominantly expresses BMPR-IB rather than BMPR-IA.

The binding of ^{125}I-GDF-5 and ^{125}I-BMP-2 to BMPR-IB was competed with unlabeled GDF-5 and also with BMP-2 (Fig. 2*C*).

To identify the endogenous receptors for GDF-5 in other cell types, we tested some other cell lines for the binding of GDF-5. In the U1240 MG glioblastoma cell line and the Mv1Lu mink lung epithelial cell line, BMPR-IB could bind GDF-5 (Fig. 3). In contrast, ^{125}I-BMP-2-cross-linked complexes to Mv1Lu were immunoprecipitated by BMPR-IA (data not shown). In most cell types investigated, including ATDC5 chondroblastic cells, MC3T3-E1 mouse osteoblastic cells, ROS17/2.8 rat osteosarcoma cells, BEC bovine endothelial cells, and C2C12 mouse myoblastic cells, binding of GDF-5 was not clear (data not shown).

Binding of GDF-5 to Type I and Type II Receptors Expressed in COS-1 Cells—In order to further investigate the type I and type II receptors for GDF-5, binding was tested using COS-1 cells transfected with the cDNAs for serine/threonine kinase receptors. For the transfection of BMPR-II cDNA, a C-terminally truncated form of BMPR-II^{His}, which encodes 530 amino acid residues with a hexahistidine tag in its C terminus and, therefore, forms about 100 kDa of cross-linked complexes (35), was used. The cross-linked complexes were precipitated using the specific antisera or Ni^{2+}-NTA agarose beads.

When singly transfected, we could observe binding of GDF-5 only to BMPR-IB among six type I-receptors. Among different type II receptors, ActR-II, ActR-IIB1, and BMPR-II^{His} bound GDF-5 (Fig. 4). GDF-5 did not bind well to other serine/threo-

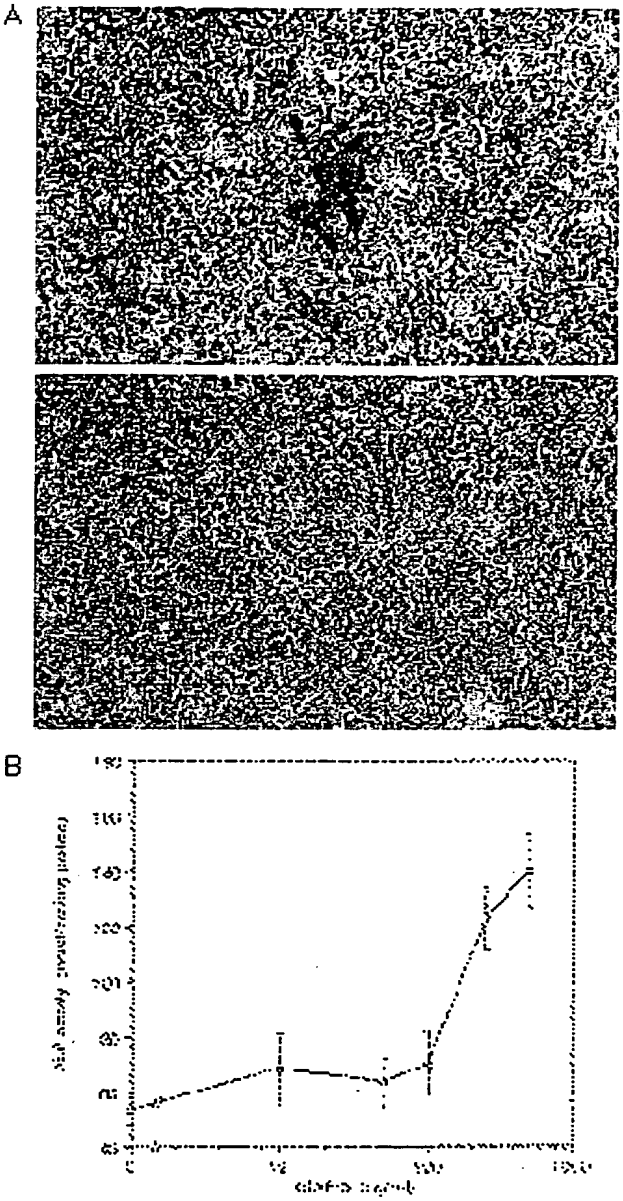

FIG. 1. **The effects of GDF-5 on induction of ALP activity in ROB-C26 cells.** ROB-C26 cells were cultured in α-minimal essential medium containing 10% FBS for 6 days with (+) or without (−) 500 ng/ml GDF-5. The cells were fixed and stained for ALP as described under "Experimental Procedures" and photographed by a phase contrast microscopy (*A*). *B*, dose-dependent induction of ALP activity by GDF-5. ROB-C26 cells in 24-well cell culture plates were treated with GDF-5 for 6 days. ALP activity was measured spectrophotometrically with *p*-nitrophenyl phosphate as a substrate. Enzyme specific activity was presented as nmol of *p*-nitrophenol produced/min/mg of protein. Values are means ± S.D. of triplicate cultures.

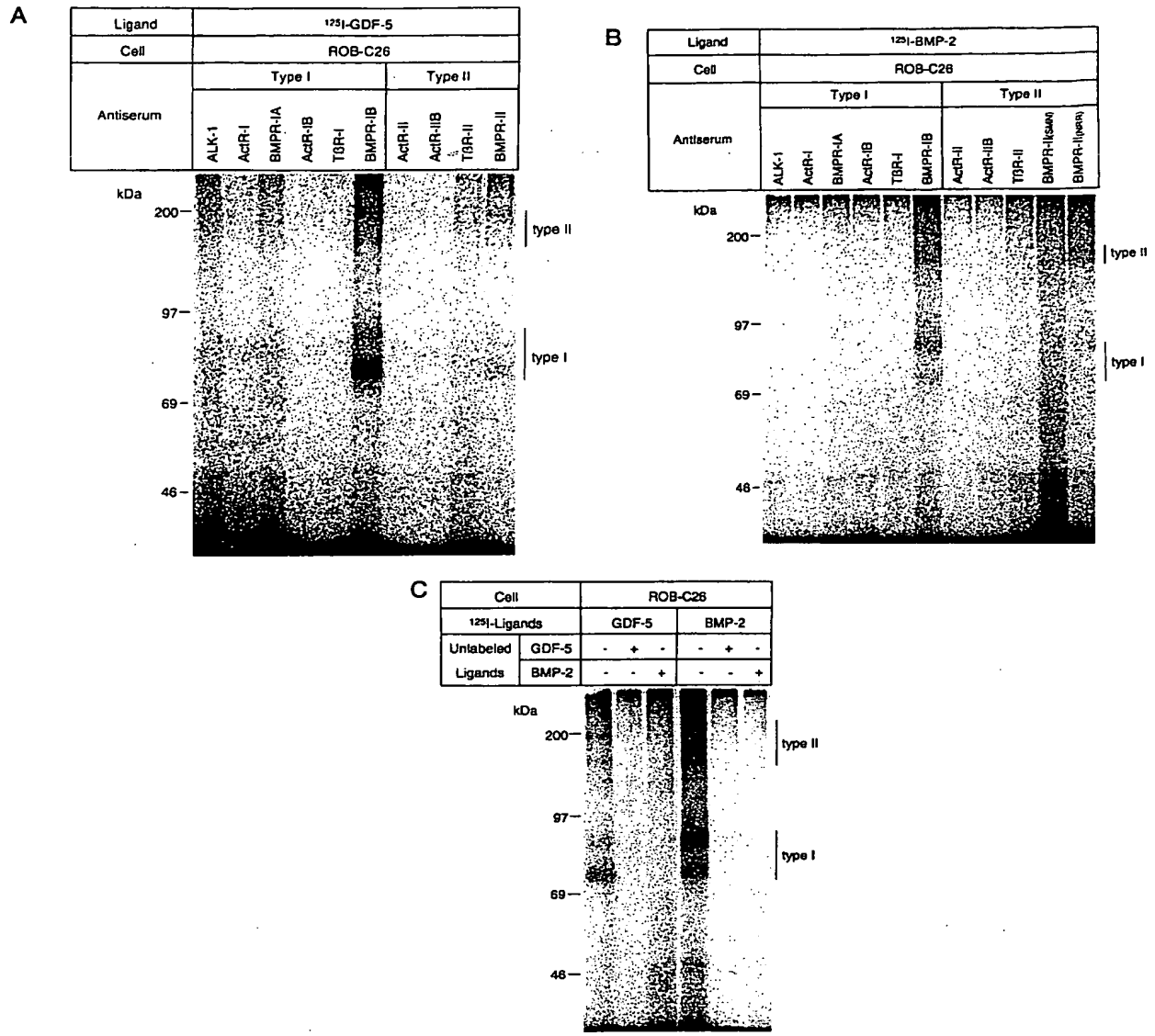

FIG. 2. **Binding of GDF-5 and BMP-2 in ROB-C26 cells.** ROB-C26 cells were affinity-labeled with ^{125}I-GDF-5 (*A*) and ^{125}I-BMP-2 (*B*), followed by cross-linking. The cross-linked complexes were immunoprecipitated with type I and type II receptor antisera. Antiserum to BMPR-II used in *A* is the NRR antiserum, which was raised against the C-terminal tail of BMPR-II (36). Two different antisera to BMPR-II (SMN and NRR; Ref. 36) were used in *B*. Binding of ^{125}I-GDF-5 and ^{125}I-BMP-2 in the presence or absence of unlabeled GDF-5 or BMP-2 was examined by immunoprecipitation using the BMPR-IB antiserum (*C*). Samples were subjected to SDS-gel electrophoresis, followed by an analysis using a Bio-Imaging Analyzer (BAS 2000; Fuji). Markers of molecular mass are indicated to the *left*.

nine kinase receptors, including BMPR-IA, ActR-I (Fig. 4), and DAF-4, a BMP type II receptor in *C. elegans* (data not shown).

When type I receptor cDNAs were co-transfected with the BMPR-II^{His}, ActR-II, or ActR-IIB1 cDNA, GDF-5 bound different sets of type I receptors. In the presence of BMPR-II^{His}, GDF-5 bound efficiently to BMPR-IB, but not to the other type I receptors (Fig. 5*A*). BMPR-IB as well as BMPR-II bands could be seen when the cross-linked complexes were immunoprecipitated by the BMPR-IB antiserum. When isolated with Ni^{2+}-NTA agarose beads, co-precipitation of the BMPR-IB complex could also be observed (Fig. 5*A*). Binding to BMPR-IB was up-regulated in the presence of BMPR-II^{His}, compared with its absence (data not shown). In the presence of ActR-II, GDF-5 bound most efficiently to BMPR-IB (Fig. 5*B*). Weak binding of GDF-5 was also seen to BMPR-IA in the presence of ActR-II (Fig. 5*B*). In the presence of ActR-IIB1, GDF-5 bound efficiently to BMPR-IB, but also to ActR-I and to BMPR-IA very weakly (Fig. 5*C*). Thus, the binding of GDF-5 is most efficient to BMPR-IB compared with the other type I receptors, and weak binding to BMPR-IA and ActR-I is observed in the presence of different type II receptors. When COS-1 cells were co-transfected with BMPR-IB and ActR-IIB1 cDNAs, the BMPR-IB complex could not be immunoprecipitated with the type II receptor antiserum (Fig. 5*C*), suggesting that BMPR-IB forms a heteromeric complex with BMPR-II and ActR-II upon GDF-5 binding but less efficiently with ActR-IIB1.

Signaling Activity in Response to GDF-5—We next investigated whether type I and type II receptors are capable of

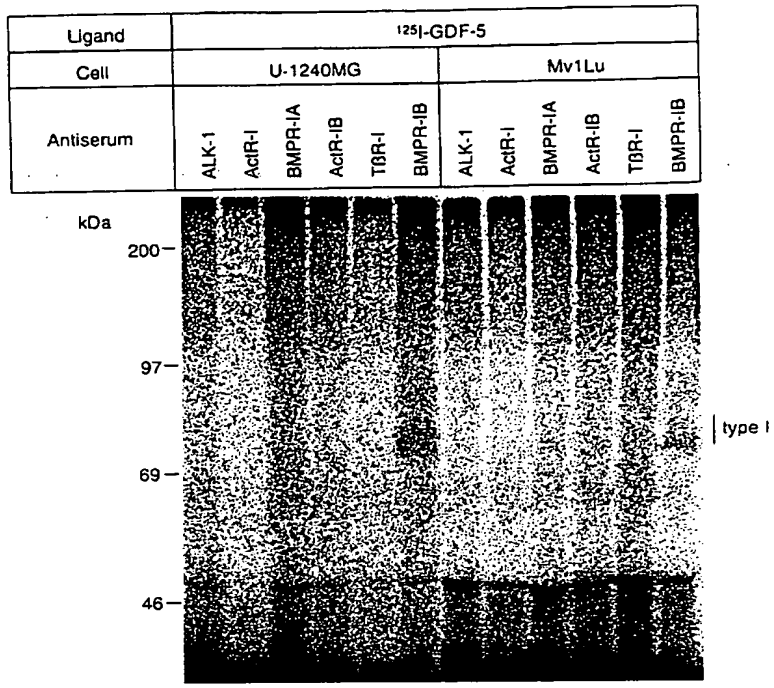

FIG. 3. **Binding of GDF-5 in U-1240 MG and Mv1Lu cells.** Binding and affinity cross-linking of ^{125}I-GDF-5 were performed with U-1240 MG human glioblastoma cells and Mv1Lu mink lung epithelial cells, followed by immunoprecipitation using antisera against type I receptors. The immune complexes were analyzed by SDS-gel electrophoresis and a Bio-Imaging Analyzer.

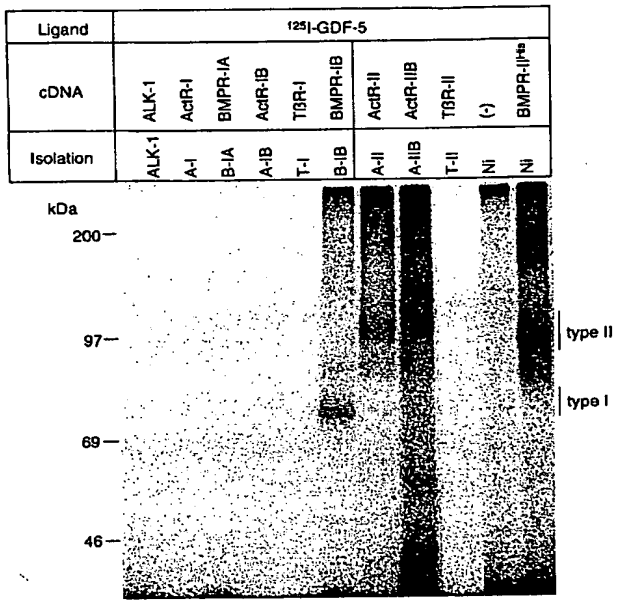

FIG. 4. **Binding of GDF-5 in COS-1 cells singly transfected with type I and type II receptor cDNAs.** COS-1 cells were transfected with cDNAs for type I and type II receptors. The cells were affinity-labeled using ^{125}I-GDF-5, followed by cross-linking. Cell lysates were precipitated with each of the corresponding antisera against type I and type II receptors or with Ni^{2+}-NTA-agarose beads. Samples were subjected to SDS-gel electrophoresis, followed by an analysis using a Bio-Imaging Analyzer. *Isolation A-I, B-IA, A-IB, T-I, B-IB, A-II, A-IIB,* and *T-II* represent immunoprecipitation by ActR-I, BMPR-IA, ActR-IB, TβR-I, BMPR-IB, ActR-II, ActR-IIB and TβR-II antisera, respectively; *Isolation Ni* represents Ni^{2+}-NTA isolation.

signaling upon binding GDF-5 using a p3TP-Lux promoter-reporter construct (54). R mutant Mv1Lu cells were transfected with type I and/or type II receptors, together with p3TP-Lux, and stimulated or not stimulated by GDF-5. Since transfection of empty pSV7d vector showed no luciferase response to GDF-5 (Fig. 6, *first set* of *bars*), these cells were used for the analysis of transfected GDF-5 receptor signaling activity. Cells transfected with ActR-II or BMPR-II alone did not respond to GDF-5 (Fig. 6). Cells transfected with BMPR-IA or BMPR-IB alone showed a very weak response to GDF-5, which may be ascribed to the presence of endogenous activin and BMP type II receptors in the R mutant cells (26, 36). When p3TP-Lux was co-transfected with ActR-II and BMPR-IB, transcriptional activation was clearly observed after stimulation by GDF-5 (Fig. 6). BMPR-IA also showed a less but significant increase in luciferase activity in the presense of ActR-II. Similarly, co-transfection of BMPR-II and BMPR-IB mediated transcriptional activation; however, co-transfection of BMPR-II and BMPR-IA did not show significant transcriptional activation (Fig. 6). In the R mutant cells co-transfected with ActR-IIB1 and type I receptors (ActR-I, BMPR-IA, and BMPR-IB), the activation of transcription by GDF-5 was not detected (data not shown).

DISCUSSION

In the present paper, we first tried to find the cell lines that respond to GDF-5 in order to identify the signaling receptors for GDF-5. In contrast to BMP-2, BMP-4, and OP-1/BMP-7, GDF-5 did not efficiently induce the ALP activity in most cell lines, including MC3T3-E1, ROS17/2.8, and C2C12 cells. Only the osteoprogenitor-like cell line, ROB-C26, could respond to GDF-5 (Fig. 1, *A* and *B*). These data suggested to us that the bioactivity of GDF-5 can be observed in limited cell types, and the receptor-binding profile of GDF-5 may be different from those of other BMPs. We then investigated the receptors in the ROB-C26 cells using antibodies against known serine/threonine kinase receptors. Interestingly, GDF-5 bound to only BMPR-IB and BMPR-II in this cell line but not to the other serine/threonine kinase receptors, including BMPR-IA (Fig. 2*A*). Since BMP-2 showed a similar binding profile in the ROB-C26 cells (Fig. 2*B*), this cell line may predominantly express BMPR-IB and BMPR-II compared with the other receptors.

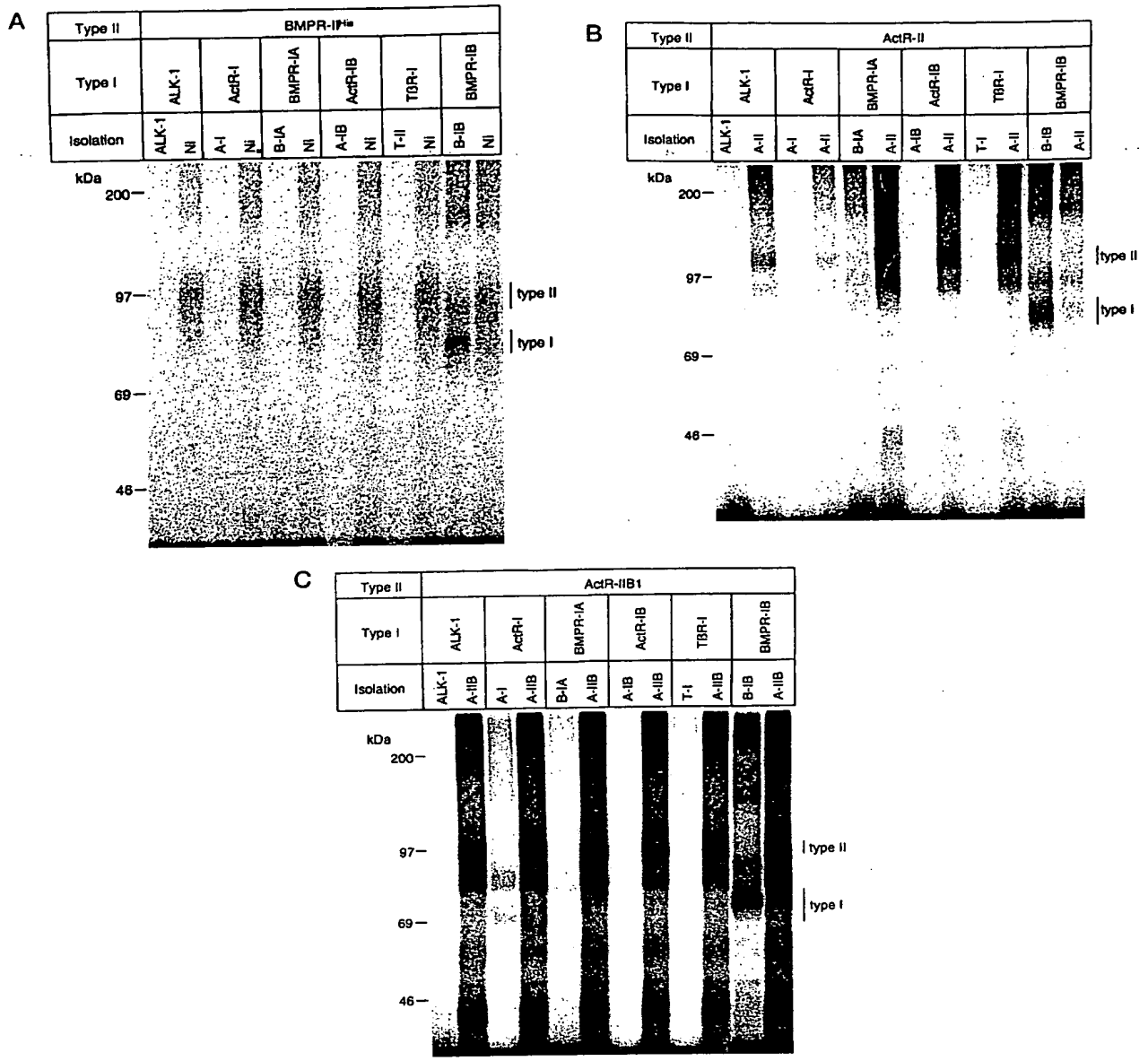

FIG. 5. **Binding of GDF-5 to type I and type II receptors in co-transfected COS-1 cells.** COS-1 cells were transfected with cDNAs for BMPR-II^{His} (*A*), ActR-II (*B*), or ActR-IIB1 (*C*) together with those for different type I receptors. The cells were affinity-labeled using ^{125}I-GDF-5, followed by cross-linking. Cell lysates were precipitated with Ni^{2+}-NTA-agarose beads for BMPR-II^{His} (*A*), or immunoprecipitated with the antisera against type I receptors (*A*, *B*, and *C*) or ActR-II (ARC-2) (*B*) or with the ActR-II antiserum that cross-reacts with ActR-IIB (*C*). Samples were analyzed by SDS-gel electrophoresis and a Bio-Imaging Analyzer. *Isolation A-I, B-IA, A-IB, T-I, B-IB, A-II, A-IIB,* and *T-II* represent immunoprecipitation by ActR-I, BMPR-IA, ActR-IB, TβR-I, BMPR-IB, ActR-II, ActR-IIB, and TβR-II antisera, respectively; *Isolation Ni* represents Ni^{2+}-NTA isolation.

Furthermore, the binding of ^{125}I-GDF-5 and ^{125}I-BMP-2 to BMPR-IB was competed by unlabeled GDF-5 or BMP-2 (Fig. 2*C*), indicating that the binding site to BMPR-IB is shared by these ligands. MC3T3-E1 cells are known to respond to BMP-4 and OP-1/BMP-7. In this cell type, ActR-I and BMPR-IA were shown to bind ^{125}I-OP-1/BMP-7 and ^{125}I-BMP-4, respectively (27). However, ^{125}I-GDF-5 did not efficiently bind to MC3T3-E1 cells, and we could not detect the cross-linked complexes with ^{125}I-GDF-5 in this cell line using any of the serine/threonine kinase receptor antisera (data not shown).

We then investigated the binding of GDF-5 to cell lines of nonskeletal origins. In U-1240 MG glioblastoma cells and Mv1Lu mink lung epithelial cells, GDF-5 bound only to BMPR-IB among the six type I receptors (Fig. 3). These cells have previously been shown to endogenously express ActR-I and BMPR-IA (27), but the cross-linked complexes with ^{125}I-GDF-5 were not immunoprecipitated by the antiserum against ActR-I or BMPR-IA. Moreover, we found that ^{125}I-BMP-2 bound to BMPR-IA as well as BMPR-IB in the Mv1Lu cells (data not shown). Taken together, the binding profile of GDF-5

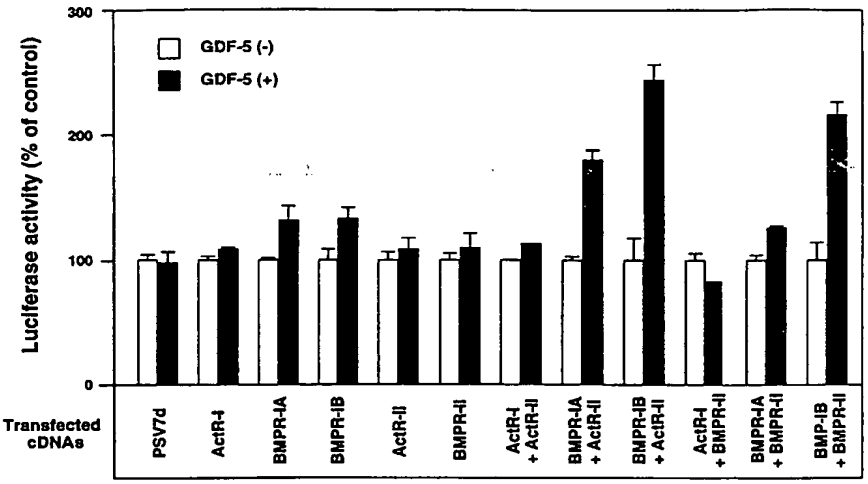

FIG. 6. **Signal transduction by GDF-5 through type I and type II receptors.** Transcriptional activation was measured using R mutant Mv1Lu cells transfected with p3TP-Lux promoter-reporter construct. cDNAs for ActR-I, BMPR-IA, BMPR-IB, ActR-II, and BMPR-II were co-transfected with p3TP-Lux into the cells, which was followed by the stimulation with GDF-5 (300 ng/ml) for 20 h. The experiments were repeated three times with similar results each time.

in nontransfected cells is different from that of BMP-2, BMP-4, or OP-1/BMP-7; *i.e.* GDF-5 preferentially binds to BMPR-IB but not to ActR-I and BMPR-IA.

We next studied the binding of GDF-5 in COS-1 cells transfected with the receptor cDNAs. Similar to BMP-4 and OP-1/BMP-7, BMPR-IB bound GDF-5 without the transfection of type II receptors. However, other type I receptors did not bind GDF-5 in the absence of type II receptors (Fig. 4). Binding of GDF-5 to the type II receptors was similar to that of OP-1/BMP-7; *i.e.* GDF-5 bound to BMPR-II as well as ActR-II and ActR-IIB1 (Fig. 4). When the type I receptors were co-transfected with the type II receptors, the binding profiles were complicated; GDF-5 formed complexes only with BMPR-IB in the presence of BMPR-II (Fig. 5*A*), but it formed complexes not only with BMPR-IB but also with BMPR-IA in the presence of ActR-II (Fig. 5*B*). In the presence of ActR-IIB1, binding of GDF-5 to ActR-I, BMPR-IA, and BMPR-IB could be seen, but BMPR-IB was not likely to form a tight complex with ActR-IIB1, because co-immunoprecipitation of neither ActR-IIB1 by the BMPR-IB antiserum nor BMPR-IB by the ActR-IIB1 antiserum could be observed (Fig. 5*C*).

Analysis of the signaling activity of GDF-5 using the p3TP-Lux construct in the R mutant Mv1Lu cells was in good agreement with the binding data observed in the transfected COS-1 cells. GDF-5 transduced the signal through BMPR-IB together with BMPR-II or ActR-II (Fig. 6). The complex of BMPR-IA and ActR-II mediated a less efficient signal than those containing BMPR-IB. GDF-5 did not transduce the p3TP-Lux signal through ActR-IIB1 and the type I receptors (data not shown). In contrast, activin was shown to activate the p3TP-Lux signal through ActR-IIB and ActR-I (25). These results in the nontransfected and transfected cells indicate that BMPR-IB and BMPR-II can act as functional type I and type II receptors for GDF-5, respectively. ActR-II may also possibly serve as a type II receptor for GDF-5 in certain cell types.

Cartilage and bone formation could be induced by GDF-5 in rodent thigh *in vivo* (14). Moreover, osteoblasts in primary culture were shown to respond to GDF-5, increasing ALP activity (14), and they formed bone-like nodules, where positive immunohistochemical staining could be seen by the antibodies against BMPR-IA and BMPR-IB.[4] In adult tissues, BMPR-IB is found mainly in brain, whereas BMPR-IA and BMPR-II are expressed in various tissues (24, 26, 28, 36). BMPR-IB is expressed in the process of bone formation during embryogenesis and after bone fracture, although the expression profile appears to be limited compared with that of BMPR-IA (55, 56). These data suggest that the bone and cartilage formation by GDF-5 observed *in vivo* is induced through BMPR-IB.

Binding of GDF-5 was observed in U-1240 MG glioblastoma cells and Mv1Lu mink lung epithelial cells. In addition to bone and cartilage, BMPR-IB and BMPR-II are expressed in various soft tissues during embryogenesis (36, 55). Moreover, both receptor transcripts are expressed in adult brain. Chang *et al.* (3) showed that although GDF-5 (CDMP-1) is predominantly expressed in skeletal muscles, GDF-6 (CDMP-2) is found in various soft tissues. Thus, GDF-5 or other highly related proteins may have broad physiological functions in different tissues. Compatible with the limited expression of GDF-5, the mutations in the GDF-5 gene result in the abnormalities only in skeletal tissues in both mouse and human (1, 19). The other GDF-5-like proteins, including GDF-6 and GDF-7, may play important roles in nonskeletal tissues.

Among the TGF-β superfamily, BMPs are classified by their ability to form bone and cartilage *in vivo*. However, BMPs include heterogenous members, and they can be subdivided into subgroups based on their amino acid sequence similarities. Moreover, the biological activities appear to be different among the members in the BMP family. Present data showed that binding profiles of GDF-5 are more limited than those of BMP-2, BMP-4, and OP-1/BMP-7, which suggests different biological functions of GDF-5 both *in vitro* and *in vivo*. Future studies including the comparison of the receptor binding properties of the other members in the BMP family, will be needed to understand the *in vivo* functions of various members of the BMP family.

Acknowledgments—We thank J. Massagué for p3TP-Lux promoter-reporter construct, BMPR-II^{His} construct, and ActR-IIB1 cDNA and L. S. Mathews and W. W. Vale for ActR-II cDNA. We also thank K. Verschueren for the antiserum against ActR-II intracellular domain. We are grateful to I. Morita for BEC cells and P. ten Dijke, K. Takeda, and M. Saitoh for valuable discussion.

REFERENCES

1. Storm, E. E., Huynh, T. V., Copeland, N. G., Jenkins, N. A., Kingsley, D. M., and Lee, S.-J. (1994) *Nature* 368, 639–643
2. Hötten, G., Neidhardt, H., Jacobowsky, B., and Pohl, J. (1994) *Biochem. Biophys. Res. Commun.* 204, 646–652
3. Chang, S. C., Hoang, B., Thomas, J. T., Vukicevic, S., Luyten, F. P., Ryöa, N. J. P., Kozak, C. A., Reddi, A. H., and Moos, M., Jr. (1994) *J. Biol. Chem.* 269, 28227–28234

[4] H. Nishitoh, H. Ichijo, M. Kimura, T. Matsumoto, F. Makishima, M. Kato, and K. Miyazono, unpublished observations.

4. Kingsley, D. M. (1994) *Genes & Dev.* **8**, 133–146
5. Reddi, A. H. (1992) *Curr. Opin. Cell Biol.* **4**, 850–855
6. Reddi, A. H. (1994) *Curr. Opin. Genet. Dev.* **4**, 737–744
7. Wozney, J. M., Rosen, V., Celeste, A. J., Mitsock, L. M., Whitters, M. J., Kriz, R. W., Hewick, R. M., and Wang, E. A. (1988) *Science* **242**, 1528–1534
8. Özkaynak, E., Rueger, D. C., Drier, E. A., Corbett, C., Ridge, R. J., Sampath, T. K., and Oppermann, H. (1990) *EMBO J.* **9**, 2085–2093
9. Vukicevic, S., Luyten, F. P., and Reddi, A. H. (1989) *Proc. Natl. Acad. Sci. U. S. A.* **86**, 8793–8797
10. Yamaguchi, A., Katagiri, T., Ikeda, T., Wozney, J. M., Rosen, V., Wang, E. A., Kahn, A. J., Suda, T., and Yoshiki, S. (1991) *J. Cell Biol.* **113**, 681–687
11. Asahina, I., Sampath, T. K., and Hauschka, P. V. (1996) *Exp. Cell Res.* **222**, 38–47
12. Paralkar, V. M., Weeks, B. S., Yu, Y. M., Kleinman, H. K., and Reddi, A. H. (1992) *J. Cell Biol.* **119**, 1721–1728
13. Perides, G., Safran, R. M., Downing, L. A., and Charness, M. E. (1994) *J. Biol. Chem.* **269**, 765–770
14. Hötten, G. C., Matsumoto, T., Kimura, M., Bechtold, R. F., Kron, R., Ohara, T., Tanaka, H., Satoh, Y., Okazaki, M., Shirai, T., Pan, H., Kawai, S., Pohl, J. S., and Kudo, A. (1996) *Growth Factors* **13**, 65–74
15. Özkaynak, E., Schnegelsberg, P. N. J., Jin, D. F., Clifford, G. M., Warren, F. D., Drier, E. A., and Oppermann, H. (1992) *J. Biol. Chem.* **267**, 25220–25227
16. Winnier, G., Blessing, M., Labosky, P. A., and Hogan, B. L. M. (1995) *Genes & Dev.* **9**, 2105–2116
17. Dudley, A. T., Lyons, K. M., and Robertson, E. J. (1995) *Genes & Dev.* **9**, 2795–2807
18. Luo, G., Hofmann, C., Bronckers, A. L. J. J., Sohocki, M., Bradley, A., and Karsenty, G. (1995) *Genes & Dev.* **9**, 2808–2820
19. Thomas, J. T., Lin, K., Nandedkar, M., Camargo, M., Cervenka, J., and Luyten, F. P. (1996) *Nature Genet.* **12**, 315–317
20. Massagué, J., Attisano, L., and Wrana, J. L. (1994) *Trends Cell Biol.* **4**, 172–178
21. Miyazono, K., ten Dijke, P., Yamashita, H., and Heldin, C.-H. (1994) *Semin. Cell Biol.* **5**, 389–398
22. Derynck, R. (1994) *Trends Biochem. Sci.* **19**, 548–553
23. Ebner, R., Chen, R.-H., Lawler, S., Zioncheck, T., and Derynck, R. (1993) *Science* **262**, 900–902
24. ten Dijke, P., Ichijo, H., Franzén, P., Schulz, P., Saras, J., Toyoshima, H., Heldin, C.-H., and Miyazono, K. (1993) *Oncogene* **8**, 2879–2887
25. Attisano, L., Cárcamo, J., Ventura, F., Weis, F. M. B., Massagué, J., and Wrana, J. L. (1993) *Cell* **75**, 671–680
26. ten Dijke, P., Yamashita, H., Ichijo, H., Franzén, P., Laiho, M., Miyazono, K., and Heldin, C.-H. (1994) *Science* **264**, 101–104
27. ten Dijke, P., Yamashita, H., Sampath, T. K., Reddi, A. H., Estevez, M., Riddle, D. L., Ichijo, H., Heldin, C.-H., and Miyazono, K. (1994) *J. Biol. Chem.* **269**, 16985–16988
28. Koenig, B. B., Cook, J. S., Wolsing, D. H., Ting, J., Tiesman, J. P., Correa, P. E., Olson, C. A., Pecquet, A. L., Ventura, F., Grant, R. A., Chen, G.-X., Wrana, J. L., Massagué, J., and Rosenbaum, J. S. (1994) *Mol. Cell. Biol.* **14**, 5961–5974
29. Bassing, C. H., Yingling, J. M., Howe, D. J., Wang, T., He, W. W., Gustafson, M. L., Shah, P., Donahoe, P. K., and Wang, X.-F. (1994) *Science* **263**, 87–89
30. Mathews, L. S., and Vale, W. W. (1991) *Cell* **65**, 973–982
31. Attisano, L., Wrana, J. L., Cheifetz, S., and Massagué, J. (1992) *Cell* **68**, 97–108
32. Mathews, L. S., Vale, W. W., and Kintner, C. R. (1992) *Science* **255**, 1702–1705
33. Lin, H. Y., Wang, X.-F., Ng-Eaton, E., Weinberg, R. A., and Lodish, H. F. (1992) *Cell* **68**, 775–785
34. Kawabata, M., Chytil, A., and Moses, H. L. (1995) *J. Biol. Chem.* **270**, 5625–5630
35. Liu, F., Ventura, F., Doody, J., and Massagué, J. (1995) *Mol. Cell. Biol.* **15**, 3479–3486
36. Rosenzweig, B. L., Imamura, T., Okadome, T., Cox, G. N., Yamashita, H., ten Dijke, P., Heldin, C.-H., and Miyazono, K. (1995) *Proc. Natl. Acad. Sci. U. S. A.* **92**, 7632–7636
37. Nohno, T., Ishikawa, T., Saito, T., Hosokawa, K., Noji, S., Wolsing, D. H., and Rosenbaum, J. S. (1995) *J. Biol. Chem.* **270**, 22522–22526
38. Wrana, J. L., Attisano, L., Wieser, R., Ventura, F., and Massagué, J. (1994) *Nature* **370**, 341–347
39. Attisano, L., Wrana, J. L., Montalvo, E., and Massagué, J. (1996) *Mol. Cell. Biol.* **16**, 1066–1073
40. Graff, J. M., Thies, R. S., Song, J. J., Celeste, A. J., and Melton, D. A. (1994) *Cell* **79**, 169–179
41. Suzuki, A., Thies, R. S., Yamaji, N., Song, J. J., Wozney, J. M., Murakami, K., and Ueno, N. (1994) *Proc. Natl. Acad. Sci. U. S. A.* **91**, 10255–10259
42. Estevez, M., Attisano, L., Wrana, J. L., Albert, P. S., Massagué, J., and Riddle, D. L. (1993) *Nature* **365**, 644–649
43. Yamashita, H., ten Dijke, P., Huylebroeck, D., Sampath, T. K., Andries, M., Smith, J. C., Heldin, C.-H., and Miyazono, K. (1995) *J. Cell Biol.* **130**, 217–226
44. Ruberte, E., Marty, T., Nellen, D., Affolter, M., and Basler, K. (1995) *Cell* **80**, 889–897
45. Letsou, A., Arora, K., Wrana, J. L., Simin, K., Twombly, V., Jamal, J., Staehling-Hampton, K., Hoffmann, F. M., Gelbart, W. M., Massagué, J., and O'Connor, M. B. (1995) *Cell* **80**, 899–908
46. Laiho, M., Weis, F. M. B., and Massagué, J. (1990) *J. Biol. Chem.* **265**, 18518–18524
47. Nistér, M., Claesson-Welsh, L., Eriksson, A., Heldin, C.-H., and Westermark, B. (1991) *J. Biol. Chem.* **266**, 16755–16763
48. Asahina, I., Sampath, T. K., Nishimura, I., and Hauschka, P. V. (1993) *J. Cell Biol.* **123**, 921–933
49. Franzén, P., ten Dijke, P., Ichijo, H., Yamashita, H., Schulz, P., Heldin, C.-H., and Miyazono, K. (1993) *Cell* **75**, 681–692
50. Ichijo, H., Yamashita, H., ten Dijke, P., Eto, Y., Heldin, C.-H., and Miyazono, K. (1993) *Biochem. Biophys. Res. Commun.* **194**, 1508–1514
51. Verschueren, K., Dewulf, N., Goumans, M.-J., Lonnoy, O., Feijen, A., Grimsby, S., Spiegle, K. V., ten Dijke, P., Morén, A., Vanscheeuwijck, P., Heldin, C.-H., Miyazono, K., Mummery, C., Van Den Eijnden-Van Raaij, J., and Huylebroeck, D. (1995) *Mech. Dev.* **52**, 109–123
52. Truett, M. A., Blacher, R., Burke, R. L., Caput, D., Chu, C., Dina, D., Hartog, K., Kuo, C. H., Maslarz, F. R., Merryweather, J. P., Najarian, R., Pachl, C., Potter, S. J., Puma, J., Quiroga, M., Rall, L. B., Randolph, A., Urdea, M. S., Valenzuela, P., Dahl, H. H., Favalaro, J., Hansen, J., Nordfang, O., and Ezban, M. (1985) *DNA* **4**, 333–349
53. Andersson, S., Davis, D. L., Dahlbäck, H., Jörnvall, H., and Russell, D. W. (1989) *J. Biol. Chem.* **264**, 8222–8229
54. Cárcamo, J., Zentella, A., and Massagué, J. (1995) *Mol. Cell. Biol.* **15**, 1573–1581
55. Dewulf, N., Verschueren, K., Lonnoy, O., Morén, A., Grimsby, S., Spiegle, K. V., Miyazono, K., Huylebroeck, D., and ten Dijke, P. (1995) *Endocrinology* **136**, 2652–2663
56. Ishidou, Y., Kitajima, I., Obama, H., Maruyama, I., Murata, F., Imamura, T., Yamada, N., ten Dijke, P., Miyazono, K., and Sakou, T. (1995) *J. Bone Miner. Res.* **10**, 1651–1659

genes by *Xbra* resembles the cooperative activation of *hunchback* by *bicoid* in *Drosophila*[19], and it will be of great interest to establish whether Xbra interacts directly with regulatory elements of mesoderm-specific genes. □

Received 12 February; accepted 15 June 1992.

1. Herrmann, B. G., Labeit, S., Poustka, A., King, T. R. & Lehrach, H. *Nature* **343**, 617–622 (1990).
2. Rashbass, P., Cooke, L. A., Herrmann, B. G. & Beddington, R. *Nature* **353**, 348–351 (1991).
3. Wilkinson, D. G., Bhatt, S. & Herrmann, B. G. *Nature* **343**, 657–659 (1990).
4. Smith, J. C., Price, B. M. J., Green, J. B. A., Weigel, D. & Herrmann, B. G. *Cell* **67**, 79–87 (1991).
5. Krieg, P. A. & Melton, D. A. *Nucleic Acids Res.* **12**, 7057–7071 (1984).
6. Hopwood, N. D. & Gurdon, J. B. *Nature* **347**, 197–200 (1990).
7. Cooke, J. & Smith, J. C. *Devl Biol.* **131**, 383–400 (1989).
8. Mohun, T. J., Brennan, S., Dathan, N., Fairman, S. & Gurdon, J. B. *Nature* **311**, 716–721 (1984).
9. Sargent, M. G. & Bennett, M. F. *Development* **109**, 967–973 (1990).
10. Jonas, E., Sargent, T. D. & Dawid, I. B. *Proc. natn. Sci. U.S.A.* **82**, 5413–5417 (1985).
11. Green, J. B. A., Howes, G., Symes, K., Cooke, J. & Smith, J. C. *Development* **108**, 173–183 (1990).
12. Kinter, C. R. & Brockes, J. P. *Nature* **308**, 67–69 (1984).
13. Ruiz i Altaba, A. & Melton, D. A. *Development* **106**, 173–183 (1989).
14. Cho, K. W. Y., Blumberg, B., Steinbesser, H. & De Robertis, E. M. *Cell* **67**, 1111–1120 (1991).
15. Green, J. B. A. & Smith, J. C. *Nature* **347**, 391–394 (1990).
16. Dale, L., Howes, G., Price, B. M. J. & Smith, J. C. *Development* **115**, 573–585 (1992).
17. Ruiz i Altaba, A. & Melton, D. A. *Cell* **57**, 317–326 (1989).
18. Cho, K. W. Y., Morita, E. A., Wright, C. V. E. & De Robertis, E. M. *Cell* **65**, 55–64 (1991).
19. Driever, W. & Nusslein-Volhard, C. *Nature* **337**, 138–143 (1989).
20. Sambrook, J., Fritsch, E. F. & Maniatis, T. *Molecular Cloning: A Laboratory Manual* 2nd edn (Cold Spring Harbor Laboratory Press, New York, 1982).
21. Slack, J. M. W. *J. Embryol. exp. Morph.* **80**, 289–319 (1984).
22. Amaya, E., Musci, T. J. & Kirschner, M. W. *Cell* **66**, 257–270 (1991).
23. Nieuwkoop, P. D. & Faber, J. *Normal Table of* Xenopus laevis (*Daudin*) (North-Holland, Amsterdam, 1967).
24. Cooke, J. *J. Embryol. exp. Morph.* **51**, 165–182 (1979).
25. Cooke, J., Smith, J. C., Smith, E. J. & Yaqoob, M. *Development* **101**, 893–908 (1987).

ACKNOWLEDGEMENTS. We thank B. Price for subcloning, W. Hatton for histology, M. Saha for the *Xhox3* plasmid, E. De Robertis for the *gsc* plasmid, and the NIMR Photographic Department for photographic work. V.C. is the recipient of a postdoctoral fellowship from the SERC.

An unusual feature revealed by the crystal structure at 2.2 Å resolution of human transforming growth factor-β2

Michael P. Schlunegger & Markus G. Grütter

Department of Biotechnology, Pharmaceuticals Division, Ciba-Geigy, CH-4002 Basel, Switzerland

TRANSFORMING growth factor type β2 (TGF-β2)[1] is a member of an expanding family of growth factors that regulate proliferation and differentiation of many different cell types[2,3]. TGF-β2 binds to various receptors[4], one of which was shown to be a serine/threonine kinase[5]. TGF-β2 is involved in wound healing[6], bone formation[7] and modulation of immune functions[8]. We report here the crystal structure of TGF-β2 at 2.2 Å resolution, which reveals a novel monomer fold and dimer association. The monomer consists of two antiparallel pairs of β-strands forming a flat curved surface and a separate, long α-helix. The disulphide-rich core has one disulphide bond pointing through a ring formed by the sequence motifs Cys-Ala-Gly-Ala-Cys and Cys-Lys-Cys, which are themselves connected through the cysteines. Two monomers are connected through a single disulphide bridge and associate such that the helix of one subunit interacts with the concave β-sheet surface of the other. Four exposed loop regions might determine receptor specificity. The structure provides a suitable model for the TGF-βs and other members of the superfamily[9–11] and is the basis for the analysis of the TGF-β2 interactions with the receptor.

Human recombinant TGF-β2 was prepared and crystallized as described earlier[12]. Table 1 describes data collection, structure solution and refinement of the TGF-β2 structure. The TGF-β2 monomer is a flat, elongated and slightly bent molecule with an overall size of $60 \times 20 \times 15$ Å^3. The unusual monomer fold consists at one end of a long α-helix with its axis perpendicular to the β-sheet and which is separated from two antiparallel pairs of β-strands (Fig. 1*a*). The core of the molecule has an additional unusual fold involving the four intramolecular disulphide bridges (Fig. 1*b*). The amino-terminal short α-helix on the outside of the monomer is followed by an exposed loop that is fixed to the core through a disulphide bridge. The other three disulphide bonds connect the different β-strands with each other. Two of these disulphide bridges form a narrow and rigid eight-membered ring consisting of the residues Cys 44-Ala 45-Gly 46-Ala 47-Cys 48-Cys 111-Lys 110-Cys 109-(Cys 44). The disulphide bridge, Cys 15 to Cys 78, connecting the N terminus with the β-strand marked C in Fig. 1*a*, points directly through this ring. We will refer to this unusual structural feature as the TGF-β 'knot'. All the intramolecular disulphide bridges are forming a tight and compact core. Similar eight-membered rings formed by two disulphide-connected backbones have also been found in endothelins, sarafatoxins, bee-venom toxins and scorpion venom toxins[13]. In these proteins the Cys-X-X-X-Cys sequence motif is part of an α-helix and the disulphide bonds are used to stabilize this helix. A similar but larger knot to that in TGF-β2 was found in the potato inhibitor of carboxypeptidase A (ref. 14). Its sequence motifs Cys-X-X-X-Cys and Cys-X-X-Cys form a nine-membered ring through which a third disulphide bridge is pointing. Comparison of the van der Waals surfaces of the two knots shows that the eight-membered ring of the TGF-β knot is the most compact ring through which a disulphide bond can pass.

The monomer has a solvent-accessible surface area of 4,400 Å^2 (ref. 15). In the dimer (Fig. 1*c*), two monomers are connected by a disulphide bridge (Cys 77) lying exactly on the crystallographic 2-fold axis ($x-y$, $-y$, $1/3-z$). The surface area of the dimer is 7,000 Å^2, indicating that about 1,800 Å^2 (900 Å^2 per

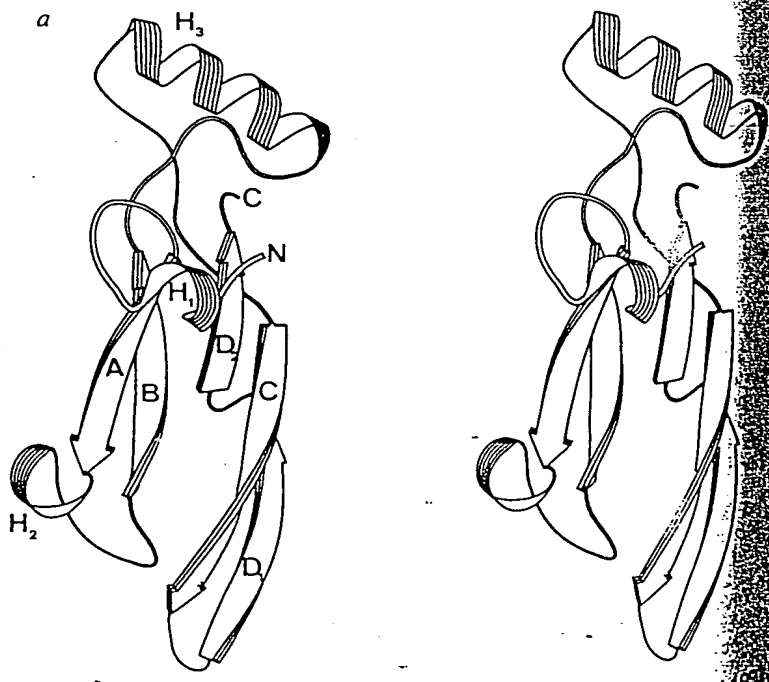

...onomer) are buried in the dimer. The long axes of the monomer ...olecules are roughly perpendicular to the 2-fold axis. The long ...helices H_3 are in tight contact with the β-sheet of the other ...ubunit. Most of the interactions between residues 56 to 65 of ...α-helix H_3 of one subunit and the β-sheet of the second ...ubunit are made between hydrophobic and aromatic residues ...hat are tightly packed and buried in the dimer interface. Addi...onal stabilization of this helix–sheet interaction is provided by ...o hydrogen bonds between the two subunits: the carbonyl ...xygens of Asn 42 and Asn 103 of one subunit to the side-chain ...His 58 and to the main-chain nitrogen of His 58 of the other ...ubunit, respectively. The packing of the two monomers is less ...ompact in the region of the intermolecular disulphide bond.

Hydrophobic interactions between Cys 77 of one subunit and Val 79 of the second subunit, as well as an extended hydrogen-bonding network in which several clearly defined water molecules are involved, also contribute to the stabilization of the dimer. Predominantly hydrophobic interactions between the monomers are found between Phe 43 (β-strand B; Fig. 1*g*) and Ala 72, Ser 73 and Ala 74 (β-strand C of the other subunit).

Possible receptor-binding sites include most of the likely side-chains of surface residues located in protruding loops. Sequence variability in TGF-β1 to β5 in such regions must be responsible for the specificity for the different receptor types. Viewed along the 2-fold axis, the biologically active dimer of TGF-β2 (Fig. 1*c*) shows three or four such regions (Fig. 2*a*, *b*).

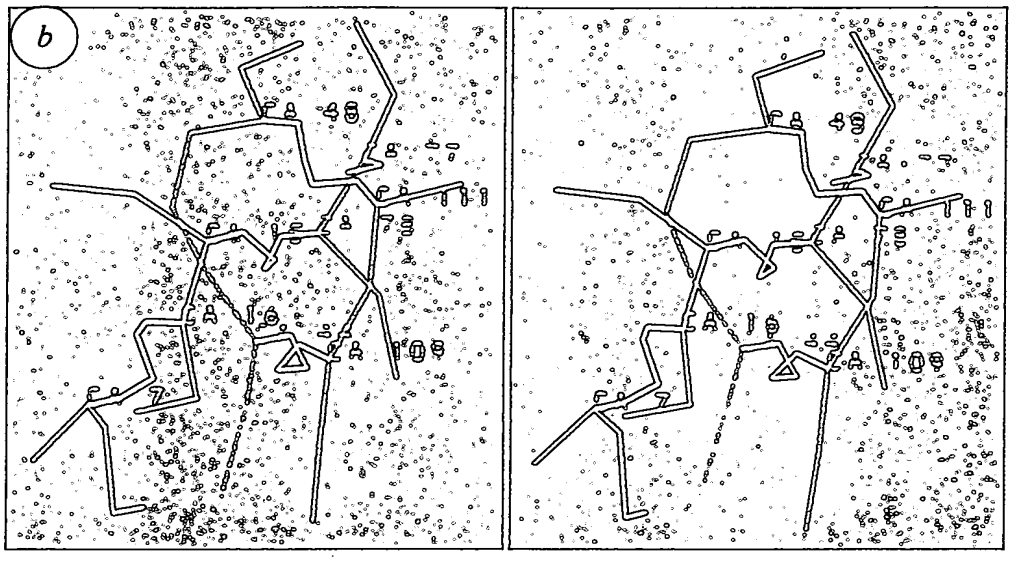

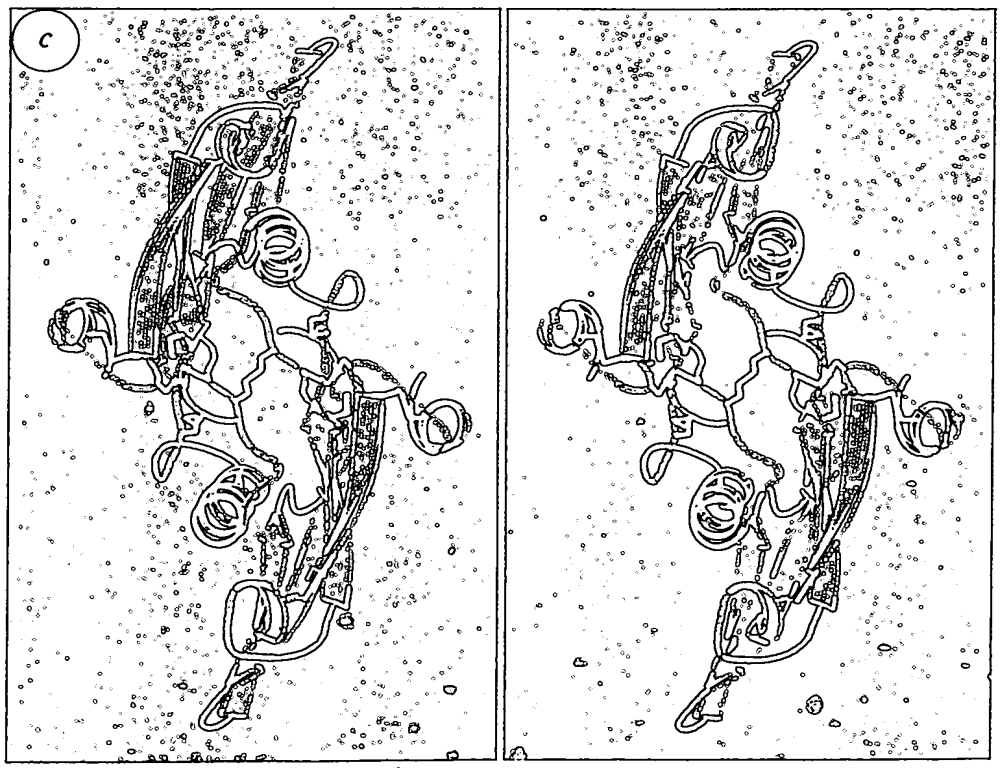

...IG. 1 *a* (opposite), Stereo RIBBON[24] ...icture of the TGF-β2 monomer fold. ...e N-terminal short α-helix H_1 ...esidues 3–8) on the outside of the ...onomer is followed by an exposed ...op, which is fixed to β-strand A ...esidues 16–23) through a disulphide ...ridge. The second β-strand B (res...dues 38–45) is connected by a long ...oop of 14 ...mino acids, including a ...mall helical turn H_2 (residues 24–28), ...β-strand A. The β-strand B is fixed ...the C terminus by two disulphide ...onds. The α-helix H_3 (residues 56–69) ...nearly four turns, situated at one ...nd of the molecule, connects β-strand ...and the long β-strand C (residues ...2–91). β-strands C and D_1 (residues ...3–102) are connected by a β-hairpin. ...085, in β-strand C, disrupts the ...drogen-bonding pattern between β-...ands C and D_1 and forces β-strand ...to wind around β-strand C in order ...continue hydrogen-bonding with the ...pposite side of β-strand C (β-strand ...esidues 105–110). *b*, Stereo pic...e showing parts of the core display...ll the cysteines and parts of the ...ckbone. The two disulphide bridges ...44–Cys 109 and Cys 48–Cys 111 ...ackbone coloured in red) are forming ...ght ring of eight residues. The disul...de bridge Cys 15–Cys 78 (backbone ...oured in blue) is pointing directly ...ough this ring. The N terminus (back...coloured in purple) is fixed by the ...phide bridge Cys 7–Cys 16. Cys 77 ...t upper corner of the picture) forms ...only intermolecular disulphide ...The rigidity is emphasized by low ...dual atomic temperature factors ...the range of 5 to 25 Å^2. *c*, Stereo ...BBON[24] picture of the TGF-β2 dimer ...ed along the crystallographic 2-...ds. The centre of the single inter...ular disulphide bond between ...of the first subunit and Cys 77* ...second subunit is lying exactly ...his 2-fold axis. All the intra- as ...as the intermolecular disulphide ...es are in yellow.

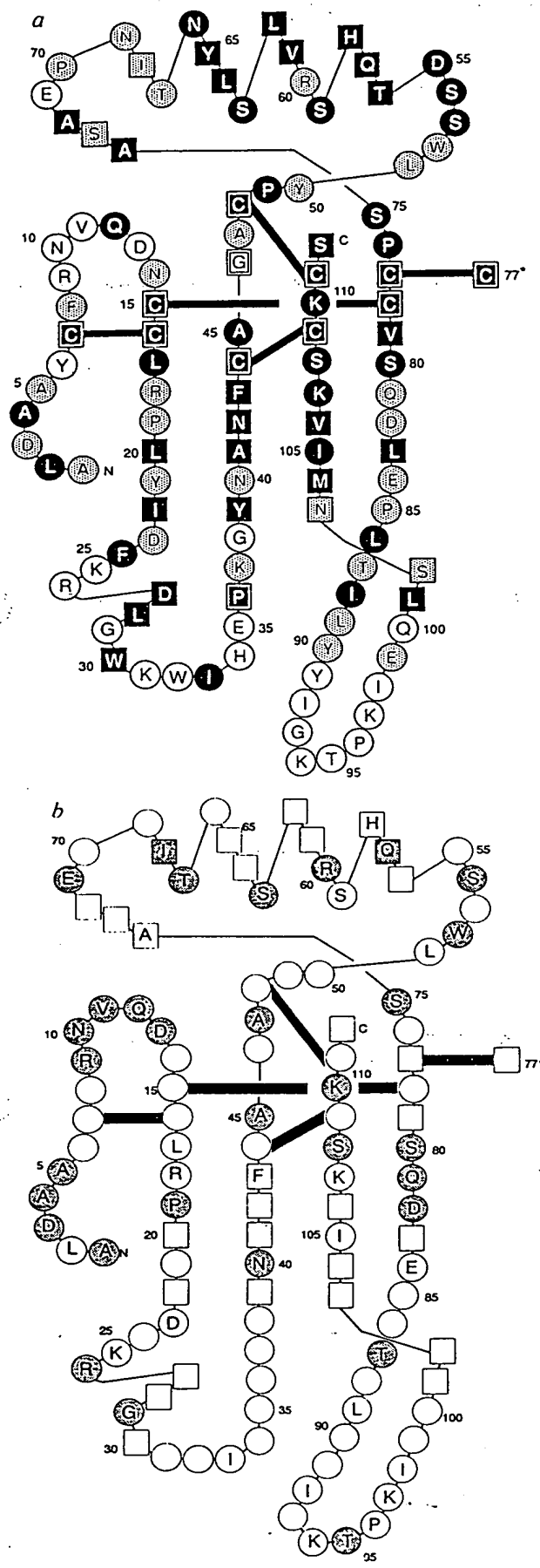

FIG. 2 *a*, Schematic representation of the TGF-β2 monomer highlighting structurally important residues. Amino acids are indicated by their one-letter code. Double squares, invariant residues for all TGFs and related proteins (Cys 7 and Cys 16 are only invariant in the five TGF-β isoforms). Characterization by the side-chain solvent-accessible area A[15]: not shaded, exposed residues ($A > 60$ Å^2); light shaded, intermediately exposed residues (20 Å$^2 < A < 60$ Å^2); dark shaded, buried residues ($A < 20$ Å^2). The single squares represent residues involved in the dimer interface having a distance of less than 4 Å from the other subunit. Glycine residues have not been included in the solvent accessibility analysis. *b*, Schematic representation of the TGF-β2 monomer highlighting residues that show changes in the five isoforms TGF-β1 to TGF-β5. Squares, residues involved in the dimer interface (as in *a*). Not shaded, residues that show conservative changes; shaded, residues that show strong changes. Residues not indicated with their one-letter code are invariant in all five isoforms. The insertion of two additional amino acids in TGF-β4 after Val 11 is not shown. *c*, Sequence alignment of the mature or proposed mature region of 20 TGF-β-like proteins beginning with the first invariant cysteine residue (which is Cys 15 and not Cys 16 of TGF-β2 as was indicated earlier[25]). The conserved residues, Cys 16, Pro 36, Cys 44, Gly 46, Cys 48, Cys 77, Cys 78, Cys 109 and Cys 111 are indicated by boxes. The superfamily has been separated into four subgroups based on the relative sequence similarities between these members[26]. TGF-β subgroup consists of human TGF-β1, TGF-β2 and TGF-β3, chicken TGF-β4 and *Xenopus* TGF-β5. Vg/dpp subgroup consists of the decapentaplegic gene product dpp of *Drosophila*, Vg-1 of the vegetal pole of *Xenopus*, mouse Vgr-1, the mammalian Vg-1 homologue mouse growth/differentiation factor 1 (GDF-1), *Drosophila* 60A, human bone morphogenetic proteins BMP-2a, BMP-2b/BMP-4, BMP-3, BMP-5, BMP-6 and BMP7/OP-1 (osteogenic protein 1). The inhibin subgroup consists of porcine inhibin α, βA and βB. The MIS subgroup contains a single member, human Müllerian inhibitory substance MIS (refs 25, 26).

c

```
TGF-β subgroup

TGF-β1      C CVRQ-LYIDFRKDLGWK-WIHE P KGYHANF C L G P C P-YIW----SLD--TQRN
TGF-β2      C CLRP-LYIDFKRDLGWK-WIHE P KGYNANF C A G A C P-YLW----SSD--TQRD
TGF-β3      C CVRP-LYIDFRQDLGWK-WVHE P KGYYANF C S G P C P-YLR----SAD--TTRN
TGF-β4      C CVRP-LYIDFRKDLQWK-WIHE P KGYMANF C M G P C P-YIW----SAD--TQRN
TGF-β5      C CVKP-LYINFRKDLGWK-WIHE P KGYEANY C L G N C P-YIW----SMD--TQTN
            15                      36          44  46  48

Vg/dpp subgroup

dpp         C -RRHSLYVDF-SDVGWDDWIVA P LGYDAYY C H G K C P-FPLADHFNS--TNHA
Vg-1        C -KKRHLYVEF-KDVGWQNWVIA P QGYMANY C Y G E C P-YPLTEILNG--SNHA
Vgr-1       C -KKHELYVSF-QDLGWQDWIIA P KGYAANY C D G E C -SFPLNAHMNA--TNHA
GDF-1       C -RTRRLHVSF-REVGWHRWVIA P RGFLANF C Q G T C ALPETLRGPGGPPALNHA
60A         C -QMQTLYIDF-KDLGWHDWIIA P EGYGAFY C S G E C N-FPLNAHMNA--TNHA
BMP-2a      C -KRHPLYVDF-SDVGWNDWIVA P PGYHAFY C H G E C P-FPLADHLNS--TNHA
BMP-2b/BMP-4 C -RRHSLYVDF-SDVGWNDWIVA P PGYQAFY C H G D C P-FPLADHLNS--TNHA
BMP-3       C -ARRYLKVDF-ADIGWSEWIIS P KSFDAYY C S G A C QFPMPKSLKPS--SNHA
BMP-5       C -KKHELYVSF-RDLGWQDWIIA P EGYAAFY C D G E C S-FPLNAHMNA--TNHA
BMP-6       C -RKHELYVSF-QDLGWQDWIIA P KGYAANY C D G E C S-FPLNAHMNA--TNHA
BMP-7/OP-1  C -KKHELYVSF-RDLGWQDWIIA P EGYAAYY C E G E C -AFPLNSYMNA--TNHA

Inhibin subgroup

Inhibin α   C -HRVALNISF-QELGWERWIVY P PSFIFHY C H G G C GLHIPPNLSLPV--PGLF
Inhibin βA  C --KKQFFVSF-KDIGWNDWIIA P SGYHANY C E G E C PSHIAGTSGSSL--SNLA
Inhibin βB  C --RQQFFIDF-RLIGWNDWIIA P TGYYGNY C E G S C PAYLAGVPGSAS--SNLA

MIS subgroup

MIS         C -ALRELSVDLRAE----RSVLI P ETYQANN C Q G V C GWPQSDRNPRY--QGLV

TGF-β subgroup

TGF-β1      VLALYN--QHNPGASAAP CC V--PQALEPLPIVYY-VGRKPKV-EQLSNMIVRS C K C S
TGF-β2      VLSLYN--TINPEASASP CC V--SQDLEPLTILYY-IGKTPKI-EQLSNMIVKS C K C S
TGF-β3      VLGLYN--TLNPEASASP CC V--PQDLEPLTILYY-VGRTPKV-EQLSNMVVKS C K C S
TGF-β4      VLALYN--QHNPGASAAP CC V--PQTLDPLPIIYY-VGRNVRV-EQLSNMIVRA C K C S
TGF-β5      VLSLYN--QNNPGASISP CC V--PDVLEPLPIIYY-VGRTAKV-EQLSNMIVRS C K C S
                                77/78                                109

Vg/dpp subgroup

dpp         VQTLVNN--MNPGKVPKA CC V--PTQLDSVAMLYLND-QSTVVLKNYQEMTVVG C G C R
Vg-1        LQTLVHS--IEPEDIPLP CC V--PTKMSPISMLFY-DNNDNVVLRHYENMAVDE C G C R
Vgr-1       VQTLVHL--MNPEYVPKP CC A--PTKLNAISVLYF-DDNSNVILKKYRNMVVRA C G C R
GDF-1       LRALMHAAA-PTPGAGSP CC V--PERLSPISVLFF-DNSDNVVLRHYEDMVVDE C G C R
60A         VQTLVHL--LEPKKVPKP CC A--PTRLGALPVLYH-LNDENVNLKKYRNMIVKS C G C R
BMP-2a      VQTLVNS---VNSKIPKA CC V--PTELSAISMLYL-DENEKVVLKNYQDMVVEG C G C R
BMP-2b/BMP-4 VQTLVNS---VNSSIPKA CC V--PTELSAISMLYL-DEYDKVVLKNYQEMVVEG C G C R
BMP-3       IQSIVRA-VGVVPGIPEP CC V--PEKMSSLSILFF-DENKNVVLKVYPNMTVES C G C R
BMP-5       VQTLVHL--MFPDHVPKP CC A--PTKLNAISVLYF-DDSSNVILKKYRNMVVRS C G C R
BMP-6       VQTLVHL--MNPEYVPKP CC A--PTKLNAISVLYF-DDNSNVILKKYRNMVVRA C G C R
BMP-7/OP-1  VQTLVHF--INPETVPKP CC A--PTQLNAISVLYF-DDSSNVILKKYRNMVVRA C G C R

Inhibin subgroup

Inhibin α   T----PAQPYSLLPGAQP CC AALPGTMRPLHVRTTSDGGYSFKYETVPNLLTQH C A C A
Inhibin βA  VINHYRMRGHSPFANLKS CC V--PTKLRPMSMLYY-DDGQNIIKKDIQNMIVEE C G C R
Inhibin βB  VVNQYRMRGLNPGT-VNS CC I--PTKLSTMSMLYF-DDEYNIVKRDVPNMIVEE C G C R

MIS subgroup

MIS         VLLL-KMQARGAALARPP CC V--PTAYAGKLLISLSEER--ISAHHVPNMVATE C
```

TABLE 1 Data collection and phasing statistics

Dataset	Resolution (Å)	Unique reflections (completeness in last resolution range)	R_{merge}* (%)	Average isomorphous difference (%) (15–3.5 Å)
native	1.8	14,995 (94.5%, 1.9–1.8 Å)	10.6	—
$K_3UO_2F_5$	2.8	4,123 (84.7%, 2.87–2.8 Å)	7.3†/5.6‡	19.6
$UO_2(NO_3)_2$	3.4	2,383 (99.9%, 3.49–3.4 Å)	8.8†/7.8‡	16.7
K_2PtCl_4	2.8	4,194 (98.6%, 2.87–2.8 Å)	8.8	9.0
K_2PtCl_6	2.8	4,161 (95.3%, 2.87–2.8 Å)	10.3	15.0

Dataset	Number of sites	R_{cullis}§ (%) (15–3.4 Å)	Anomalous data	Phasing power‖ (15–3.4 Å)	Binding site
$K_3UO_2F_5$	1	41.7	yes	2.92	Glu 35
$UO_2(NO_3)_2$	1	46.0	yes	2.42	Glu 35
K_2PtCl_4	1	68.4	no	1.73	Asn 69
K_2PtCl_6	1	62.0	no	1.64	Asn 69

Diffraction data were collected using a FAST area detector (Enraf-Nonius, Delft, The Netherlands). Data were evaluated using the program MADNES[18]. All other crystallographic calculations were done using the CCP4 program package (Daresbury Laboratory). The space group was determined as $P3_121$ or $P3_221$ by examining the 00l and the hk0 reflections. Heavy-atom derivative sites were determined by inspection of the Harker sections of the difference Patterson maps. Heavy-atom parameters x, y, z and occupancy were refined and then atomic temperature factors were also refined. The structure was solved using the $K_3UO_2F_5$ derivative alone with the aid of the anomalous scattering signal of the derivative, which provided SIRAS phases. The initial map at 3.4 Å had a mean figure of merit of 0.596 for 2,343 reflections between 15.0 and 3.4 Å. It was improved by a solvent-flattening procedure[19] (ref. 3a), estimating a solvent content of 50% and iteration for four cycles. The map allowed the determination of the space group ($P3_221$), the unambiguous chainfold and the location and fitting of 104 of 112 (93%) of the amino-acid side-chains from the known amino-acid sequence[20] using the program FRODO[21]. Only the regions 70–71 and 91–96 were unclear before refinement. The heavy-atom site of UO_2^{2+} was found to be near Glu 35, which is reasonable owing to its location on the surface of the molecule and its negative charge. The model had a crystallographic R-factor of 39.4% before refinement, which was done by using a combination of simulated annealing using the program X-PLOR[22] and restrained least-squares refinement as implemented in the program TNT[23]. Electron density maps were inspected with coefficients $2F_o - F_c$ and $F_o - F_c$ at different refinement stages or after omitting parts (typically 8–10 residues) of the structure before the interpretation (Fig. 3b). The model includes 78 water molecules. The atomic temperature factors range from 3 to 99 Å^2 for protein atoms and 15 to 92 Å^2 for water molecules. The current R-factor is 18.1% for reflections between 8.0 and 2.2 Å. The root-mean-square deviation from ideal bond length is 0.01 Å and from bond angles 1.98 degrees. All but one non-glycine residue ϕ, ψ angles lie in the 'allowed' regions of the Ramachandran plot, the exception being residue Asn 42.

*$R_{merge} = \Sigma(|I - \{I\}|)/\Sigma I$, where I is intensity measurement for symmetry-related reflections, and $\{I\}$ is the mean intensity for this reflection.

†Including anomalous differences.

‡Anomalous dispersion signals included.

§$R_{cullis} = \Sigma||F_{PH} - F_P| - F_{H(calc)}|/\Sigma|F_{PH} - F_P|$, where F_P and F_{PH} are the structure amplitudes of the protein and the heavy-atom derivative, respectively, and $F_{H(calc)}$ is the calculated heavy-atom structure factor amplitude (over centric data only.

‖Phasing power $= \langle F_H \rangle / E$, the r.m.s. heavy-atom structure factor amplitude divided by the residual lack-of-closure error.

First, the N-terminal segment (Ala 1 to Asp 13) is a region in the sequences of TGF-β1 to β5 where many nonconservative amino-acid substitutions are concentrated. The second region of interest is the loop connecting β-strand A and B. The charged and polar residues 25, 26, 31 and 35 are solvent-exposed and residues 23, 25 and 26 show sequence changes between TGF-β1 to β5. The third region is the C-terminal end of the long α-helix H_3 (Thr 67 to Ser 73), where the solvent-accessible residue 71 is either Glu or Gly. The fourth region is the most flexible β-turn (Tyr 91 to Pro 96) which connects β-strands C and D_1. Because interactions between a TGF-β molecule and its receptor must be very specific as binding constants are in the picomolar range[4], it is still unclear whether one or more of these segments interact. The existence of heterodimers like TGF-β1.2 (refs 1, 16) and TGF-β2.3 (ref. 16), purified from natural sources, might indicate that one TGF-β-dimer could bind to two different receptors at the same time, as was suggested for receptor types II and III (ref. 17).

So far all isolated or predicted proteins of the TGF superfamily show sequence invariance in the cysteines 15, 44, 48, 77,

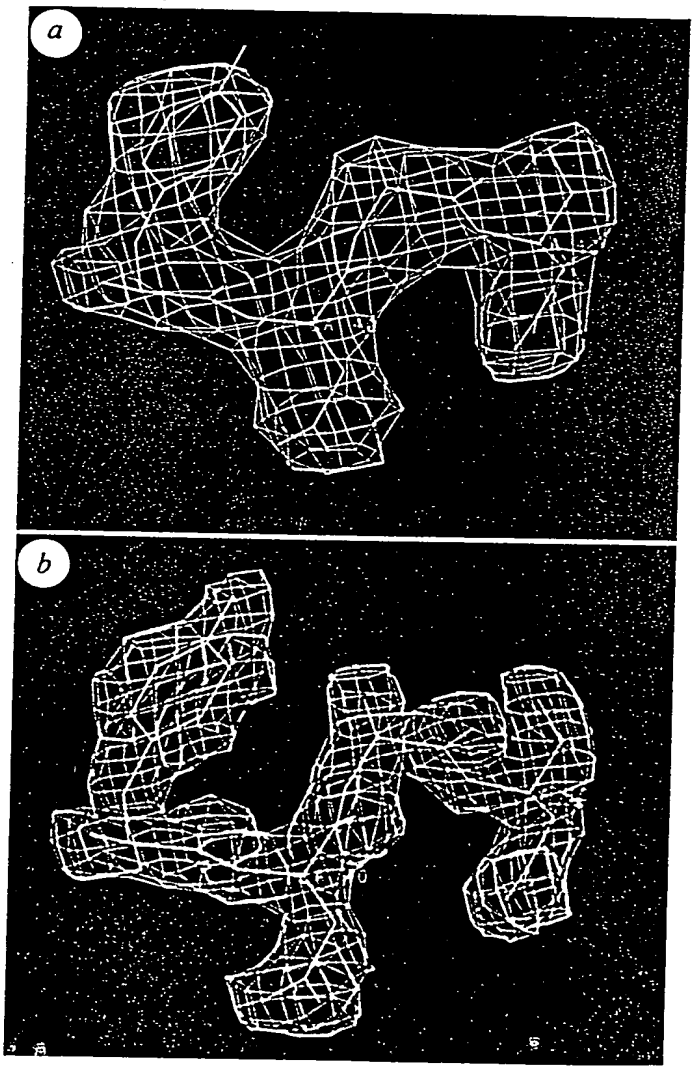

FIG. 3 *a*, Solvent flattened electron density map at 3.4 Å displaying the region Tyr 39 to Asn 42 calculated with the phases derived from the $K_3UO_2F_5$ derivative alone and its anomalous signal. *b*, An equivalent region of the electron density of a $3F_o - 2F_c$ map at 2.2 Å after refinement. Both maps are contoured at 1 r.m.s. above the mean.

78, 109 and 111, as well as Pro 36 and Gly 46 (Fig. 2*c*; numbering as in TGF-β2). All the cysteines are involved in the disulphide pattern of TGF-β2 as well as in the intermolecular disulphide bridge between the monomers. Amino acid 46 in the eight-residue ring has to be a Gly because of steric hindrance and because of the atypical conformation angles ($\phi = 135.1°$, $\psi = 160.9°$). Proline 36 was found to be the only *cis*-Pro in TGF-β2 and is necessary for ending the long loop and continuing in a β-strand. Many of the amino acids involved in the dimer interface are invariant or show conservative changes in most members of the TGF superfamily. We therefore propose the general fold, including the TGF-β knot, of all the proteins of the TGF superfamily to be the same with variations in the loop regions. The five more closely related members of the TGF subfamily (TGF-β1 to TGF-β5) show an overall sequence homology of 64 to 76% (compared to TGF-β2). The residues involved in the helix-sheet interactions or in the hydrogen-bonding network with the water molecules in the interface are invariant or show conservative changes. Of the 29 amino acids of TGF-β2 that are involved in the dimer interface (Fig. 2*b*), 24 are absolutely invariant in all five isoforms. Conservative changes were observed for three positions (residues 43 (Phe to Tyr), 58 (His to Tyr) and 74 (Ala to Ile)), whereas only two amino acids (residues 57 (Gln to Thr) and 68 (Ile to His)) show nonconservative changes. Both variable residues are located in the long α-helix H_3. This might lead to small positional changes of the α-helix H_3 of one subunit and the β-sheet of the other subunit. All other varying residues are found fairly evenly distributed over the whole surface of the dimer. The general fold of all five TGF-β isoforms, including the TGF-β knot, is therefore likely to be the same and only small changes are expected. The fact that heterodimers TGF-β1.2 (refs 1, 16), as well as TGF-β2.3 (ref. 16), have been isolated from natural sources support this proposal.

The first crystal structure of a protein of the TGF superfamily reveals a new fold including a very unusual disulphide pattern, the TGF-β knot. With this information, other three-dimensional structures of TGF isoforms or even of more distantly related proteins could be solved and modelled. Future work must include the analysis of the TGF-β receptor complexes. This will help us understand the biochemical roles of these members of the TGF superfamily and will help in the development of new therapeutic agents, such as for wound healing, bone formation and immune modulation. □

Received 14 May; accepted 17 July 1992.

1. Cheifetz, S. *et al. Cell* **48**, 409–415 (1987).
2. Roberts, A. B. & Sporn, M. B. *Adv. Cancer Res.* **51**, 107–145 (1988).
3. Massagué, J. *A. Rev. Cell Biol.* **6**, 597–641 (1990).
4. Cheifetz, S. & Massagué, J. *J. biol. Chem.* **266**, 20767–20772 (1991).
5. Lin, H. Y., Wang, X.-F., Ng-Eaton, E., Weinberg, R. A. & Lodish, H. F. *Cell* **68**, 775–785 (1992).
6. Cox, D. A., Kunz, S., Cerletti, N., McMaster, G. K. & Bürk, R. R. in *Angiogenesis: Key Principles. Science, Technology, Medicine* (eds Steiner, R., Weisz, B. & Langer, R.) 287–295 (Birkhäuser, Basel, Switzerland, 1992).
7. Joyce, M. E., Roberts, A. B., Sporn, M. B. & Bolander, M. E. *J. Cell Biol.* **110**, 2195–2207 (1990).
8. Wrann, M. *et al. EMBO J.* **6**, 1633–1636 (1987).
9. Mason, A. J. *et al. Nature* **318**, 659–663 (1985).
10. Wozney, J. M. *et al. Science* **242**, 1528–1534 (1988).
11. Wozney, J. M. *Prog. Growth Factor Res.* **1**, 267–280 (1989).
12. Schlunegger, M. P. *et al. FEBS Lett.* **303**, 91–93 (1992).
13. Tamaoki, H. *et al. Prot. Engng.* **4**, 509–518 (1991).
14. Rees, D. C. & Lipscomb, W. N. *Proc. natn. Acad. Sci. U.S.A.* **77**, 4633–4637 (1980).
15. Janin, J. & Wodak, S. *J. molec. Biol.* **125**, 357–386 (1978).
16. Ogawa, Y. *et al. J. biol. Chem.* **267**, 2325–2328 (1992).
17. Wang, X.-F. *et al. Cell* **67**, 797–805 (1991).
18. Messerschmidt, A. & Pflugrath, J. W. *J. appl. Crystallogr.* **20**, 306–315 (1987).
19. Wang, B.-C. *Meth. Enzym.* **115**, 90–112 (1985).
20. Ikeda, T., Lioubin, M. N. & Marquardt, H. *Biochemistry* **26**, 2406–2410 (1987).
21. Jones, T. A. *J. appl. Crystallogr.* **11**, 268–272 (1987).
22. Brünger, A. T., Kuriyan, J. & Karplus, M. *Science* **235**, 458–460 (1987).
23. Tronrud, D. E., Ten Eyck, L. F. & Matthews, B. W. *Acta Crystallogr.* **A43**, 489–451 (1987).
24. Priestle, J. P. *J. appl. Crystallogr.* **21**, 572–576 (1988).
25. Lee, S.-J. *Molec. Endocrin.* **4**, 1034–1040 (1990).
26. Wharton, K. A., Thomson, G. H. & Gelbart, W. M. *Proc. natn. Acad. Sci. U.S.A.* **88**, 9214–9218 (1991).

ACKNOWLEDGEMENTS. We thank J. P. Priestle for discussions during structure determination and critical review of this manuscript, N. Cerletti, D. A. Cox and G. K. McMaster for providing TGF-β2 and for discussions, K. von Meyenburg for encouragement and support for this project, M. Carvajal for technical assistance in the crystallization experiments and F. Winkler for bringing the structure of the potato inhibitor of carboxypeptidase A to our attention. The coordinates will be deposited in the Brookhaven Data Bank.

CORRECTIONS

Cloning of cDNAs for Fanconi's anaemia by functional complementation

Craig A. Strathdee, Hanna Gavish, William R. Shannon & Manuel Buchwald

Nature 356, 763–767 (1992)

WE have discovered that the sequence of our *FACC* gene in Fig. 1*c* is in error. The corrected sequence appears below, starting at position 787 of the cDNA.

GAG	CGA	GTG	GCG	TCC	CTG	TCA	CGA	GTT
E	R	V	A	S	L	S	R	V
TGT	GTC	CCA	CTT	ATT	ACC	CTG	ACA	
C	V	P	L	I	T	L	T	

The change does not alter any of the conclusions of the paper. The length of the open reading frame remains 557 amino acids. No new significant homologies to the cDNA sequence nor to the translated protein were detected in GenBank, EMBL or Swiss-Prot databases, nor were any new functional motifs detected with the corrected sequence. The correct version has been submitted to the EMBL database. The accession number is X66184. We regret any inconvenience caused by this mistake.

A new type of synthetic peptide library for identifying ligand-binding activity

Kit S. Lam, Sydney E. Salmon, Evan M. Hersh, Victor J. Hruby, Wieslaw M. Kazmeierski & Richard J. Knapp

Nature 354, 82–84 (1991)

IN this paper we inadvertently omitted to cite the work of Fu and colleagues (A. Fukura, F. Sebestyen, M. Asgedom, G. Dibo *14th Int. Congr. Biochem.* FR013; 1988), who independently described a similar synthetic method for producing multiple peptide sequences (which we called "split synthesis"). However, Fukura *et al.* did not describe the concept of 'one bead, one peptide' which was central to our approach.

were most probably made by predators. It should be recognized, however, that there is an intergradation between parasitism and predation that is usually not resolvable in the fossil record, and also that a mineralized shell is useful to hold off any attacking organism, whether parasite or predator.

Predator pressure may induce a variety of responsive strategies with great evolutionary potential for differentiation and speciation (*10*). With regard to shell-boring, the best investigated cases concern gastropod predation on bivalves. The main factors in prey selection appear to be the ratio between prey biomass and shell thickness, and the relative size of predator and prey (*22*). Responses by nonmotile prey would thus involve reduction in shell penetrability and modifications of ontogenetic growth (*26, 27*).

The low percentage of bored *Cloudina* is comparable to the generally low levels of shell-boring predation through the Palaeozoic, before the Mesozoic evolution of shell-boring gastropods (*10, 24, 28, 29*). The apparent predator on *Cloudina* selected its prey for size, as do shell-boring gastropods. Due to the secondarily phosphatized preservation of the *Cloudina* walls in our material, the original shell thickness is difficult to measure in specimens isolated from the rock. Thus there are currently no data indicating whether the predator also preferred individuals with a high ratio of biomass to shell thickness. Furthermore, as *Cloudina* is nowhere known to span a substantial stratigraphic interval and no evolutionary ancestors or descendants have been positively identified, there is currently no time frame available in which to study the possible evolutionary effects of early predation.

Nevertheless, the apparent predation on *Cloudina* is highly significant for our understanding of the dramatic biotic events around the Precambrian-Cambrian boundary. First, it would mean that the marine food web already extended to macrophagous predation in the late Precambrian ecosystems. Second, the occurrence of borings, in particular the unsuccessful ones, suggests that at least one function of the first mineralized skeletons was to thwart predators. Third, the possibility of active selection for size by this Precambrian predator indicates a level of neural complexity usually associated with bilaterian animals. Fourth, the evidence fits the prediction of those models of Precambrian-Cambrian evolution that affix a high significance to the appearance of carnivory (and herbivory) both for the origin of mineralized skeletons and for the general ecological diversification. Fifth, we have a possible way to obtain the data necessary for more rigorous testing of such hypotheses in the future.

REFERENCES AND NOTES

1. F. H. T. Rhodes and T. W. Bloxam, *Proceedings of the North American Paleontological Convention* (1971), vol. K, p. 1485.
2. E. T. Degens, *Chem. Geol.* 25, 257 (1979).
3. J. Kaźmierczak, V. Ittekott, E. T. Degens, *Palaeontol. Z.* 59, 15 (1985).
4. J. Kaźmierczak and E. Degens, *Mitt. Geol.-Palaeontol. Inst. Univ. Hamburg* 61, 1 (1986).
5. M. F. Glaessner, *The Dawn of Animal Life. A Biohistorical Study* (Cambridge Univ. Press, Cambridge, 1984), p. 244.
6. J. W. Valentine and D. H. Erwin, *Mar. Biol. Lab. Lect. Biol.* 8, 71 (1987).
7. J. W. Evans, *Compte Rendu de la XI:e Session du Congrès Géologique International (Stockholm 1910), Premier Fascicule* (1912), p. 542.
8. G. E. Hutchinson, in *Oceanography*, M. Sears, Ed. (AAAS, Washington, DC, 1967), p. 85.
9. S. Bengtson, *Acta Univ. Ups. Abstr. Upps. Diss. Fac. Sci.* 415, 71 (1977).
10. G. J. Vermeij, *Evolution and Escalation. An Ecological History of Life* (Princeton Univ. Press, Princeton, NJ, 1987).
11. G. J. Vermeij, *Palaios* 4, 585 (1990).
12. S. Conway Morris, *Am. Sci.* 75, 157 (1987).
13. J. W. Valentine, S. M. Awramik, P. W. Signor, P. M. Sadler, *Evol. Biol.* 25, 279 (1991).
14. S. M. Stanley, *Proc. Natl. Acad. Sci. U.S.A.* 70, 1486 (1973).
15. ———, *Am. J. Sci.* 276, 56 (1976).
16. G. J. B. Germs, *Chamb. Mines Precambr. Res. Unit Bull.* 12, 250 (1972).
17. G. Hahn and H. D. Pflug, *Senckenbergiana Lethaea* 65, 413 (1985).
18. S. Conway Morris, B. W. Mattes, Chen Menge, *Am. J. Sci.* 290A, 245 (1990).
19. S. W. F. Grant, *Am. J. Sci.* 290(A), 261 (1990).
20. Chen Menge, Chen Xianggao, Lao Qiuyuan, *Sci. Geol. Sinica* 1975(2), 181 (1975).
21. Xing Yusheng *et al.*, *Bull. Inst. Geol. Chin. Acad. Geol. Sci. Spec. Issue* 10 (1984).
22. J. A. Kitchell, C. H. Boggs, J. F. Kitchell, J. A. Rice, *Paleobiology* 7, 533 (1981).
23. L. N. Popov, K. K. Khazanovich, N. G. Borovko, S. P. Sergeeva, R. F. Sobolevskaya, *Akad. Nauk SSSR, Min. Geol. SSSR, Mezhvedomstv. Stratigr. Komitet SSSR, Trudy* 18 (1989).
24. A. R. Kabat, *Malacologia* 32, 155 (1990).
25. D. K. Young, *Am. Zool.* 9, 903 (1969).
26. J. A. Kitchell, *3rd North Am. Paleontol. Conv. Proc.* 2, 301 (1982).
27. D. L. DeAngelis, J. A. Kitchell, W. M. Post, *Am. Nat.* 126, 817 (1985).
28. N. F. Sohl, *Am. Zool.* 9, 725 (1969).
29. S. Conway Morris and S. Bengtson, *J. Paleontol.*, in press.

30. We are grateful to S. Conway Morris, S. W. F. Grant, B. Runnegar, P. W. Signor, III, and G. J. Vermeij for constructive comments on the manuscript. Supported by the Swedish Natural Science Research Council and the National Natural Science Foundation of China.

12 March 1992; accepted 1 June 1992

Crystal Structure of Transforming Growth Factor–β2: An Unusual Fold for the Superfamily

Sun Daopin, Karl A. Piez, Yasushi Ogawa, David R. Davies*

The transforming growth factors–β (TGF-β1 through -β5) are a family of homodimeric cytokines that regulate proliferation and function in many cell types. Family members have 66 to 80% sequence identity and nine strictly conserved cysteines. A crystal structure of a member of this family, TGF-β2, has been determined at 2.1 angstrom (Å) resolution and refined to an *R* factor of 0.172. The monomer lacks a well-defined hydrophobic core and displays an unusual elongated nonglobular fold with dimensions of approximately 60 Å by 20 Å by 15 Å. Eight cysteines form four intrachain disulfide bonds, which are clustered in a core region forming a network complementary to the network of hydrogen bonds. The dimer is stabilized by the ninth cysteine, which forms an interchain disulfide bond, and by two identical hydrophobic interfaces. Sequence profile analysis of other members of the TGF-β superfamily, including the activins, inhibins, and several developmental factors, imply that they also adopt the TGF-β fold.

The transforming growth factors–β (TGF-βs) are a family of multifunctional growth and differentiation factors that act on most cell types with activities dependent upon the cell type, stage of proliferation, and environment [for reviews, see (*1–5*)]. Of particular interest are their abilities to stimulate connective tissue synthesis, to suppress proliferation and function of immune cells, to inhibit proliferation of endothelial and other epithelial cells, to stimulate osteogenic activity, and to be chemotactic for monocytes and fibroblasts. Five isoforms that have similar but not identical activities (TGF-β1 to -β5) have been discovered and have 66 to 80% sequence identity (*6–17*).

A larger group of proteins, referred to as the TGF-β superfamily, have ~30% sequence identity to TGF-β1 and seven invariant cysteines [see (*2*)]. They include the activins and inhibins, Mullerian inhibiting substance (MIS), the bone morphogenetic proteins (BMPs), the decapentaplegic (DPP-C) gene complex of *Drosophila*, and the closely homologous *Vg1* and *Vgr-1* genes of *Xenopus* and mouse, respectively.

The TGF-βs are homodimers with molecular masses of ~25,000 daltons. Each

S. Daopin and D. R. Davies, Laboratory of Molecular Biology, National Institute of Diabetes, Digestive and Kidney Diseases, National Institutes of Health, Bethesda, MD 20892.
K. A. Piez, Fogarty International Center, National Institutes of Health, Bethesda, MD 20892.
Y. Ogawa, Celtrix Pharmaceuticals, Inc., 3055 Patrick Henry Drive, Santa Clara, CA 95052.
*To whom correspondence should be addressed.

subunit consists of 112 amino acids, except TGF-β4, which has 114. Heterodimers, designated TGF-β1.2 and TGF-β2.3, are also known to exist in small amounts in certain tissues (*18*, *19*). Each polypeptide chain has nine disulfide-bonded cysteines, which are invariant among the five forms (*19*). The TGF-βs are synthesized in precursor forms of ~400 residues per chain and are secreted as latent complexes, which are activated later by proteolytic processing and dissociation of the latent forms.

We report the three-dimensional (3-D) structure of the mature form of human TGF-β2 determined by x-ray crystallography at 2.1 Å resolution. Sequence comparisons among the members of the superfamily were made by using a profile (*20*, *21*) based on the local environment of the residues in TGF-β2 that enables us to draw conclusions about the putative structures of the other members.

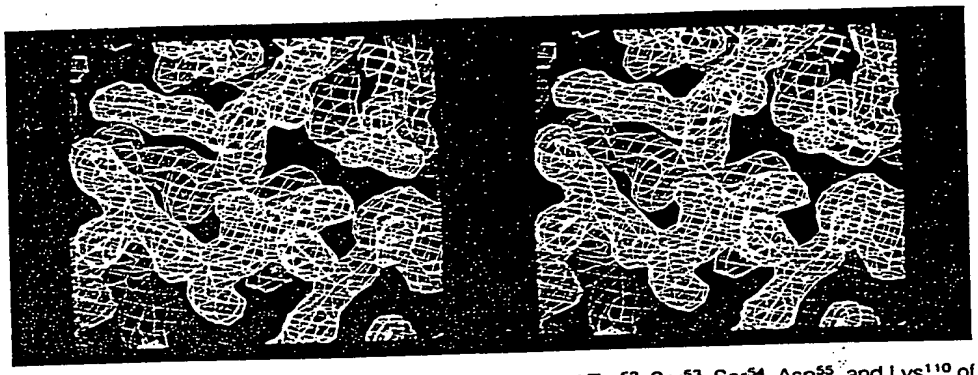

Fig. 1. Stereo pair showing a representative region around Trp^{52}, Ser^{53}, Ser^{54}, Asp^{55}, and Lys^{110} of the refined ($2F_o - F_c$) electron density map contoured at a level corresponding to one σ (standard deviation of the map).

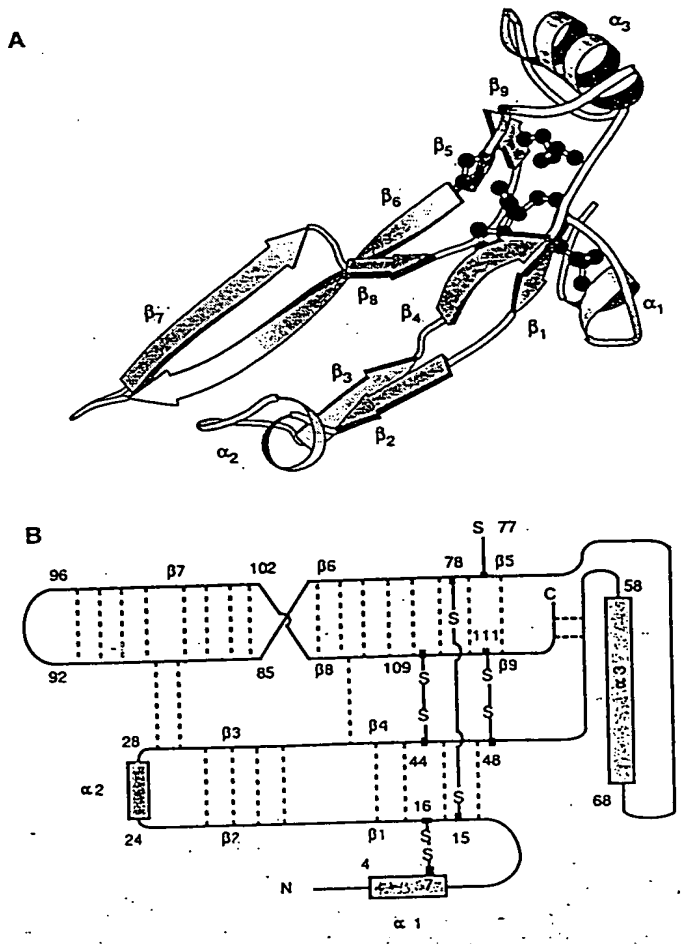

Fig. 2. (A) Topology diagram of a TGF-β2 subunit. The α helices are labeled as α1, α2, and α3 and peptide strands in β sheets are labeled from β1 through β9. The residues involved in the regular secondary structure are: α1, residues 4 to 8; α2, 24 to 28; α3, 58 to 68; β1, 15 to 18; β2, 20 to 23; β3, 37 to 40; β4, 42 to 46; β5, 77 to 80; β6, 82 to 91; β7, 96 to 102; β8, 104 to 106; and β9, 109 to 112. (B) Schematic drawing of the primary and secondary structure of a TGF-β2 subunit. Hydrogen bonds in the β strands and loops are indicated by dashed lines. The analogy to a left hand can be seen. The heel (helix α3) is to the right and the fingers (β strands) are to the left with the third and fourth fingers twisted.

The structure determination is describ... in Table 1. A typical section of the electr... density map ($2F_o - F_c$) with refined pha... is shown in Fig. 1. The 112–amino ac... subunit of TGF-β2 displays a very unus... fold (Figs. 2 and 3). The secondary stru... ture consists largely of short, two-strand... antiparallel β sheets, the longest of whi... extends from residue 82 to 91 and 96 ... 105, in agreement with the secondary stru... ture assignments of TGF-β1 from nucle... magnetic resonance (NMR) data (*22*). There are three α helices in the structur... helix α1, residues 4 to 7; helix α2, residu... 24 to 28, which consist of one turn on... and helix α3, residues 58 to 68, which ... longer. All three helices have also be... observed in TGF-β1 by NMR (*22*). Of th... seven Pro residues, only Pro^{36} adopts the ... peptide configuration. The Ramachandra... plot shows no residues in forbidden region...

The 112-residue subunit has the over... shape of a slightly curled left hand wi... fingers, formed by β strands and loop... extended in pairs (Figs. 2 and 3). Th... three-turn helix α3 forms the heel of th... hand. The amino- and carboxyl-termin... ends are in the same region and are he... tightly to the body of the hand; the t... amino-terminal residues form the thumb ... the hand. The loop at the end of the ma... extended pair of fingers, corresponding ... residues 91 to 96, is poorly defined in th... electron density map. The dimensions ... the subunit are approximately 60 Å by 20 Å by 15 Å. There is no defined hydrophobic core in the subunit as a result of the extended shape of the molecule, suggesting that the only stable form of the molecule in solution is a dimer.

The strictly conserved nine cysteines in the sequence of the TGF-βs suggest an important role in structure and function. In the crystal structure, all nine cysteines form disulfide bonds. Eight form four intrachain disulfide bonds between residues 7 and 16, 15 and 78, 44 and 109, and 48 and 111; one participates in an interchain disulfide bond between residue 77 of one monomer and residue 77 of the other. The four intrachain disulfides form a core (Fig. 3) that is essentially inaccessible to solvent and have very low crystallographic *B* factors. The accessible side chain (Cβ-S-S-Cβ) areas of the four disulfides (7-16, 15-78, 44-109, and 48-111), measured in the dimer, are 0.1, 1.9, 2.4, and 0.8 Å² (*23*), respectively, and the averaged side chain *B* factors are 20.1, 17.2, 18.4, and 17.2 Å², respectively. In contrast, the interchain disulfide is much more exposed and has greater mobility. Its side chain solvent accessible area is 58 Å² and the averaged side chain *B* factor is 3... Å². Consistent with this result, chemical studies have shown that the two subunits can be separated by mild reduction (*18*...

dditional discussion of disulfide bonding ppears below in the context of the superfamily.

The two chains of the dimer are related by a twofold axis going through the middle of the 77-77 disulfide bond (Fig. 4). The interface is made largely of hydrophobic residues. The twofold symmetry results in two identical hydrophobic cores on either side of the interchain disulfide. Helix α3 in one subunit (the heel of the hand) lies against the curved β-sheet area of the other subunit, involving strands β6, β7, and β8 (third and fourth fingers of the hand), parts of strands β2 and β3, and the long loop between β2 and β3 (first and second fingers of the hand). The hydrophobic residues involved in this core packing are Val^{61}, Leu^{62}, Leu^{64}, Tyr^{65}, and Ile^{68} of helix α3 and Ile^{22}, Phe^{24}, Leu^{28}, Trp^{30}, Trp^{32}, Ile^{33}, Phe^{43}, Ile^{88}, Leu^{101}, and Met^{104} of the β-sheet region. The total hydrophobic interface between the subunits (defined as the surface area of carbon and sulfur atoms per subunit removed from solvent contact upon dimerization) was calculated to be 940 $Å^2$ versus the monomer surface area of 6400 $Å^2$ (23). This value corresponds to 19 kcal mol^{-1} of stabilization energy per monomer when a conversion of 20 cal mol^{-1} $Å^{-2}$ is used (24–26).

There are two twofold-related solvent-accessible cavities between the interchain disulfide bridge and the hydrophobic cores in the interface area. Four water molecules were observed in the electron density map to fill each void. It is not clear whether these voids and the accessible interchain disulfide bond have any functional role.

The TGF-β superfamily includes cytokines that share at least 25% sequence identity with TGF-β1 and that have seven invariant cysteines in the amino acid sequence of each chain. Of particular importance is the role of these invariant cysteines in the structure and function of this cytokine superfamily. As mentioned above, among the nine cysteines in the structure of TGF-β2, eight are essentially not accessible to solvent. This result argues strongly that they are important mainly for structural reasons rather than for direct functional reasons. The two cysteines missing in some members are residues 7 and 16, which form a disulfide bond in the amino-terminal region of TGF-β2, where homology with other members of the superfamily is weak. The other disulfides constitute a core structure that is complementary to the hydrogen bond network. As illustrated in Fig. 2B, there are extensive hydrogen bonds between fingers one and two, three, and four, but few between the thumb and finger one, fingers two and three, and fingers one and four. Instead, these adjacent strands that are not extensively joined by hydrogen

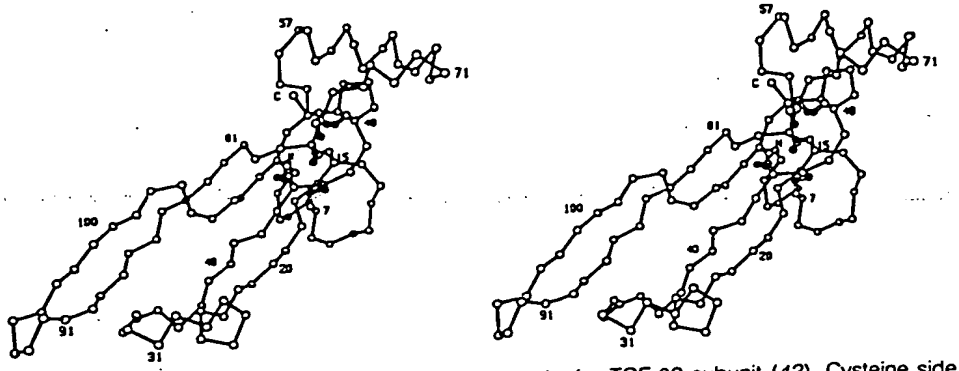

Fig. 3. ORTEP drawing of the Cα backbone (in stereo) of a TGF-β2 subunit (*42*). Cysteine side chains (open bonds and solid spheres for sulfurs) are shown.

Table 1. Structure determination. Crystals were grown by vapor diffusion, by using standard hanging-drop methods (*31*). They belong to space group $P3_221$ with cell dimensions $a = b = 60.7$ Å and $c = 75.3$ Å. With one subunit of TGF-β2 per asymmetric unit, the Matthew's volume, V_m, is 3.2, corresponding to a solvent content of 61%. Both the native and derivative data were collected with a Siemens area detector mounted on a Rigaku rotating-anode x-ray generator and were processed by using the program XDS (*32, 33*). Three derivatives were used. The major binding site of UO_2SO_4 was solved by using the Patterson vector search part of the program PROTEIN. The binding sites of the iodine and mercury derivatives were solved by a cross-Fourier technique by using the major site of UO_2SO_4 as the phasing site. The heavy-atom parameters were refined by using the program PHASIT (*34*). The initial phases were deduced from the multiple isomorphous replacement (MIR) by using the three heavy atom derivatives at 3.2 Å resolution and the single anomalous scattering (SAS) of UO_2SO_4 at 3.5 Å (*35*). The mean figure of merit was 0.68. A slightly improved, solvent-flattened map (*36*) was largely interpretable and allowed 70% of the sequence to be traced by using the graphic program (O) (*37*). A second electron density map was calculated at 2.8 Å resolution by using combined phases from the 3.2 Å MIR, the 3.5 Å SAS, and 2.8 Å single isomorphous replacement of UO_2SO_4, and the partial model phases. This map allowed the entire amino acid sequence, except residues 91 to 96, to be traced. The model was refined with the program package TNT by using all of the reflections between 15 and 2.1 Å resolution for which $F > 2\sigma(F)$ (*38*). The initial refinement included data to 2.8 Å resolution (with the TNT solvent model included) with positional parameters only. The resolution was subsequently increased to 2.4 Å with restrained crystallographic *B* factors and to 2.1 Å with individual isotropic *B* factors. The final model has a crystallographic *R* factor of 0.172 and consists of all 890 protein atoms, including both amino and carboxyl termini, and 32 solvent molecules. The density corresponding to residues 91 to 96 was weak and ill-defined.

Parameter	Native	UO_2SO_4	I_2	Hg_2O
Diffraction data				
Observations (no.)	54,248	11,726	15,886	20,624
Unique reflections (no.)	9,706	4,129	2,793	2,820
Resolution (Å)	2.1	2.8	3.2	3.2
Completeness (%)	87	95	97	99
R_{sym}*	0.047	0.022	0.052	0.089
Phasing statistics				
R_{iso}†		0.14	0.136	0.10
Heavy atom sites		2	7	3
Isomorphous difference (no.)		3,994	2,737	2,722
Anomolous difference (no.)		1,652		
R_{Cullis}‡		0.40	0.48	0.55
Phasing power§		1.9	1.8	1.7
Mean figure of merit at 3.2 Å		0.68		
Mean figure of merit at 2.8 Å		0.69		
Refinement				
Resolution (Å)	15–2.1			
Protein atoms	890			
Water molecules	32			
R factor‖	0.172			
RMS bond length (Å)¶	0.012			
RMS bond angle (degree)	2.3			
RMS planar groups (Å)	0.016			

*$R_{sym} = \Sigma_h\Sigma_i|I(h)_i - \langle I(h)\rangle|/\Sigma_h\Sigma_i I(h)_i$; $I(h)$ is the intensity of reflection h, Σ_h, sum over all reflections, and Σ_i, sum over the *i*th measurement. †$R_{iso} = \Sigma_h|F_{PH} - F_P|/\Sigma_h F_P$; F_P and F_{PH} are the native and derivative structure factor amplitudes, respectively. ‡$R_{Cullis} = \Sigma_h|F_H(obs) - F_H(calc)|/\Sigma_h F_H(obs)$. F_H is the heavy atom structure factor amplitude. §Phasing power = $F_H(calc)/E$ or $2F_H(calc)/E$, for isomorphous and anomalous differences, respectively. *E* is the estimated error. ‖*R* factor = $\Sigma_h|F(obs) - F(calc)|/\Sigma_h F(obs)$. ¶RMS, root-mean-square.

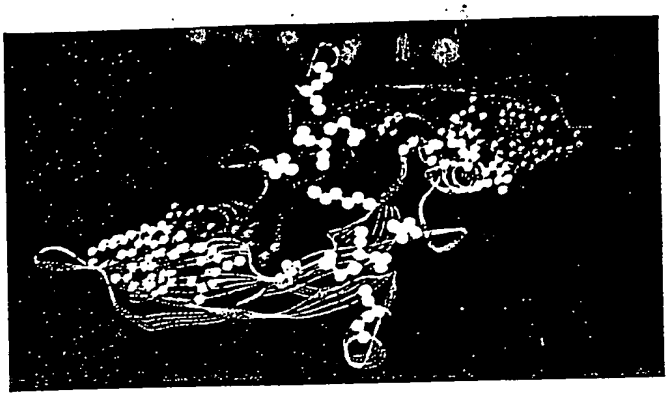

Fig. 4. Ribbon drawing of a dimer of TGF-β2. The two subunits are colored yellow and blue. Shown in white are the cysteine side chains and disulfide bonds. The residues shown in yellow and blue are the hydrophobic residues that form the interface between the two subunits. The twofold axis is at the interchain disulfide bond and perpendicular to the page. The drawing was made with the program Ribbons (*43*).

Table 2. Sequence comparisons and 3-D–1-D profile scores for the TGF-β superfamily. The sequences were first aligned by the GCG program package (*39*). A penalty of −0.1 was applied if a gap or an insertion was in a loop region and −1.0 if it was in an α helix or a β sheet. Included as controls are the variable domains of two mouse immunoglobulin light chains, J539 and McPC603, which are known to have similar structures by x-ray diffraction (*40, 41*). The *Z* scores indicate similarity among TGF-β2 and other TGF-β family members.

Sequence	Source	Length	*Z*	Sequence identity (%)
TGF-β 1 to 5*				
TGF-β2	Human	112	50.5	100
TGF-β1	Human	112	48.5	72
TGF-β3	Human	112	47.6	80
TGF-β4	Chicken	114	51.9	66
TGF-β5	*X. laevis*	112	49.8	66
TGF-β superfamily*				
Inhibin βA	Human	112	21.2	39
Inhibin βB	Human	111	16.7	35
BMP 2	Human	100	21.0	34
BMP 4	Human	104	19.6	35
Vg1	*X. laevis*	109	23.7	36
DPP-C	*Drosophila*	102	20.8	36
MIS	Human	107	12.2	23
Inhibin α	Human	113	6.5	26
Immunoglobulin VL†				
J539	Mouse	107	44.6	100
McPC603	Mouse	114	27.9	55

*The profile deriving sequence is TGF-β2 and the sequence identity is calculated between β2 and each of the superfamily members. †The profile deriving sequence is J539. The structure and sequence of the antibody J539 is obtained from the Brookhaven Data Bank entry 2FBJ and the sequence of McPC603 is obtained from Brookhaven Data Bank entry 1MCP. In both J539 and McPC603 cases, only the light chains of the variable domain are compared.

bonds are linked by disulfides. This core structure (the palm of the hand) can be expected to be common to all of the members of the TGF-β superfamily. The amino-terminal domain, the heel of the hand, and the design of the fingers can be expected to be variable features of the backbone structure among superfamily members.

The members of the superfamily can be further divided into subfamilies, for example, TGF-β1 through -β5, within which there is much greater sequence identity. Model building has shown that the TGF-β1 sequence can be fit to the TGF-β2 backbone without significant distortion of the backbone coordinates. All of the differences are in surface residues, except for residue 58, which is in the hydrophobic interface (His in TGF-β2 and Tyr in TGF-β1), strongly suggesting that the differences in biological activity between these two family members depend on differences in surface side chains rather than in tertiary structure.

A method has recently been proposed that scores the compatibility of amino acid sequences with a known 3-D structure (*20, 21*). We have applied this method to compare the sequences of the proteins in the TGF-β superfamily and scored the compatibility of each individual sequence to the 3-D profile generated from the structure of TGF-β2 (Table 2).

TGF-β1 through -β5 have similar profile scores (Z score), implying similar 3-D structures, which is not surprising since there is ~70% sequence identity among them. The other members of the superfamily share 25 to 40% sequence identity with TGF-β2 (Table 2). The profile analysis shows that most of these proteins cluster with Z values near 20 except for MIS and inhibin α chain, which have lower scores than the rest. This result indicates a close structural similarity between the superfamily members and TGF-β2.

The 3-D structure of TGF-β2, as described here, should provide a rational basis for understanding structure and function of this important cytokine and other members of the family. Of particular importance is the binding of these cytokines to cell-surface receptors. Several receptors present on most cells have been identified [see (*2*)] and two have been cloned (*27, 28*). Different affinity constants have been observed for TGF-β1 and -β2. Recently, receptors that are less ubiquitous but very selective for TGF-β1 or -β2 have been reported (*29*).

Recent studies of a chimeric TGF-β1 and -β2 have shown that differences in specificity can be associated with residues 40 to 82 (*30*). Of the 42 residues, 14 differ between TGF-β1 and -β2 and thus must be responsible for the differences in specific activity mediated by receptors in the endothelial cell growth inhibition assay used. Examination of the structure of TGF-β2 reveals that these residues are mostly located in the heel of the subunit (Fig. 2A). All but one (His[58] to Tyr) are surface residues. Furthermore, they form a surface patch consisting of residues from both subunits in this region of the molecule. It is therefore conceivable that this patch participates in the interaction with receptors. Although the exact binding site is yet to be defined, the structure of TGF-β2 provides a framework upon which further studies of structure-function relations can be based.

REFERENCES AND NOTES

1. M. B. Sporn and A. B. Roberts, in *Peptide Growth Factors and Their Receptors I*, M. B. Sporn and A. B. Roberts, Eds. (Springer-Verlag, New York, 1990), chap. 8.
2. J. Massagué, *Annu. Rev. Cell Biol.* 6, 597 (1990).
3. K. A. Piez and M. B. Sporn, Eds., *Transforming Growth Factor-βs. Chemistry, Biology and Therapeutics, Ann. N.Y. Acad. Sci.* 593 (1990).
4. R. M. Lyons and H. L. Moses, *Eur. J. Biochem.* 187, 467 (1990).
5. M. B. Sporn and A. B. Roberts, *Cell Regul.* 1, 875 (1990).
6. C. A. Frolik, L. L. Dart, C. A. Meyers, D. M. Smith, M. B. Sporn, *Proc. Natl. Acad. Sci. U.S.A.* 80, 3676 (1983).
7. R. K. Assoian, A. Komoriya, C. A. Meyers, D. M. Miller, M. B. Sporn, *J. Biol. Chem.* 258, 7155 (1983).
8. A. B. Roberts *et al.*, *Biochemistry* 22, 5692 (1983).
9. S. M. Seyedin *et al.*, *J. Biol. Chem.* 262, 1946 (1987).
10. S. Cheifetz *et al.*, *Cell* 48, 409 (1987).
11. M. Wrann *et al.*, *EMBO J.* 6, 1633 (1987).
12. S. K. Hanks *et al.*, *Proc. Natl. Acad. Sci. U.S.A.* 85, 79 (1988).
13. P. ten Dijke, P. Hanson, K. K. Iwata, C. Pieler

3. J. G. Foulkes, *ibid.*, p. 4715.
4. R. Derynck *et al.*, *EMBO J.* 7, 3737 (1988).
5. S. B. Jakowlew, P. J. Dillard, P. Kondaiah, M. B. Sporn, A. B. Roberts, *Mol. Endocrinol.* 2, 747 (1988).
6. S. B. Jakowlew, P. J. Dillard, M. B. Sporn, A. B. Roberts, *ibid.*, p. 1186.
7. P. Kondaiah *et al.*, *J. Biol. Chem.* 265, 1089 (1990).
8. Y. Ogawa, D. K. Schmidt, J. R. Dasch, R.-J. Chang, C. B. Glaser, *ibid.* 267, 2325 (1992).
9. Y. Ogawa, personal communication.
10. J. U. Bowie, R. Lüthy, D. Eisenberg, *Science* 253, 164 (1991).
11. R. Lüthy, J. U. Bowie, D. Eisenberg, *Nature* 356, 83 (1992).
12. S. Archer and D. Torchia, personal communication.
13. T. J. Richmond and F. M. Richards, *J. Mol. Biol.* 119, 537 (1978).
14. C. Chothia, *Nature* 248, 338 (1974).
15. M. Matsumura, W. J. Becktel, B. W. Matthews, *ibid.* 334, 406 (1988).
16. A. E. Eriksson *et al.*, *Science* 255, 178 (1992).
17. X.-F. Wang *et al.*, *Cell* 67, 797 (1991).
18. F. Lopéz-Casillas *et al.*, *ibid.*, p. 785.
19. S. Cheifetz and J. Massagué, *J. Biol. Chem.* 266, 20767 (1991).
20. S. W. Qian *et al.*, *Proc. Natl. Acad. Sci. U.S.A.*, in press.
21. Purified mature TGF-β2, a recombinant form expressed in mammalian cells, was provided by Celtrix Pharmaceuticals, Inc. (Santa Clara, CA). The protein was supplied at 40 mg/ml in 0.1% trifluoroacetic acid, 40% acetonitrile, and was diluted four times with 10 mM acetate buffer pH 4.0. Crystals were grown from 10-μl drops consisting of equal parts of the diluted protein solution and well solvent. The well solvent contained 20% PEG 200, 50 mM sodium acetate buffer at pH 4.2 and 30 to 50 mM unbuffered sodium acetate added as precipitant. Typical crystals, measuring 0.5 mm by 0.5 mm by 0.3 mm, grew in about 10 days and diffracted to better than 2.0 Å. Crystals were stabilized with 10% PEG 200, 50 mM buffered sodium acetate at pH 4.2, and 50 mM unbuffered sodium acetate prior to data collection.
32. W. Kabsch, *J. Appl. Crystallogr.* 21, 67 (1988).
33. ———, *ibid.*, p. 916.
34. The program package PHASIT was written and kindly provided by W. Furey.
35. W. A. Hendrickson and E. E. Lattman, *Acta Crystallogr.* B26, 136 (1970).
36. B.-C. Wang, *Methods Enzymol.* 115, 90 (1985).
37. T. A. Jones, J.-Y. Zou, S. W. Cowan, *Acta Crystallogr.* A47, 110 (1991).
38. D. E. Tronrud, L. F. Ten Eyck, B. W. Matthews, *ibid.* A34, 489 (1987).
39. The sequence analysis program package GCG is the product of Genetics Computer Group, University of Wisconsin Biotechnology Center.
40. Y. Satow, G. H. Cohen, E. A. Padlan, D. R. Davies, *J. Mol. Biol.* 190, 593 (1986).
41. T. N. Bhat, E. A. Padlan, D. R. Davies, Brookhaven Protein Data Bank entry 2FBJ.
42. C. K. Johnson, *ORTEP: A Fortran Thermal-Ellipsoid Plot Program For Crystal Structure Illustrations* (Oak Ridge National Laboratory, Oak Ridge, TN, 1970).
43. M. Carson, *J. Mol. Graphics* 5, 103 (1987).

44. We thank D. Eisenberg for kindly providing the 3-D–1-D profile analysis programs and D. Torchia and M. B. Sporn for access to their unpublished results. Part of this work was done while K.A.P. was a Scholar-in-Residence at the Fogarty International Center, National Institutes of Health. The refined coordinates are being deposited in the Brookhaven Protein Data Bank.

22 May 1992; accepted 24 June 1992

Ocean Warming and Sea Level Rise Along the Southwest U.S. Coast

Dean Roemmich

Hydrographic time-series data recorded during the past 42 years in the upper 500 meters off the coast of southern California indicate that temperatures have increased by 0.8°C uniformly in the upper 100 meters and that temperatures have risen significantly to depths of about 300 meters. The effect of warming the surface layer of the ocean and thereby expanding the water column has been to raise sea level by 0.9 ± 0.2 millimeter per year. Tide gauge records along the coast are coherent with steric height and show upward trends in sea level that vary from about 1 to 3 millimeters per year.

Global sea level appears to be rising at a rate of about 2 mm/year (*1*, *2*). A variety of factors may contribute to sea level rise (*3*), including steric expansion of the water as a result of warming, an increase in the mass of water in the oceans as a result of glacial melting, and changes in the shape and volume of the ocean basins. A major step toward predicting future sea level rise and the impact of human activity on sea level is to distinguish the individual factors affecting the present sea level record. Moreover, if sea level rise is indicative of ocean warming, it is critical to determine the vertical distribution of the temperature change. The extent to which warming is concentrated in the surface layer must influence the ultimate impact of climate change on marine life. In this paper, I describe a study of long-term upper-ocean steric change with the use of a comprehensive regional hydrographic time series off California. The study focuses on the distribution of changes in steric height over position, depth, and time, and the relation of these changes to coastal sea level.

Repeated hydrographic and biological sampling along the California coast was initiated in 1950 and continues to the present. Stations in the sampling grid (Fig. 1) are typically 30 to 60 km apart, and the coverage at each station extends to depths of about 500 m in water up to 4 km deep. This survey, the California Cooperative Oceanic Fisheries Investigations (CalCOFI), has been carried out jointly by the state of California, the Scripps Institution of Oceanography, and the National Marine Fisheries Service. During the 1950s CalCOFI cruises were conducted up to ten times per year and coverage was extensive from Oregon to Baja California. The survey has been redefined several times. A serious hiatus in temporal resolution occurred during the 1970s, with only five cruises off southern California from 1969 to 1976. From 1984 to the present, sampling has been carried out quarterly along the six lines from San Diego to Point Conception (Fig. 1). I focus on this region.

CalCOFI Line 90 (Fig. 1) is the most heavily sampled of all the lines, with 170 repetitions. For each transect along Line 90, I interpolated the temperature and salinity data onto an evenly spaced grid with the use of an objective mapping procedure (*4*). I removed seasonal cycles independently at each grid point by subtracting the difference between the average over all cruises during a given month and the average over the 12 months. Nonseasonal residuals showed warming of nearly 1°C in the upper 100 m at all stations; at some stations warming was evident to depths of 300 m or more.

In order to help suppress sampling noise, data from each cruise were averaged horizontally over the highly sampled interval from station 90.35 (50 km offshore) to 90.70 (315 km offshore). For this interval, the vertically integrated effect of the temperature and salinity changes on the height of the sea surface is shown in a time series of steric height (*5*) (Fig. 1). Large positive offsets that occurred during the major El Niño episodes of 1957 to 1958 and 1982 to 1983 are notable in the steric height record. Steric height subsequently decreased after each episode but never fully returned to the pre–El Niño values. The trend in steric height from 1950 to the present shown in Fig. 1 amounts to 0.9 ± 0.2 mm/year. This trend is due to temperature change (Fig. 2B), with no substantial contribution from salinity. Line 93 off San Diego and Line 80 near Point Conception were also well sampled during the 42-year interval (138 and 132 transects); the results from these lines are similar to those from Line 90.

Net changes over the total length of the record are illustrated by averaging over the initial and final 7-year periods, from 1950 to 1956 and 1985 to mid-1991. These two intervals contained no major El Niño episodes. The steric height increase (Fig. 2A) was nearly 3 cm and, within the statistical uncertainty of the estimates, was spatially

Marine Life Research Group, Scripps Institution of Oceanography, La Jolla, CA 92093.

...chemistry and Molecular Biology, Inc. Vol. 267, No. 28, Issue of October 5, pp. 20352-20362, 1992 Printed in U.S.A.

Recombinant Human Osteogenic Protein-1 (hOP-1) Induces New Bone Formation *in Vivo* with a Specific Activity Comparable with Natural Bovine Osteogenic Protein and Stimulates Osteoblast Proliferation and Differentiation *in Vitro**

(Received for publication, April 30, 1992)

T. Kuber Sampath‡, James C. Maliakal, Peter V. Hauschka§¶, William K. Jones, Halina Sasak, Ronald F. Tucker, Kerry H. White, John E. Coughlin, Marjorie M. Tucker, Roy H. L. Pang, Clare Corbett, Engin Özkaynak, Hermann Oppermann, and David C. Rueger

From Creative BioMolecules Inc., Hopkinton, Massachusetts 01748 and the §Children's Hospital and ¶Harvard School of Dental Medicine, Boston, Massachusetts 02115

We reported previously that a 32-36-kDa osteogenic protein purified from bovine bone matrix is composed of dimers of two members of the transforming growth factor (TGF)-β superfamily: the bovine equivalent of human osteogenic protein-1 (OP-1) and bone morphogenetic protein-2a, BMP-2a (BMP-2). In the present study, we produced the recombinant human OP-1 (hOP-1) in mammalian cells as a processed mature disulfide-linked homodimer with an apparent molecular weight of 36,000. Examination of hOP-1 in the rat subcutaneous bone induction model demonstrated that hOP-1 was capable of inducing new bone formation with a specific activity comparable with that exhibited by highly purified bovine osteogenic protein preparations. The half-maximal bone-inducing activity of hOP-1 in combination with a rat collagen matrix preparation was 50-100 ng/25 mg of matrix as determined by the calcium content of day 12 implants. Evaluation of hOP-1 effects on cell growth and collagen synthesis in rat osteoblast-enriched bone cell cultures showed that both cell proliferation and collagen synthesis were stimulated in a dose-dependent manner and increased 3-fold in response to 40 ng of hOP-1/ml. Examination of the expression of markers characteristic of the osteoblast phenotype showed that hOP-1 specifically stimulated the induction of alkaline phosphatase (4-fold increase at 40 ng of hOP-1/ml), parathyroid hormone-mediated intracellular cAMP production (4-fold increase at 40 ng of hOP-1/ml), and osteocalcin synthesis (5-fold increase at 25 ng of hOP-1/ml). In long-term (11-17 day) cultures of osteoblasts in the presence of β-glycerophosphate and L(+)-ascorbate, hOP-1 markedly increased the rate of mineralization as measured by the number of mineral nodules per well (20-fold increase at 20 ng of hOP-1/ml). Direct comparison of TGF-β1 and hOP-1 in these bone cell cultures indicated that, although both hOP-1 and TGF-β1 promoted cell proliferation and collagen synthesis, only hOP-1 was effective in specifically stimulating markers of the osteoblast phenotype.

Demineralized bone matrix when implanted in non-bony sites in rats induces a sequence of cellular events leading to the formation of new bone and bone marrow (1, 2). The finding that the bone-inducing activity elicited by demineralized bone matrix could be dissociated into a soluble component and assayed by implanting with an appropriate collagenous matrix carrier in rats (3) permitted the isolation of several osteogenic proteins (OPs),[1] also called bone morphogenetic proteins (BMPs) (4-7). The subsequent isolation of the genes encoding these proteins from human cDNA libraries identified a family of proteins, including BMP-2 through BMP-6, and osteogenic protein OP-1 (also referred to as BMP-7) (8-10). The predicted amino acid sequences of the proteins indicated that all are members of the TGF-β superfamily sharing a high degree of homology within the COOH-terminal 7 cysteine domain (11).

After purification and characterization, the 32-36-kDa bovine bone-derived osteogenic protein was found to be composed of disulfide-linked dimers of 18- and 16-kDa polypeptides (7); whether these exist exclusively as homodimers *in vivo* has not been established. Amino acid sequence data obtained from the proteolytically digested 18- and 16-kDa subunits indicate that the 18-kDa subunit is the bovine equivalent of mature human OP-1, whereas the 16-kDa subunit is the bovine equivalent of mature BMP-2. Recently, it was reported that homodimers of recombinant BMP-2 are capable of inducing bone when implanted with a collagenous matrix in rats (12) with a reported specific activity that was lower than that of naturally purified bovine bone inductive protein preparations.

A number of well known growth factors have been isolated and characterized from bone matrix extracts and from media conditioned by bone cells and bone organ cultures (13-19). They include: insulin-like growth factors I and II, transforming growth factors β1 and β2, acidic and basic fibroblast growth factors, platelet-derived growth factor, and hematopoietic factors. The synthesis and action of these local factors are in turn modulated by systemic factors, *e.g.* growth hormone, parathyroid hormone, and vitamin D (19). These peptide growth factors are stored in bone and possibly released during bone remodeling. While they may play a critical role in the coupling of bone formation to bone resorption (21, 22), they have not been shown to induce new bone formation in the rat subcutaneous bone induction model (4). The newly identified family of osteogenic proteins isolated from bone matrix, on the other hand, are capable of inducing the commitment of stem cells to differentiate into osteoblastic cell lineages both *in vivo* (5-7) and *in vitro* (23-28). The action of these osteogenic proteins on bone cell cultures has been reported (23-28). Natural preparations of osteogenin (BMP-3), purified from bovine bone matrix, have been shown to stimulate chondrogenic and osteogenic phenotypes in culture (23, 24). Recombinant human BMP-2 induces the maturation of osteoblast precursor cells into osteoblast-like cells, although it has not been shown to have an effect on established osteoblast-like cells in culture (25-27). A recent study with recombinant BMP-4 (BMP-2b), a gene product closely related to BMP-2, showed that this protein is capable of stimulating DNA and collagen synthesis, as well as alkaline phosphatase activity in rat osteoblast-enriched cultures (28).

This report describes the characterization of purified recombinant hOP-1 and demonstrates that the recombinant human OP-1 is able to induce new bone formation in the rat subcutaneous assay with a specific activity that is comparable with highly purified bovine OP preparations and to promote cell proliferation and collagen synthesis of osteoblasts in culture. In addition, hOP-1 is shown to be effective in specifically stimulating markers characteristic of the osteoblast phenotype, *e.g.* alkaline phosphatase, osteocalcin, PTH-mediated cAMP, and deposition of mineralized nodules.

MATERIALS AND METHODS

Expression of hOP-1—The full-length hOP-1 cDNA was expressed in mammalian cells.[2] Briefly, the cDNA was inserted into a mammalian expression vector containing the amplifiable DHFR gene and stably transfected into dhfr(−) Chinese hamster ovary (CHO) cells. After methotrexate-mediated gene amplification, a cell line was selected, cultured in roller bottles or cell factories, and the conditioned media collected periodically. Alternatively, the cDNA was inserted into a mammalian expression vector containing the neomycin selective marker and the SV40 origin of replication and transfected into the BSC-1 ts58 cell line. BSC-1 is a modified monkey kidney-derived cell line that contains ts58, a temperature-sensitive mutant of the SV40 T-antigen (29). At 39 °C, the ts58 antigen is not active, whereas a temperature shift to 33 °C results in the expression of active T-antigen and the subsequent expression of appropriately transfected genes. The clones for BSC cells were selected by resistance to the drug G418 and subcultured.

Purification of hOP-1—During purification, the recombinant hOP-1 protein was detected by Western blot analysis using hOP-1 antisera. hOP-1 was purified from conditioned medium using three chromatography steps: S-Sepharose, phenyl-Sepharose (Pharmacia LKB Biotechnology Inc.), and reverse phase HPLC (C18 Vydac). A typical purification of hOP-1 utilized 2 liters of conditioned medium containing 0.5% fetal calf serum. The medium was diluted with 2 volumes of 9 M urea, 20 mM HEPES, pH 7.0 and applied to a 100-ml column of S-Sepharose equilibrated with 6 M urea, 20 mM HEPES, pH 7.0, containing 50 mM NaCl. After washing with equilibration buffer, step elution of bound protein was accomplished with the same buffer containing 100 and 300 mM NaCl. The 300 mM NaCl fraction was made 1.0 M in ammonium sulfate and applied to a 10-ml column of phenyl-Sepharose, pre-equilibrated with 6 M urea, 1.0 M ammonium sulfate, 0.3 M NaCl, 20 mM HEPES, pH 7.0. After washing with the equilibration buffer, the column was step-eluted with the same buffer containing 0.6 and 0 M ammonium sulfate. The protein eluted with 0 M ammonium sulfate was then sequentially dialyzed against water and 30% acetonitrile, 0.1% trifluoroacetic acid, and finally subjected to C18 reverse phase HPLC as described previously (7). Fractions containing hOP-1, as determined by immunoblot analysis and by Coomassie staining, were pooled. The purity of the hOP-1 was determined by gel scanning densitometry.

In Vivo Assay of hOP-1—Purified bovine OP (7), or recombinant human OP-1, in varying concentrations was combined with rat collagen carrier in 50% acetonitrile, 0.1% trifluoroacetic acid, lyophilized as described previously (7) and implanted in a subcutaneous site in the thorax region of 28-35-day-old male Long-Evans rats. Briefly, 25 mg of demineralized and 4 M guanidine HCl extracted rat bone matrix (rat collagen carrier) was added to osteogenic protein dissolved in 200 μl of 50% acetonitrile, 0.1% trifluoroacetic acid, mixed, and then lyophilized. The response exhibited by intact demineralized diaphyseal rat bone matrix (particle size 74-420 μm, 25 mg) was used as the maximal bone-forming activity and compared with the activity exhibited by bovine OP and recombinant hOP-1 containing implants. Rat bone collagen carrier was used alone as the negative control. The day of implantation was designated as day 0 of the assay. Implants were removed on days 5, 7, 9, 12, 14, and 21 for evaluation. Bone-forming activity in the implants was monitored by the specific activity of alkaline phosphatase, calcium content, and histological evaluation. The specific activity of alkaline phosphatase and the calcium content of the 0.5 M HCl-soluble fraction of the sediment were determined as described previously (2). For histological examination, implants were fixed in Bouin's Solution, embedded in JB4 plastic medium, cut into 1-μm sections, and stained by toluidine blue (American HistoLab, Gaithersburg, MD). The specific bone-forming activity was determined by analysis of the calcium content of day 12 implants and expressed as the amount of protein required to exhibit half maximal bone-forming activity, as compared with the bone-forming activity of the demineralized rat bone matrix implants.

Cell Cultures—Primary cultures of rat calvarial cells were obtained from 1-2-day-old CD and Long-Evans strain rats (Charles River Laboratories, Wilmington, MA) by sequential collagenase digestion essentially following the methods described by Wong and Cohn (30). Briefly, six sequential 20-min digests were performed on fetus-free calvarial fragments at 37 °C in phosphate-buffered saline containing collagenase CLS-2 (2 mg/ml) (Worthington, Freehold, NJ). Single-cell suspensions were obtained at each digest interval and numbered as individual populations 1-6 and were pooled as populations 1-2, 3-5, and 6. The cells were plated in 24-multiwell plates (Falcon Labware, Lincoln Park, NJ) or 48-well tissue culture plates (Coster Corp, Cambridge, MA) at varying cell densities as described in the text in α-MEM (GIBCO) containing 10% fetal bovine serum (FBS, Hyclone Laboratories, Logan, UT) with L-glutamine and antibiotics (100 units/ml penicillin and 100 μg/ml streptomycin). After culturing at 37 °C, 5% CO_2, and 88% humidity for 3-5 days without changing the medium, and after achieving a density of approximately 5×10^4 cells/cm^2, the medium was replaced with serum-free medium for 24 h prior to the addition of hOP-1 or TGF-β1 (R & D Systems, Minneapolis, MN).

To evaluate the effect of hOP-1 on osteocalcin synthesis and the mineralization process, the medium was supplemented with 10% FBS. On day 2, cells were fed with fresh medium supplemented with fresh 10 mM β-glycerophosphate (Sigma). Beginning on day 5 and at twice weekly intervals, the cells were fed with a complete mineralization medium containing all of the above components plus fresh L(+)-ascorbate at a final concentration of 50 μg/ml. Purified hOP-1, stored at −20 °C in 50% acetonitrile (or 50% ethanol) containing 0.1% trifluoroacetic acid, was added to tissue culture wells directly at ≤5 μl/ml of medium with thorough mixing. Control wells received the solvent vehicle only. After refeeding, each conditioned medium sample was diluted 1:1 in radioimmunoassay buffer containing protease inhibitors (31), which was stored at −20 °C until assayed for osteocalcin.

Cell Growth—The effect of hOP-1 on osteoblast cultures was examined by determining the rate of [^{3}H]thymidine incorporation into total acid-insoluble DNA and cell number. DNA synthesis rates were determined in triplicate cultures after 24 h of hOP-1 treatment by adding [*methyl*-^{3}H]thymidine (2 μCi/ml, 80 Ci/mmol; Du Pont-New England Nuclear) for 6 h before the termination of the culture. Incorporation was terminated by aspiration of the medium, and after washing three times with phosphate-buffered saline, the trichloroacetic acid (10%)-precipitated radioactive DNA was extracted with 1.0% (w/v) sodium dodecyl sulfate, 0.1 M NaOH and quantitated by liquid scintillation counting. For cell number determination, 1×10^5 cells were plated in T-25 flasks (Falcon Labware, Lincoln Park, NJ)

* This work was supported in part by National Institutes of Health Grant AR 38349 (to P. V. H.). The costs of publication of this article were defrayed in part by the payment of page charges. This article must therefore be hereby marked "*advertisement*" in accordance with 18 U.S.C. Section 1734 solely to indicate this fact.

‡ To whom correspondence should be addressed: Creative BioMolecules, 35 South St., Hopkinton, MA 01748. Tel.: 508-435-9001; Fax: 508-435-6951.

[1] The abbreviations used are: OP, osteogenic protein; hOP, bovine osteogenic protein; hOP, human osteogenic protein; BMP, bone morphogenetic protein; TGF, transforming growth factor; PTH, parathyroid hormone; CHO, Chinese hamster ovary; HPLC, high performance liquid chromatography; HEPES, 4-(2-hydroxyethyl)-1-piperazineethanesulfonic acid; MEM, minimum Eagle's medium; FBS, fetal bovine serum; SDS-PAGE, sodium dodecyl sulfate-polyacrylamide gel electrophoresis; IGF, insulin-like growth factor; FGF, fibroblast growth factor.

[2] H. Oppermann, W. K. Jones, J. C. Maliakal, H. Sasak, E. Özkaynak, T. K. Sampath, D. C. Rueger, and R. H. L. Pang, unpublished data.

α-MEM containing 10% FBS, and after 24 h the growth medium was replaced with serum-free medium containing various concentrations of hOP-1. For comparison, control cultures received fresh 10% FBS. Triplicate cultures were harvested every 24 h for the duration of 7 days, and the cell number was determined by counting of the cells released by trypsin digestion (GIBCO) in a fixed volume hemacytometer.

Collagen Synthesis—The rate of collagenous and noncollagenous protein synthesis was measured in osteoblast-enriched cultures by pulse labeling with 25 μCi/ml [2,4-^{3}H]proline (0.2–0.5 Ci/mmol, Du Pont-New England Nuclear) for the last 6 h of culture. Various concentrations of growth factors were added to confluent cultures (in triplicate) in 24-well plates containing serum-free medium. Following incubation, the cell layers were lysed by three freeze thaw cycles and extracted with 1 M NaCl, Tris-HCl buffer, pH 7.4, containing 10 mM *N*-ethylmaleimide, 250 nM EDTA, and 0.2 mM phenylmethylsulfonyl fluoride. Proteins from both cell culture medium and cell lysates were precipitated with 10% trichloroacetic acid and chilled; pellets were washed with acetone:ether (3:1 v/v), dried, resolubilized in 0.5 M acetic acid, and neutralized with NaOH. The amount of [^{3}H]proline incorporated into collagenase-digestible protein and nondigestible noncollagenous protein was determined as described by Peterkofsky and Diegelmann (32). The percent collagen synthesis was calculated after correcting for the relative abundance of proline in collagenase-digestible protein (multiplying the values of noncollagenous proteins by 5.4).

Alkaline Phosphatase Activity—Alkaline phosphatase activity in cultured cells was determined by the method of Reddi and Huggins (2). Following removal of culture medium, cell layers were subjected to three freeze/thaw cycles and sonicated in 200 μl of assay buffer (0.15 M NaCl, 3 mM $NaHCO_3$, pH 7.4, containing 0.1% Triton X-100). Recovered samples (10 μl) were assayed for enzyme activity in 96-well plates with *p*-nitrophenyl phosphate (Sigma) as a substrate in glycine-NaOH buffer, pH 9.3, in a total volume of 100 μl; after 30 min at 37 °C the reaction was stopped with 100 μl of 0.1 M NaOH and absorbance was measured at 400 nm on a Dynatech MR700 plate reader with *p*-nitrophenol as a standard. Results are presented in units/μg of protein, where 1 unit = 1 nmol of *p*-nitrophenol liberated per 30 min at 37 °C.

3′,5′ cAMP Production in Response to PTH—To determine the cAMP production in the presence of PTH, cells were preincubated for 20 min with α-MEM containing 0.5% bovine serum albumin and 1 mM 3-isobutyl-1-methylxanthine (Sigma), and then 200 ng/ml of human PTH(1–34) (Sigma) was added and incubation continued for 8 min. The cell layers were solubilized in 0.1% Triton X-100, and the concentration of cAMP in the cell layer was determined using a cAMP assay kit (Amersham).

Osteocalcin Radioimmunoassay—Rat osteocalcin levels in the cell culture supernatant and cell-associated extracellular matrix were determined by a 3-day nonequilibrium radioimmunoassay as described previously (31), employing goat anti-rat osteocalcin (first antibody) and donkey anti-goat IgG (second antibody). Data are reported as nanograms of osteocalcin/ml of medium or as total nanograms of osteocalcin/culture. Osteocalcin associated with the extracellular matrix was detected by extracting washed cell layers with 0.5 ml of 0.5 M EDTA containing protease inhibitors (31).

Histochemical Analysis—Cell layers were rinsed with cold 0.9% NaCl, fixed in fresh 4% paraformaldehyde at 23 °C for 10 min, and stained for endogenous alkaline phosphatase at pH 9.5 for 10 min using the commercially available kit (Sigma). Purple-stained wells were then dehydrated with methanol and air-dried. Mineralization was determined by a modified von Kossa staining technique on fixed cell layers. After a 30-min incubation with 3% $AgNO_3$ in the dark, H_2O rinsed samples were exposed for 30 s to 254-nm UV light (Fotodyne) to develop the black silver-stained calcium phosphate nodules. Individual mineralized foci (≥20 μm) were counted under a dissecting microscope and expressed as nodules/culture.

hOP-1 Antibody—The cDNA clone that encodes the COOH-terminal conserved 7-cysteine region (TGF-β-like domain) of the hOP-1 gene (9) (amino acids 324–431, approximately 12.5 kDa) was expressed as fusion proteins in *Escherichia coli* (33). The OP-1 fusion proteins, which were produced intracellularly as inclusion bodies, were solubilized and cleaved using mild acid to release the leader peptide. Following renaturation and purification, the hOP-1 polypeptide was used to raise polyclonal antibodies in rabbits. Antisera were tested for reactivity to nonreduced and reduced bovine OP by immunoblot analysis.

Analytical Methods—Protein fractions were characterized by SDS-PAGE on 15% minigels (0.5 mm thick) with a 3% stacking gel (7). Samples dissolved in Laemmli sample buffer were heated in boiling water for 3 min with or without dithiothreitol (100 mM) prior to electrophoresis. For Western blot analysis, samples subjected to SDS-PAGE were transferred to immobilon (Millipore Corp.) and reacted with specific anti-OP-1 rabbit sera and subsequently with goat anti-rabbit linked to peroxidase. To examine the presence of carbohydrate on hOP-1, immobilon-transferred proteins were blotted with concanavalin A linked to peroxidase (34). Amino acid sequence analysis was performed using an Applied Biosystems Protein/Peptide Sequencer (model 470A) as described (7). hOP-1 concentration was determined by HPLC, based on the absorbance of the hOP-1 peak at 214 nm in reference to a known amount of a hOP-1 standard, which had been previously quantitated by amino acid analysis.

RESULTS

Recombinant hOP-1—The full-length hOP-1 cDNA clone encoding the hOP-1 precursor, including the signal sequence, was expressed in mammalian cells in order to obtain correctly processed and fully active protein. Cell clones expressing hOP-1 were selected on the basis of Northern hybridization and Western blot analysis, using hOP-1-specific probes and antisera. Purification of hOP-1 from either BSC- or CHO-conditioned medium yielded preparations of processed mature hOP-1 that were greater than 90% pure. Fig. 1 shows immunoblotted and Coomassie-stained aliquots of the purified preparations of hOP-1 after SDS-PAGE. The CHO hOP-1 showed four to five major dimer bands in the 34–38-kDa range, which migrated as two major bands of 19 and 17 kDa, as well as a minor band of 23 kDa upon reduction. The BSC hOP-1 migrated as a dimer of approximately 36 kDa, which after reduction migrated at approximately 18 kDa. In some preparations, the reduced CHO hOP-1 and BSC hOP-1 samples showed degradation products in varying amounts that migrated at 15–16 kDa (data not shown).

The hOP-1 precursor contains 431 amino acids and is approximately three times larger than the mature hOP-1 (Fig. 2*A*). The processing site for the mature protein was identified by NH_2-terminal amino acid sequencing of the mature hOP-1 and is located following arginine residue 292. Amino-terminal sequence analysis of the hOP-1 CHO-sourced 23-, 19-, and 17-kDa species and the BSC-sourced 18-kDa species demonstrated that each possessed the same NH_2-terminal sequence Ser-Thr-Gly-Ser-. The COOH terminus of each species was intact as determined by *in situ* cyanogen bromide digestion and subsequent sequence analysis. Apparent degradation products migrating at approximately 15 kDa in some CHO hOP-1 preparations displayed four NH_2-terminal sequences corresponding to subunits with 119, 117, 116, and 114 amino acids of mature OP-1, whereas the 16-kDa degradation product of BSC hOP-1 preparations presented two NH_2-terminal sequences corresponding to subunits with 116 and 114 amino acids (Fig. 2*B*).

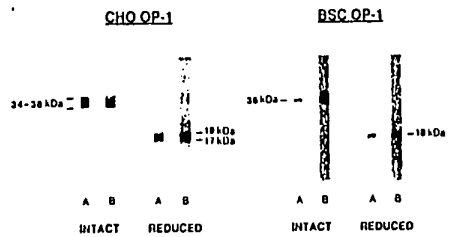

FIG. 1. SDS-PAGE and immunoblot analysis of the purified mammalian cell produced human OP-1. Lanes designated as *A* are immunoblots and lanes designated as *B* are Coomassie-stained. These OP-1 preparations were 90% pure, as determined by gel-scanning methods. Approximately 0.05 μg of OP-1 was used for immunoblots, and 0.5 μg of OP-1 was used for Coomassie staining.

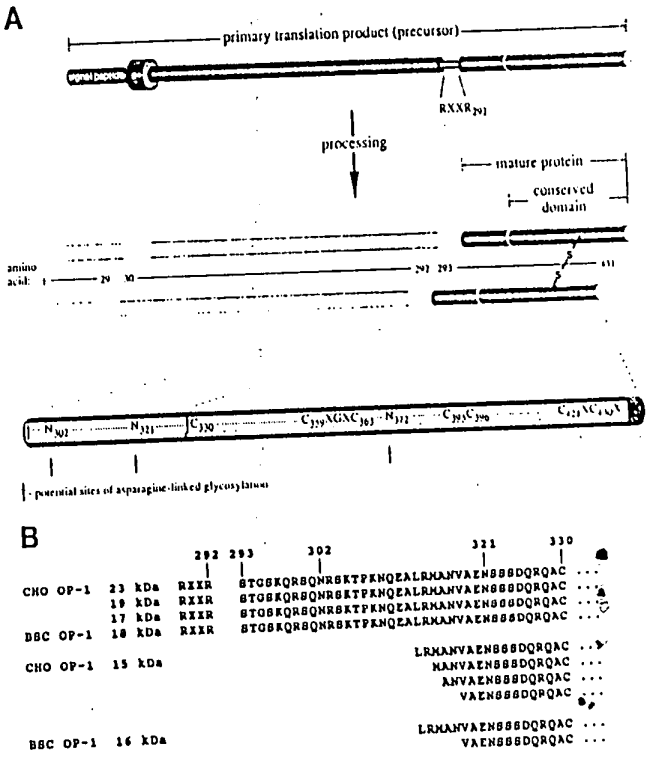

FIG. 2. *A*, structure of hOP-1. *B*, NH_2 terminus of CHO- and BSC-produced hOP-1 subunits.

Both the dimers and subunits of the mammalian expressed hOP-1 bound concanavalin A after SDS-PAGE and transfer to immobilon (data not shown). Identical NH_2-terminal sequences and the fact that the CHO hOP-1 and BSC hOP-1 subunits are reduced to a 14-kDa subunit after digestion with *N*-glycanase support the hypothesis that the apparent molecular weight differences of the CHO produced hOP-1 species are related to differences in glycosylation. Mature hOP-1 has three potential *N*-linked glycosylation sites at residues 302 (*N*-R-S), 321 (*N*-S-S), and 372 (*N*-S-T). Two of the three potential glycosylation sites are within the NH_2-terminal region and the third is within the TGF-β domain (conserved 7 cysteine) region. Amino acid sequence analysis indicated that the glycosylation site at residue 372 in the TGF-β domain region is heavily or completely glycosylated, whereas the other two sites do not appear to be glycosylated to any measurable degree.

Bone-inducing Activity—The purified recombinant hOP-1 in combination with rat collagen as a carrier induced new bone formation *in vivo* as determined by histological examination of subcutaneous implants in the rat. Rat collagen carrier implants without hOP-1 did not show any sign of bone formation (Fig. 3*A*). In the rat subcutaneous implant assay, the bone collagen matrix carrier serves as a scaffold for the attachment and proliferation of mesenchymal cells which, in response to hOP-1, differentiate to form new bone at the implant site. In the absence of hOP-1 the collagen carrier implants contained mesenchymal cells and formed fibrous tissue which was slowly resorbed. On days 5–7, hOP-1 implants showed numerous chondrocytes in the implanted matrix (Fig. 3*B*). The degree of response was dependent on the dose of hOP-1 in that higher concentrations of protein elicited a more uniform response throughout the implant. Fig. 3*C* shows that day 9 implants exhibited calcification of cartilage and vascularization in the region of hypertrophied chondrocytes. Also, new bone formation was seen in apposition to calcified and cartilaginous matrix and basophilic osteoblasts surrounded the vascular endothelium. With higher doses of hOP-1, signs of remodeling were already apparent at day 9 as indicated by the presence of multinucleated osteoclasts. Although the implant predominantly induced endochondral bone, some intramembranous bone was seen at the outer surface of the implant (Fig. 3*D*). By day 12, chondrolysis was almost complete in that the implanted bone matrix was extensively resorbed and replaced by remodeled bone (Fig. 3*E*). Abundant osteocytes were seen surrounding the newly formed extracellular bone matrix (osteoid), and signs of hemopoiesis were apparent in the implant. Implants containing high doses of OP-1 showed evidence of further remodeling and recruitment of bone marrow elements. At 21 days, the carrier was almost completely resorbed and replaced with ossicles filled

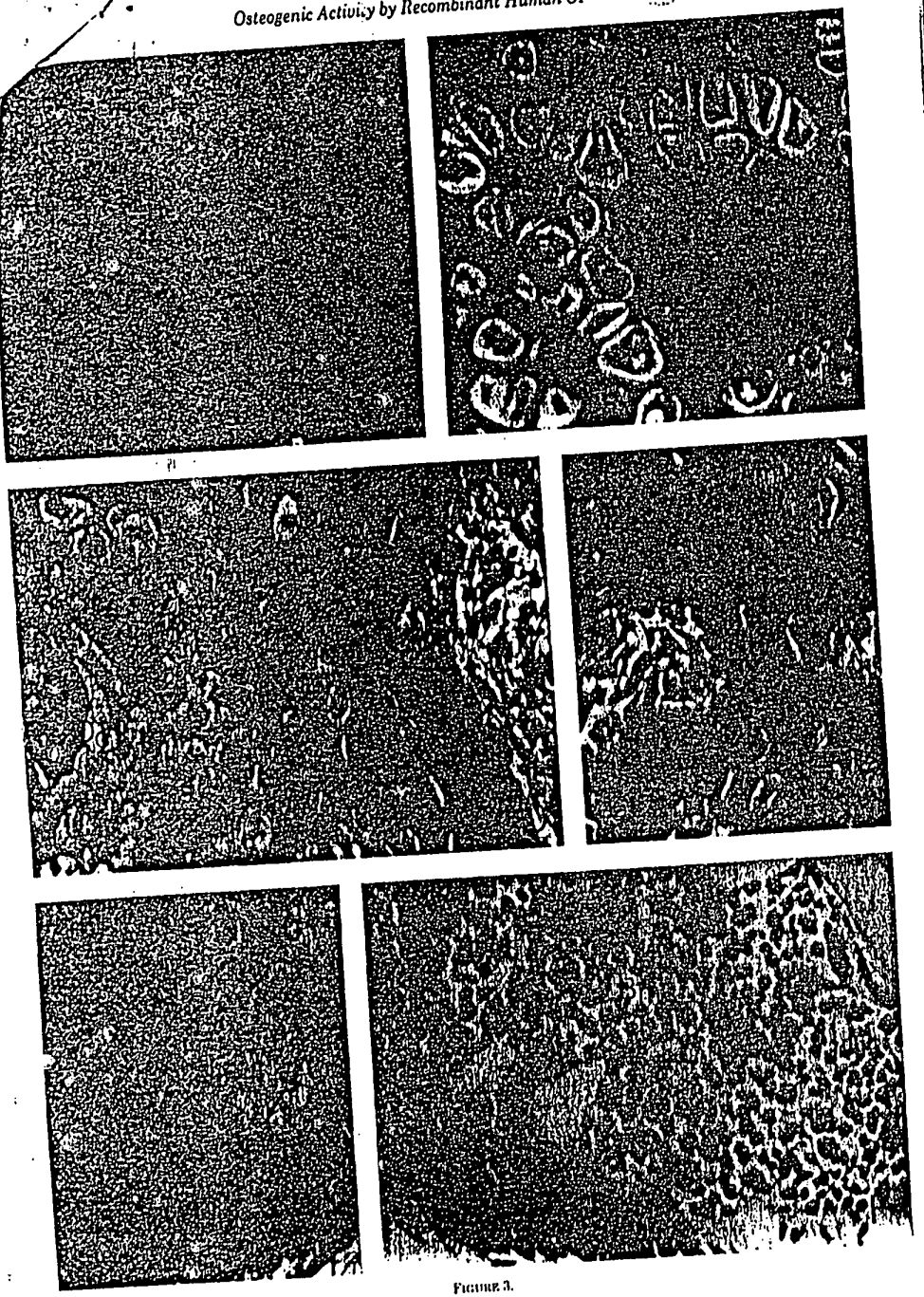

FIGURE 3.

with numerous bone marrow elements, including erythrocytic, granulocytic, and megakaryocytic cell lineages (Fig. 3F). Throughout the differentiation process the size of the newly formed bone was dependent upon the volume of the initial implant.

The bone-forming activity elicited by recombinant hOP-1 was monitored by alkaline phosphatase specific activity and quantitated by the calcium content of day 12 implants. Various quantities of hOP-1 protein (in nanograms) were used to develop a dose curve, and the hOP-1 bone-inducing activity was found to be reproducible and dose-dependent. Fig. 4*A* compares the specific activities of CHO and BSC cell-derived hOP-1 preparations to that of a highly purified natural bovine osteogenic protein preparation. The specific bone-forming activity of CHO hOP-1, as defined by the amount of protein required to exhibit half-maximal bone-inducing activity when compared with the activity of intact demineralized bone powder, was approximately 50–100 ng/25 mg of matrix implant. Control protein (mock) preparations from cells lacking the OP-1 expression vector obtained under identical conditions were not active. A broad range of doses including high concentrations of hOP-1 (0.025–50 μg/25 mg of matrix) were employed in order to evaluate the maximal bone-inducing activity of hOP-1 in the rat subcutaneous assay. Fig. 4*B* clearly illustrates the dependence of bone formation on the dose of hOP-1, as measured by the calcium content of day 12 implants. Bone formation plateaued at approximately 1 μg of hOP-1/25 mg of rat matrix. The bone-inducing activity exhibited by 1 μg of hOP-1/25 mg of matrix is approximately four times greater than that exhibited by the intact demineralized bone matrix. Evaluation of CHO hOP-1 preparations that contained predominantly the degraded dimer species (migrating at 15–16 kDa on SDS-PAGE under reducing condition) indicated that the bone-forming potential of these NH$_2$-terminally truncated forms of OP-1 were equivalent to that of intact mature OP-1 (data not shown).

Cell Proliferation—To evaluate the effect of hOP-1 on osteoblasts, we employed osteoblast-enriched primary cultures prepared through sequential collagenase digestions of newborn suture-free rat calvaria. Although these cultures have a heterogenous population of osteoblasts at various stages of differentiation (including preosteoblasts, lining cells, osteoblasts, and osteocytes), they are a standard model (30, 35) and are known to express phenotype characteristics of osteoblasts, including high levels of alkaline phosphatase, synthesis of type I collagen without type III collagen, secretion of osteocalcin into the medium, increased intracellular cAMP production in response to PTH, and the capacity to mineralize in long term culture (39–42). The osteoblast-enriched cultures used in our studies express these properties, and it is generally believed that these cultures are metabolically and functionally more representative of osteoblasts present in bone than are the established osteoblast-like osteosarcoma-derived cell lines.

The effect of hOP-1 on mitogenesis of osteoblast-enriched calvarial cells (preparations 3–5) was examined in the absence of serum using sparse, subconfluent, and confluent cultures and compared with the mitogenic response elicited by TGF-β1 and fresh fetal bovine serum (0.5–10%). The results showed that hOP-1 stimulated DNA synthesis in subconfluent and confluent cultures but not in sparse cultures, as examined by [^{3}H]thymidine incorporation into total acid-insoluble DNA (Fig. 5, *A–C*). Compared with control cultures, hOP-1 showed 3–5-fold maximal mitogenic stimulation at approximately 40 ng/ml in serum-free medium, whereas TGF-β1 showed a biphasic effect with 2–3-fold maximal stimulation between 0.01 and 10.0 ng/ml. Like hOP-1, TGF-β1 was effective in mediating mitogenesis in subconfluent and confluent cultures and showed no effect in sparse cultures (Fig. 5, *A–C*). The mitogenic activity of 40 ng of hOP-1/ml in serum-free medium was comparable with that elicited by 10% fetal calf serum alone (Fig. 1, *B′* and *C′*).

The stimulatory effect of hOP-1 on the growth of osteoblasts was further examined by cell number measurements using subconfluent cultures in serum-free medium and compared with that elicited by 10% fetal calf serum. The growth of osteoblasts was stimulated by hOP-1 at a concentration of 80 ng/ml in serum-free medium as measured by the cell number at 24-h intervals over a period of 5 days (Fig. 6). At 5 days the growth-promoting activity of hOP-1 was approximately 80% of that produced by 10% fetal calf serum.

Collagen Synthesis—The effect of hOP-1 on collagen synthesis was examined using osteoblast-enriched cultures in serum-free medium and compared with the effect of TGF-β1. The results indicated that hOP-1 not only enhanced the absolute amount of collagen synthesized, as determined by the total incorporation of [^{3}H]proline into collagenase-digestible proteins, but also selectively increased collagen synthesis relative to the synthesis of noncollagenous proteins (Table I). The enhancement of collagen synthesis by hOP-1 was dose-dependent, exhibiting a maximum stimulation of 3-fold at a concentration of 40 ng/ml. TGF-β1 also promoted osteoblastic collagen synthesis in agreement with previously reported data and showed a maximum response at 5–10 ng/ml (36).

Osteoblast Phenotypic Markers—Effects of hOP-1 on osteoblast markers or activities known to be associated with their cellular functions were examined using osteoblast-enriched cultures and compared with TGF-β1 effects. The specific

FIG. 3. Photomicrographs of the implants (stained with toluidine blue × 280) representing the various hOP-1-induced developmental stages of endochondral bone differentiation on days 7, 9, 12, and 21. *A*, negative control (day 12), guanidine-extracted rat demineralized bone matrix (*m*) (rat carrier). Note the absence of new bone formation. The implant consists of bone matrix (*m*) and surrounding mesenchyme. *B*, rat carrier reconstituted with 125 ng of recombinant hOP-1 (day 7). Evidence of extensive chondrogenesis is seen. Newly formed cartilage cells, chondroblasts, and chondrocytes (*Cy*) are in close contact with the rat carrier matrix (*m*). *C* and *D*, rat carrier reconstituted with 250 ng of recombinant OP-1 (day 9). Note evidence of endochondral bone differentiation: *e.g.* cartilage calcification, hypertrophy of chondrocytes, vascular invasion, and the onset of new bone formation. Observe the appearance of basophilic osteoblasts (indicated by *arrows*) in close proximity to the vascular endothelium. Signs of remodeling are already apparent as indicated by the presence of multinucleated osteoclasts. Also, some intramembranous bone can be seen at the outer surface of the implant (*D*). *E*, rat carrier reconstituted with 125 ng of recombinant OP-1 (day 12), note the extensive bone formation and remodeling. The newly formed bone matrix deposited by the osteoblasts is being remodeled by multinucleated osteoclasts (*Oc*), and the implanted matrix is being slowly resorbed and replaced by remodeled bone. There are early signs of bone marrow recruitment in the newly formed ossicles. *F*, rat matrix reconstituted with 500 ng of recombinant OP-1 (day 21). Note hematopoietic bone marrow differentiation in the newly formed ossicles. Most of the implanted matrix (*m*) has been replaced by newly formed bone containing ossicles filled with bone marrow elements, including cells of erythrocytic, granulocytic, and megakaryocytic lineages.

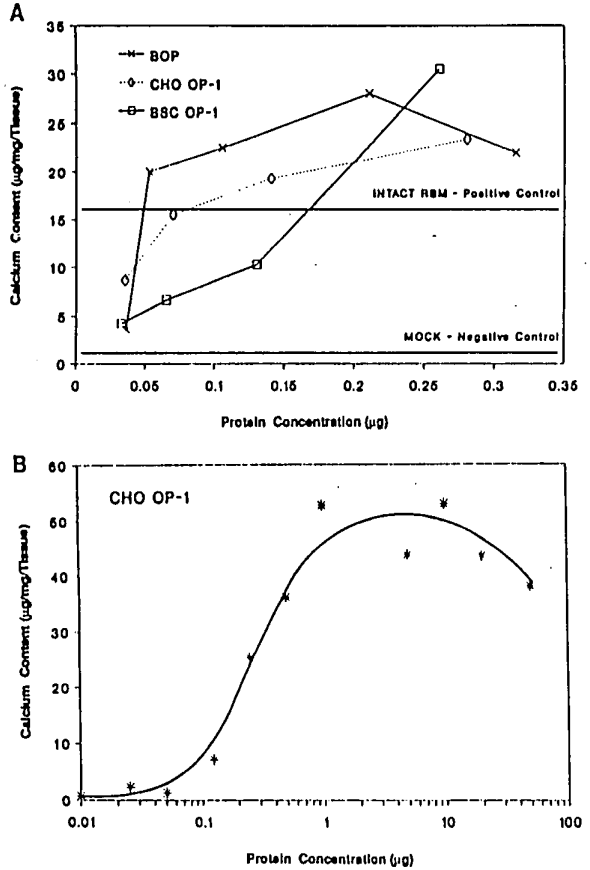

FIG. 4. *A*, comparison of bone-inducing activity exhibited by CHO- and BSC-produced recombinant hOP-1 with highly purified natural bovine OP. Calcium content in the day 12 implant was used to determine the extent of osteogenesis induced by increasing concentrations of hOP-1 or bovine OP in the implant. Bone-forming activity exhibited by the intact demineralized rat bone matrix was defined as maximal response and thus the half-maximal response is represented as 8 μg Ca^{++}/mg of tissue. The rat carrier that contained a mock hOP-1 preparation was used as negative control. Values are average of six to ten observations from three to five rats. *B*, CHO hOP-1 dose curve. Bone-forming activity was quantitated by calcium content of the day 12 implant. The values are average of ten observations from five rats.

properties examined included: alkaline phosphatase activity (a marker enzyme for osteogenesis), PTH-mediated cAMP production (a marker for hormonal responsiveness of osteoblasts), synthesis of osteocalcin (a bone-specific protein and a marker for mature osteoblast activity and bone formation), and mineralization (a process characteristic of differentiated osteoblasts *in vivo* and of differentiated osteoblasts in long-term cultures containing ascorbate and β-glycerophosphate).

hOP-1 enhanced the specific activity of alkaline phosphatase in cell lysates of osteoblast-enriched cultures (Fig. 7, *B* and *C*). The effect of hOP-1 on alkaline phosphatase induction was dose-dependent and appeared to be specific to osteoblasts, since it did not stimulate alkaline phosphatase activity in non-osteoblastic cultures (Fig. 7*A*). Osteoblast-enriched cultures treated with 40 ng of hOP-1/ml for 3 days exhibited a 4-fold stimulation in the specific activity of alkaline phosphatase when compared with serum-depleted controls. In contrast, TGF-β1 did not increase the specific activity of alkaline phosphatase in osteoblast-enriched cultures and in fact diminished the enzyme activity at the higher concentrations tested. Examination of the effect of hOP-1 on the induction of alkaline phosphatase activity in osteoblast-enriched cultures over 6 days demonstrated a dose-dependent hOP-1 stimulation that reached a maximum at 48 h of incubation and remained at an elevated level thereafter (data not shown).

Table II shows that hOP-1 did not increase the level of intracellular cAMP in osteoblasts in the absence of PTH, suggesting that cAMP is not a second messenger for hOP-1. However, pretreatment with hOP-1 increased PTH-stimulated cAMP production in a dose-dependent manner; the addition of 200 ng of hOP-1/ml to osteoblast-enriched cultures in serum-depleted medium for 72 h produced a 6-fold increase in PTH-stimulated cAMP levels compared with control cultures not exposed to hOP-1. Under identical conditions to those tested with hOP-1, TGF-β1 did not affect PTH-mediated cAMP production.

Osteocalcin synthesis by osteoblast-enriched cultures was examined on days 3–21 by a specific radioimmunoassay. hOP-1 stimulated the induction of osteocalcin synthesis starting from day 7, reaching a peak on day 13 and then slowly declining (data not shown). Because of the long culture period required for the production of osteocalcin and subsequent mineralization, these studies were performed in the presence of 10% serum. Fig. 8 shows the effect of varying concentrations of hOP-1 on osteocalcin production in day 13 cultures, as measured by radioimmunoassay. The hOP-1 effect produced approximately a 5-fold increase at 25 ng/ml compared with controls. The increase in osteocalcin synthesis correlated with increased mineralization in long-term osteoblast cultures as monitored by the appearance of mineral nodules (Fig. 9). hOP-1 increased the initial mineralization rate approximately 20-fold compared with untreated cultures. Evaluation of TGF-β1 effects on osteocalcin synthesis, and the rate of mineralization indicated that TGF-β1 neither induced osteocalcin synthesis nor promoted the mineralization process (data not shown).

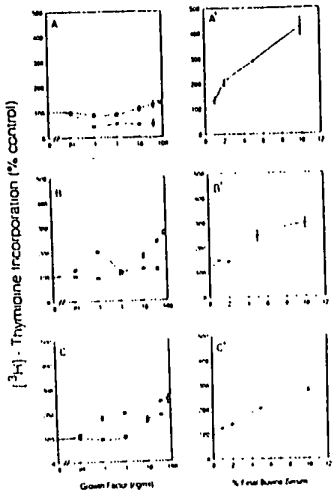

FIG. 5. Effect of cell density on DNA synthesis by hOP-1 (□), TGF-β1 (■), and fetal calf serum (♦) in osteoblast-enriched cultures. Population 3–5 cells were cultured in sparse (*A* and *A'*), subconfluent (*B* and *B'*), and confluent (*C* and *C'*) densities as described under "Materials and Methods." Cultures were incubated in serum-free medium for 24 h and then treated with either increasing concentrations of growth factors (*A–C*) or various percentage of fetal calf serum (*A'–C'*). After 18 h, the cultures were labeled with 2 μCi/ml [^{3}H]thymidine for 6 h. The incorporation of trichloroacetic acid-insoluble ^{3}H into cells was analyzed by solubilization of cells in SDS/NaOH and is represented as percent of serum-free medium control. Values are means ± S.E. of three cultures.

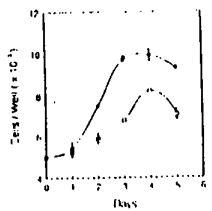

FIG. 6. Effect of hOP-1 (□) and 10% serum (■) on cell numbers in osteoblast-enriched cultures. Population 3–5 cells were plated at subconfluent density (10^5 cells/T-25 flask) in medium containing 10% FBS, and after 24 h the growth medium was replaced with serum-free medium containing hOP-1 (80 ng/ml). For comparison, control cultures received fresh 10% FBS. Triplicate cultures were harvested every 24 h, and the cell number was determined in trypsin-released single cell suspensions using a hemocytometer. Values are means ± S.E. from triplicate cultures.

TABLE I

Influence of hOP-1 and TGF-β1 on collagen synthesis in osteoblast-enriched cultures

Cultures were grown to confluence, at which time the medium was replaced with serum free medium alone or containing growth factors. After 72 h [^{3}H]proline was added to the cultures for the final 6 h, and protein synthesis was measured (see "Materials and Methods"). Expressed as mean ± S.E. of triplicate cultures.

Concentration of protein		Collagenase-digestible protein	Noncollagenase protein	Collagen synthesis
hOP-1	TGF-β1			
ng/ml		*cpm × 10⁻³*		%
		3.26 ± 0.06	4.36 ± 0.04	13.3
1		4.22 ± 0.05	4.86 ± 0.05	13.6
10		9.76 ± 0.12	7.32 ± 0.06	19.6
40		12.14 ± 0.10	8.02 ± 0.10	23.0
80		11.56 ± 0.08	6.50 ± 0.10	25.0
	1	8.51 ± 0.08	5.65 ± 0.05	21.0
	10	10.35 ± 0.16	5.26 ± 0.06	24.6
	40	11.45 ± 0.07	7.11 ± 0.10	24.3

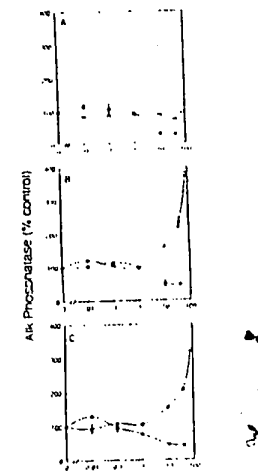

FIG. 7. Effect of hOP-1 (□) and TGF-β1 (■) on stimulation of alkaline phosphatase (*AP*) activity in collagenase-released suture-free calvarial cells. Cultures included: *A*, a pool of population 1 and 2 cells; *B*, a pool of population 3–5 cells; and *C*, population 6 cells. Confluent cultures in serum-free medium were treated with increasing concentrations of growth factors for 72 h. Cells were extracted with 0.15 M NaCl, 3 mM $NaHCO_3$, pH 7.4, and 0.1% Triton X-100 and incubated with substrate *p*-nitrophenyl phosphate for 30 min. The activity was determined by production of *p*-nitrophenol quantitated by absorbance at 400 nm. The specific activity of alkaline phosphatase (units/mg of protein) is presented as the percent of serum-free medium controls. Values are means ± S.E. of triplicate cultures.

DISCUSSION

We reported previously that the purified bovine osteogenic protein (bOP) preparations are composed of dimers of the bovine equivalents of OP-1 and BMP-2, two members of the TGF-β superfamily (7). Since previous data did not establish whether the bone-inducing activity of bovine OP is due to

TABLE II

Effect of hOP-1 on cAMP production in response to PTH in osteoblast-enriched cultures

Cultures treated with hOP-1 at various concentrations for 72 h were then washed and exposed to 0 (PTH(−)) or 200 ng/ml synthetic PTH(1-34) (PTH(+)) for 8 min in the presence of 1 mM 3-isobutyl-1-methylxanthine. Intracellular cAMP was extracted and measured by radioimmunoassay (see "Materials and Methods").

Growth factors	Amounts of cAMP produced		
	PTH(−)	PTH(+)	PTH(+)/PTH(−) ratio
ng/ml	pmol/well		
hOP-1			
0	1.87 ± 0.50	2.50 ± 0.03	1.3
1	2.15 ± 0.40	3.83 ± 0.57	1.7
10	1.50 ± 0.10	3.96 ± 0.35	2.6
40	2.05 ± 0.70	7.50 ± 0.50	3.6
100	1.55 ± 0.05	8.50 ± 1.40	5.4
200	1.90 ± 0.30	12.00 ± 0.70	6.3
1000	1.43 ± 0.05	14.75 ± 1.06	10.3
TGF-β1			
0	1.01 ± 0.07	2.26 ± 0.28	2.2
0.1	0.92 ± 0.15	1.38 ± 0.22	1.5
1	0.82 ± 0.09	1.25 ± 0.15	1.5
5	0.71 ± 0.32	0.90 ± 0.05	1.2

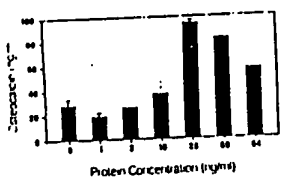

FIG. 8. Effect of hOP-1 on osteocalcin synthesis in osteoblast-enriched cultures. Population 3–5 cells in confluence were cultivated in medium containing 10% FBS. Beginning on day 5 cells were supplemented twice a week with fresh 10 mM β-glycerophosphate and L(+)-ascorbate (see "Materials and Methods"). Varying concentrations of hOP-1 were added to the cultures at day 5 and at every feeding. Control cultures received equal volumes of the hOP-1 solvent vehicle. Osteocalcin in the medium on day 13 was measured by radioimmunoassay and represented as nanograms/ml culture medium. Values are means ± S.E. of triplicate cultures.

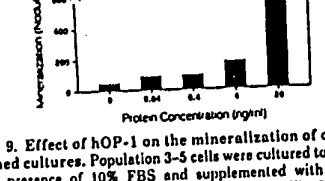

FIG. 9. Effect of hOP-1 on the mineralization of osteoblast-enriched cultures. Population 3–5 cells were cultured to confluence in the presence of 10% FBS and supplemented with 10 mM β-glycerophosphate and 50 μg of L(+)-ascorbate as in Fig. 8. On day 11, cells were rinsed with cold 0.9% NaCl, fixed in fresh 4% paraformaldehyde at 23 °C for 10 min and stained with 3% $AgNO_3$ (von Kossa Staining). Individual mineralized foci (≥20 μm) were counted in triplicate wells and represented as nodules/well. Three independent experiments yielded similar results.

homodimers and/or heterodimers of OP-1 and BMP-2, we produced recombinant hOP-1 to demonstrate that the homodimer of this polypeptide is capable of inducing new bone formation *in vivo* with a specific activity that is comparable with that of naturally sourced bovine OP. Additional studies have demonstrated that pure recombinant hOP-1 promotes the growth of osteoblasts and stimulates expression of markers characteristic of the osteoblast phenotype in culture.

This present study describes the purification and characterization of recombinant hOP-1 homodimers produced in mammalian cells (CHO and BSC). As predicted by analogy to the other members of the TGF-β superfamily, the hOP-1 gene is produced as a processed mature disulfide-linked homodimer as determined by 1) NH_2-terminal amino acid sequence analysis, 2) Western blot analysis with OP-1 antisera, and 3) SDS-PAGE analyses under nonreducing and reducing conditions. The NH_2-terminal amino acid sequences obtained from the purified hOP-1 subunit indicate that the cleavage site in the hOP-1 precursor occurs following the sequence, arginine-*X*-*X*-arginine, which is a consensus processing site for other members of TGF-β superfamily and a number of prohormones (37). The correctly processed mature hOP-1 subunit contains 139 amino acids. The mammalian-expressed hOP-1 is glycosylated as shown by its ability to bind concanavalin A and wheat germ agglutinin lectins. Studies on the CHO cell-produced protein show that hOP-1 can exhibit heterogeneity due to differential glycosylation.

The recombinant hOP-1 induces new bone formation *in vivo* in a manner that is highly reproducible and dose-dependent, irrespective of the cell used for production of hOP-1. Histological evaluation showed that as little as 5–10 ng of hOP-1 in 25 mg of matrix carrier is sufficient to induce endochondral bone formation in day 12 implants. In the absence of hOP-1, the collagen carrier induced formation of fibrous tissue that was eventually resorbed. The specific activity of hOP-1, defined as the amount of protein required to exhibit half-maximal bone-forming activity when compared with the activity of intact demineralized bone powder, is approximately 50–100 ng/25 mg of matrix implant (Fig. 4, *A* and *B*). This activity is comparable with that exhibited by the purified natural bOP. The sequence of cellular events leading to endochondral bone formation that occurs in response to rat matrix implants containing recombinant hOP-1 is identical to that induced by purified natural bOP and intact demineralized bone matrix. A uniform response is observed throughout the implant site during the developmental stages of cartilage, bone, and bone marrow differentiation. Histological evaluation showed that in implants containing higher amounts of hOP-1 (more than 1 μg of hOP-1/25 mg of matrix) bone development, *viz.* onset of bone formation, bone remodeling, and hematopoiesis, occurs 3–5 days earlier than when elicited by the rat demineralized bone matrix implants. Furthermore, implants containing higher amounts of hOP-1 showed that the matrix carrier is almost resorbed by 12 days after implantation and has become filled with newly formed bone and bone marrow elements. In contrast, implants of intact demineralized matrix show complete resorption of matrix by 18–21 days after implantation (2).

The quantitation of bone formation by calcium content of implants on day 12 after implantation demonstrates that the quantity and rate of bone formation is dependent upon the amount of hOP-1. Thus, the rate of bone formation can be modulated to levels less than, equivalent to, or greater than that exhibited by intact demineralized rat bone matrix by varying the amount of hOP-1 in the implant. The bone-forming activity, however, plateaus at a hOP-1 concentration of 1 μg/25 mg of matrix carrier. At this concentration of hOP-1 the bone-forming activity of the implant is four times greater than the activity elicited by intact demineralized bone matrix.

Homodimers of recombinant hBMP-2 have been reported to induce bone formation when implanted with rat collagen carrier in the rat subcutaneous assay model (12). In these studies, approximately 10 times more rhBMP-2 was required to achieve the same level of bone-forming activity as that observed with the corresponding naturally sourced bovine bone inductive protein preparations (5, 12). Although we have not directly compared the activities of recombinant hOP-1 and hBMP-2, the present study demonstrates that the specific bone-inducing activity of hOP-1 is comparable with the naturally sourced bovine OP in the rat subcutaneous model.

Comparison of amino acid sequences of the TGF-β domains demonstrates that the other members of the TGF-β superfamily exhibit the following degrees of identity to human OP-1: BMP-5 (90%), murine Vgr-1 (BMP-6) (88%), *Drosophila melanogaster* 60A (70%), BMP-2 (60%), BMP-4 (58%), *D. melanogaster* DPP (58%), *Xenopus laevis* Vg-1 (57%), growth and differentiation factor, GDF-1 (42%), inhibin βA (44%), BMP-3 (42%), inhibin βB (39%), TGF-β1 (34%), and Müllerian inhibiting substance, MIS (32%) (8–10, 38). The homology in the conserved 7-cysteine domain of the TGF-β superfamily members suggests that some of these members may have *in vivo* osteogenic activity. Hammonds *et al.* (22) have recently reported that homodimers of recombinant hBMP-4, which is closely related to BMP-2, is also capable of inducing bone *in vivo*, whereas recombinant activin does not. TGF-β1 does not induce new bone formation under the same assay conditions (4, 22). Evaluation of the bone formation potential of other TGF-β superfamily members will provide valuable insight into the functional relationships of this family of proteins.

In cell culture studies, hOP-1 stimulates osteoblast proliferation which is dependent on both the concentration of hOP-1 and cell density. The mitogenic response elicited by hOP-1 in serum-free medium is comparable with the response obtained by adding fresh 10% FBS. The mitogenic effect of hOP-1 observed for the calvarial cells released initially following treatment with collagenase suggests that these mesenchymal cells (preosteoblasts) are also capable of responding to hOP-1 and may have hOP-1 binding sites or surface receptors (data not shown). Natural preparations of osteogenin (BMP-3) from bovine bone (23, 24) and recombinant BMP-2 (25–27) have been shown to stimulate the growth of preosteoblasts, periosteal cells, and C26 clonal rat osteoblast progenitors and to inhibit the proliferation of established osteoblast-like cells, MC3T3-E1 cells, and C20 clonal rat osteoblast cells. Recombinant human BMP-4, a gene product closely related to BMP-2, has been shown recently to stimulate DNA synthesis in rat osteoblast-enriched cultures (28). Our results show that recombinant hOP-1 stimulates the proliferation of both preosteoblasts and mature osteoblasts in culture.

Recombinant hOP-1 enhances the synthesis of collagenase-digestible protein and increases the percent collagen synthesis relative to that of noncollagenous proteins when added to osteoblast-enriched cultures in serum-depleted medium. Recombinant BMP-2, on the other hand, has been reported to have no effect on the expression of type I collagen mRNA or collagen synthesis by osteoblast-like cells, calvarial cells, and embryonic fibroblasts in culture (27). Osteogenin purified from bovine bone has been reported to stimulate the synthesis of collagenase-digestible protein by calvarial osteoblasts in culture (24). It is possible that a portion of this response can be attributed to small amounts of OP-1 or related proteins present in naturally sourced preparations of osteogenin (6). Recently, BMP-4 has been shown to enhance Type I collagen synthesis in osteoblast-enriched cultures (28).

The specific activity of alkaline phosphatase, the production of cAMP in response to PTH, osteocalcin synthesis, and extracellular matrix mineralization are all enhanced in osteoblast-enriched cultures in response to recombinant hOP-1. The effect of hOP-1 on alkaline phosphatase induction appears to be specific to osteoblasts, since it was not observed with non-osteoblastic cultures of population 1 and 2 rat calvarial cells and NIH-3T3 fibroblasts. hOP-1-induced alkaline phosphatase activity remained elevated over the entire period after the hOP-1 exposure. Recombinant BMP-2, BMP-4, and natural preparations of osteogenin have also been shown to stimulate alkaline phosphatase in calvarial osteoblasts, MC3T3-E1 cells, periosteal cells, and mouse 10T1/2 cells (23–28). With respect to hOP-1 regulation of other markers of the osteoblast phenotype, the production of cAMP in response to PTH is not only maintained by the presence of hOP-1 but also increases with increasing hOP-1 in these cultures. Adenylate cyclase activity which is subject to PTH stimulation is a biochemical marker of the mature osteoblastic phenotype (30), and hOP-1 increases this activity. Our study shows that hOP-1 is also capable of stimulating osteocalcin synthesis in osteoblast-enriched cultures without the addition of 1,25-$(OH)_2$ vitamin D_3. Osteocalcin, a bone-specific protein, is known to be synthesized by mature rat and human primary osteoblasts in long-term culture (39, 42). Furthermore, the hOP-1 induction of osteocalcin synthesis correlates with an increase in osteocalcin mRNA levels (data not shown). Vitamin D is known to up-regulate osteocalcin mRNA expression and osteocalcin synthesis when added to cultured osteoblasts (19, 43–45). BMP-2 has been shown to stimulate osteocalcin synthesis when added to osteoblast precursors in the presence of vitamin D *in vitro* (27). The hOP-1-induced osteocalcin synthesis, as evaluated here by radioimmunoassay and Northern blot mRNA analysis, appears to correlate with increased mineralization. Although osteoblast-enriched cultures used in these studies are capable of mineralizing in long term culture without addition of hOP-1, the initial rate at which mineralized foci appear can be enhanced at least 20-fold in the presence of hOP-1.

As hOP-1 is a member of the TGF-β superfamily, we evaluated the direct effect of TGF-β1 on calvarial-derived cell populations under identical conditions. Like hOP-1, TGF-β1 stimulates the proliferation of calvarial cells and synthesis of collagenase-digestible proteins in osteoblast-enriched cultures. TGF-β1, known to be synthesized by osteoblasts as an autocrine factor (36, 46), also exhibits biphasic effects on osteoblast proliferation and is reported to enhance collagen synthesis by osteoblasts *in vitro* (36). However, unlike hOP-1, TGF-β1 does not enhance the expression of markers characteristic of the osteoblast phenotype. In fact, significant decreases are caused by TGF-β1 in alkaline phosphatase specific activity (Fig. 5), PTH-mediated cAMP production (Table II), and osteocalcin synthesis (47) in osteoblast-enriched cultures. Other peptide growth factors that are known to stimulate bone cell proliferation *in vitro* include IGF-I, IGF-II, TGF-β2, TGF-β3, and acidic and basic FGF (20, 21). IGF-I and TGF-β1 have also been shown to enhance the collagen synthesis by calvarial osteoblasts in culture (36, 48).

In general, the concentrations of hOP-1 which exhibit biological activity *in vitro* appear to be higher than the concentrations typically employed for other cytokines and growth factors in similar experiments. The effective dose range for hOP-1 in the assays performed in our study is 1–40 ng/ml. In comparison the effective dose for TGF-β1 is in the range of 0.01–10 ng/ml. Results from *in vitro* studies have recently been reported for BMP-2 (25–27). BMP-2 enhancement of cell proliferation and induction of alkaline phosphatase in C26 clonal osteoblast precursor cells occurs at doses of 1–1000 ng/ml (27). BMP-4, on the other hand, has been report-

that are modified with the phenylboronic acid groups, and are characterizing the association of the polymers with a monolayer presenting the catechol groups. We will then introduce catechol groups on to the collagen fibrils and show that the polymer can aggregate them. We have worked out chemical methods for introducing synthetic groups on to the fibrils. It will also be important to show that the fibrils disaggregate when the catechol groups are oxidized to the orthoquinones.

Having established a method to dynamically control the cross-linking of natural fibrils, we will use the same biomechanical methods that we have used for natural tissues to evaluate the mechanics of the modified tissues. The next step will be to translate these approaches into a synthetic system with similarly controlled properties. Ultimately, this stepwise approach is expected to lead to the development of a fully synthetic fibrous composite with dynamically controlled stiffness.

This work has been supported by grants from the U.S. National Science Foundation, the U. S. Office of Naval Research, the U.S. Defense Advanced Research Projects Agency and the Shriners of North America. The authors thank Dr Greg Szulgit and Dr Robert Shadwick for providing a copy of their in-press paper.

References

1 Kadler, K. E., Holmes, D. F., Trotter, J. A. and Chapman, J. A. (1996) Biochem. J. **316**, 1–11
2 Ayad, S., Boot-Handford, R. P., Humphries, M. J., Kadler, K. E. and Shuttleworth, C. A. (1998) The Extracellular Matrix Facts Book, 2nd edn, Academic Press, San Diego
3 Reinhardt, D. P., Keene, D. R., Corson, G. M., Poschl, E., Bachinger, H. P., Gambee, J. E. and Sakai, L. Y. (1996) J. Mol. Biol. **258**, 104–116
4 Wilkie, I. C. (1996) in Echinoderm Studies, vol. 5 (Jangoux, M. and Lawrences, J., eds), pp. 61–102, A. A. Balkema, Brookfield
5 Trotter, J. A. and Koob, T. A. (1995) J. Exp. Biol. **198**, 1951–1961
6 Trotter, J. A., Lyons-Levy, G., Luna, D., Koob, T. J., Keene, D. R. and Atkinson, M. A. L. (1996) Matrix Biol. **15**, 99–110
7 Koob, T. J., Koob-Emunds, M. M. and Trotter, J. A. (1999) J. Exp. Biol. **202**, 2291–2301
8 Trotter, J. A., Salgado, J. P. and Koob, T. J. (1997) Comp. Biochem. Physiol. **116A**, 329–335
9 Trotter, J. A., Chapman, J. A., Kadler, K. E. and Holmes, D. F. (1998) J. Mol. Biol. **284**, 1417–1424
10 Trotter, J. A. and Koob, T. J. (1989) Cell Tissue Res. **258**, 527–539
11 Trotter, J. A., Thurmond, F. A. and Koob, T. A. (1994) Cell Tissue Res. **275**, 451–458
12 Trotter, J. A., Lyons-Levy, G., Thurmond, F. A. and Koob, T. J. (1995) Comp. Biochem. Physiol. **112A**, 463–478
13 Trotter, J. A. and Koob, T. J. (1993) Comp. Biochem. Physiol. **107B**, 125–134
14 Thurmond, F. A. and Trotter, J. A. (1994) J. Mol. Biol. **235**, 73–79
15 Holmes, D. F. (1995) Biochem. Soc. Trans. **23**, 720–725
15a Trotter, J. A., Kadler, K. E. and Holmes, D. F. (2000) J. Mol. Biol., in the press
16 Thurmond, F. A., Koob, T. J., Bowness, M. and Trotter, J. A. (1997) Connect. Tiss. Res. **36**, 211–222
17 Thurmond, F. A. and Trotter, J. A. (1996) J. Exp. Biol. **199**, 1817–1828
18 Trotter, J. A., Lyons-Levy, G., Chino, K., Koob, T. J., Keene, D. R. and Atkinson, M. A. L. (1999) Matrix Biol. **18**, 569–578
19 Szulgit, G. K. and Shadwick, R. E. (2000) J. Exp. Biol. **203**, 1539–1550
20 Koob-Emunds, M. M., Trotter, J. A. and Koob, T. J. (2000) Bull. Mount Desert Island Biol. Lab. 39, in the press

Received 29 February 2000

Inductive activity of recombinant human growth and differentiation factor-5

R. C. Spiro*[1], L.-S. Liu*, M. A. Heidaran*, A. Y. Thompson*, C. K. Ng*, J. Pohl† and J. W. Poser*
*Orquest, Inc., 365 Ravendale Drive, Mountain View, CA 94043, U.S.A., and †Biopharm GmbH, Czernyring 22, 69115 Heidelberg, Germany

Abstract

Growth and differentiation factor-5 (GDF-5) is a divergent member of the transforming growth factor-β/bone morphogenetic protein (BMP) superfamily that is required for proper skeletal patterning and development in the vertebrate limb. Based on the homology of GDF-5 with other bone-inducing BMP family members, the inductive activity of a recombinant form of human GDF-5 (rhGDF-5) was evaluated in a series of *in vitro* assays and *in vivo* bone-formation models. The *in vitro* response to rhGDF-5 resulted in the formation of chondrogenic nodules in fetal rat calvarial cells cultured in the context of collagen or collagen/hyaluronate extracellular matrices. Matrices loaded with rhGDF-5 induced ectopic

Key words: bone graft matrix, bone morphogenetic protein, segmental bone defect, spine fusion.
Abbreviations used: ECM, extracellular matrix; GDF-5, growth and differentiation factor-5; rhGDF-5, recombinant human GDF-5; BMP, bone morphogenetic protein; QHMA, quantitative histomorphometric analysis; PNB, percentage of new bone; PRD, percentage of residual defect; CT, computerized tomographic; L, lumbar.
[1]To whom correspondence should be addressed (e-mail bspiro@orquest.com).

cartilaginous and osseous tissue when implanted in subcutaneous or intramuscular sites. In non-human primate long-bone-defect and spinal-fusion models, rhGDF-5 combined with a mineralized collagen matrix induced bone formation in a manner equivalent to autogenous bone. These results highlight the unique potential of rhGDF-5 in a wide variety of orthopaedic applications.

Introduction

The skeletal elements of the vertebrate limb are derived during embryonic development from mesenchymal cells, which condense and initiate a differentiation program that results in the formation of cartilage and bone. It is well established that members of the bone morphogenetic protein (BMP) family play a direct role in the developmental events that dictate skeletal patterning [1,2]. Growth and differentiation factor-5 (GDF-5), also termed cartilage-derived morphogenetic protein-1 (CDMP-1) and MP52, is a member of the BMP family that defines a distinct structural and functional subgroup. GDF-5 shares 40–50% protein-sequence homology with the BMP-2 and BMP-7 (osteogenic protein-1, or OP-1) family-member subgroups and plays a pivotal role in the process of joint formation [3–6]. A null mutation in *gdf*-5 at the mouse brachypodism (*bp*) locus disrupts the formation of approx. 30% of the joints of developing limbs, including the complete absence of joint development between the proximal and medial phalanges of the fore- and hind-feet [1,5]. In addition to joint development, GDF-5 has shown activity in promoting the survival of dopaminergic neurons, inducing angiogenesis *in vivo*, and in tendon/ligament morphogenesis [7–9]. Based on the homology of GDF-5 with other BMP family members and the activity of this growth factor in skeletal development, a recombinant version of human GDF-5 (rhGDF-5) was evaluated as a potential inductive component of a matrix/growth factor bone-graft substitute.

Materials and methods

Growth factors and matrix components

Purified rhGDF-5 was provided by Hoechst Marion Roussel (Kawagoe, Saitama, Japan) and Biopharm (Heidelberg, Germany) and was prepared from prokaryotic expression systems as described previously [4,10]. Demineralized bone preparations were isolated as described previously [11]. Type-I bovine collagen was purchased from Kensey-Nash (Exton, PA, U.S.A.) or Collagen Corp. (Palo Alto, CA, U.S.A.). Hyaluronate was purchased from Lifecore Biomedical (Chasca, MN, U.S.A.).

Matrix and matrix/growth factor fabrication

Type-I collagen, mineralized collagen (Healos®) and collagen/hyaluronate matrices were prepared as described previously [12,13]. Stock rhGDF-5 solution was diluted in 20 mM sodium acetate buffer, pH 4.0, prior to adding to sterile collagen, mineralized collagen or collagen/hyaluronate matrices at concentrations ranging from 10 to 1500 $\mu g/cm^3$ of matrix material. Matrix/GDF-5 combinations were then lyophilized and stored at 4 °C.

In vivo assays

Rat soft-tissue implants

Matrix/growth factor combinations were implanted either subcutaneously in the thoracic region or intramuscularly in posterior tibial muscle pouches created by blunt dissection in 8-week-old male Sprague–Dawley rats. At 14–21 days post-surgery, implants were harvested, weighed and processed for routine histology (fixed in 10% formalin, paraffin-embedded, sectioned to 6 μm and haematoxylin- and eosin-stained). Alternatively, implants were extracted and assayed for alkaline phosphatase activity using commercially available assay kits (Sigma, St. Louis, MO, U.S.A.).

Primate long-bone-defect model

Bilateral 1.5-cm osteotomy defects were created in the mid-diaphysis of the fibulae of 16 skeletally mature male baboons (*Papio cynocepthalus*; four animals per group). Defects were stabilized with a customized stainless steel plate and implanted unilaterally with two strips ($1.8 \times 1.0 \times 0.6$ cm, 1.1 cm^3 volume) of mineralized collagen matrix with or without three dose levels of rhGDF-5 (10, 100 and 1000 $\mu g/cm^3$ or total dose of 22, 220 and 2200 μg). Contralateral defects were left as untreated controls. Radiographic analysis was performed immediately after surgery and every 4 weeks thereafter. Implant materials were retrieved at 21 weeks for qualitative and quantitative histological analysis. Quantitative histomorphometric analysis (QHMA) was performed using a BioQuant Four Image Analysis system. Representative slides were selected for examination at 1.6 × original magnification. The defect was centred within the microscopic field and all area measurements (mm^2) were made within this stand-

ardized area. Both the percentage of new bone (PNB) and percentage of residual defect (PRD) were measured.

Primate spinal-fusion model

A non-instrumented, posterolateral lumbar intertranverse process fusion of one motion segment was performed in 36 skeletally mature female baboons using mineralized collagen matrix with or without rhGDF-5 (500 and 1500 $\mu g/cm^3$ of matrix) or autograft (5 cm^3 per side) harvested from the iliac crest. Vertebrae lumbar (L)2–L6 were exposed through a posterior approach and the graft site was prepared bilaterally by decortication of the transverse processes. Two strips of graft material per side (5 cm^3 per strip) were placed across the transverse processes of L4 and L5 for total doses of 5 and 15 mg of rhGDF-5 per side at the 500 and 1500 $\mu g/cm^3$ concentrations, respectively. Radiographic evaluation was performed at 0, 8, 12, 16 and 20 weeks post-treatment. At 20 weeks, spines were harvested for *ex vivo* radiographic, computerized tomographic (CT) and qualitative histological evaluation. Radiographic and qualitative histological data were evaluated blind and correlated with reconstructed CT data to determine the extent and quality of each fusion mass. Histological evidence of fusion was assessed through review of stained thin plastic sections, unstained and backlit thick sections, and blocks of fixed calcified tissue. Histological scores were assigned to each animal based on independent interpretation of the response achieved on each side of the motion segment. Four performance outcomes were assessed: complete fusion, discontinuous fusion mass, periosteal reactive bone formation or no bone formation. The left and right side outcomes were paired into equivalent ranking of left/right matched observations to form ten levels of response score (scored 0–9). A frequency of 100 % complete bilateral fusion in nine animals would result in a maximum total score of 81.

Statistical methods

In the long-bone model, paired t tests were performed on the QHMA data to compare PNB and PRD in treated and untreated sites within each treatment group. In the spinal-fusion model, a rule of reasonable decision was the primary criterion for scoring equivalence between treatment groups. Based on a prospective decision, equivalence existed for groups with total scores that were within ± 8 points. A Wilcoxon rank sum test for non-uniform samples was used to test the null hypothesis that mean responses to two treatments was equivalent. Significance was tested at $\alpha = 0.05$.

Results

In vitro activity of rhGDF-5

In contrast to most BMP family members, the response of cultured cells to GDF-5 as measured by alkaline phosphatase activity has been shown previously to be diminished and restricted to a subset of osteoblast-like cell lines such as ROB-C26 [10]. GDF-5 has also been shown to stimulate mesenchyme aggregation and chondrogenesis in rat limb-bud cells *in vitro* [14]. Using fetal rat calvarial cells as an alternative cell source for osteo- and chondro-progenitor cells [15,16], we have observed that rhGDF-5 stimulates the *in vitro* formation of chondrogenic nodules in cells that are seeded in the context of type-I collagen or collagen/hyaluronate extracellular matrix (ECM) components. The dependence of this *in vitro* response on specific components of the ECM was unique to rhGDF-5 in comparison with other members of the BMP family (M. Heidaran and R. C. Spiro, unpublished work).

In vivo activity of rhGDF-5

GDF-5 has been previously shown to induce ectopic cartilage and bone formation in rodents *in vivo* [14]. Collagen/hyaluronate matrices loaded with rhGDF-5 (30 μg) and implanted intramuscularly in rats for 21 days formed ectopic cartilaginous foci within the matrix. Cells with distinct chondrocyte-like morphology were observed within the foci and were surrounded by an extensive metachromatic staining matrix. Subcutaneous implants of collagen or mineralized collagen matrices loaded with rhGDF-5 (10 and 100 μg) showed a dose-dependent increase in alkaline phosphatase activity. The alkaline phosphatase activity induced by 100 μg of rhGDF-5 was an order of magnitude less than that observed with comparable amounts of demineralized bone powder (0.87 ± 0.4 versus 13.5 ± 2.1 nmol/min per mg of implant, respectively). In general, the ectopic bone formation in response to rhGDF-5 was less than that observed with other BMP family members (A. Thompson and R. C. Spiro, unpublished work).

In the primate long-bone-defect model, a 1.5-cm fibular defect treated with rhGDF-5-loaded mineralized collagen matrices (10, 100 and

1000 μg of rhGDF-5 per cm^3 of matrix) showed radiographic evidence of healing that stratified with dose (Figure 1). The deposition of radiopaque tissue indicative of a bone-healing response was evident at earlier time points in sites treated with matrices containing the higher doses of rhGDF-5. Qualitative histological evaluation at 21 weeks showed 100% union in the high-dose group, 75% union in the mid-dose group and 50% union in the low-dose group. Only 25% of the untreated or matrix-alone-treated specimens showed any histological evidence of bony union. Fibular unions were characterized by mature bone closure with distinct cortices and medullary tissue. Bone modelling was advanced and composed of lamellar structures, osteonal architecture and quiescent osteoclast and osteoblast activity.

QHMA measurements of mean PNB ranged from 23.1 to 34.3% in matrix and matrix/rhGDF-5-treated sites compared with a range of 10.9–24.2% for untreated sites. Paired t tests did not demonstrate significant differences in PNB between treated and untreated groups. QHMA measurements of PRD and t test analysis did, however, demonstrate that the residual defect area in the high-dose group was significantly lower than the untreated group ($P = 0.002$).

In the primate spinal fusion model, the implantation of mineralized collagen matrices containing 500 μg/cm^3 rhGDF-5 induced the highest frequency of bilateral fusion, as judged by radiographic/CT analysis (Figure 2). Four bilateral fusions and two unilateral fusions were observed in this group based on assessment by two independent reviewers. Surprisingly, only one of the 1500 μg/cm^3 rhGDF-5-treated specimens was scored as a bilateral fusion and only two achieved unilateral fusion, with disagreement between the two reviewers on one of the unilateral fusions. Autograft-treated specimens were scored as bilateral fusions in two specimens and as unilateral fusions in four specimens, with disagreement between the reviewers on two of the unilateral fusion specimens. None of the mineralized collagen-matrix-alone-treated specimens had radiographic/CT evidence of fusion.

Histological evaluation revealed that all specimens showed some evidence of new bone, ranging from complete bony fusion across the motion segment to limited focal periosteal reactive bone formation. The matrix 500 μg/cm^3 rhGDF-5 specimens showed the most robust bone formation, with well-organized fusion masses consisting of inner zones with a high volume of trabecular bone, lamellar in nature, and a pro-

Figure 1

21-Week plain-film radiographs of primate 1.5-cm fibular defects

Fibular defects were grafted with mineralized collagen matrix (**A**), matrix with 10 μg/cm^3 rhGDF-5 (**B**), matrix with 100 μg/cm^3 rhGDF-5 (**C**) and matrix with 1000 μg/cm^3 rhGDF-5 (**D**).

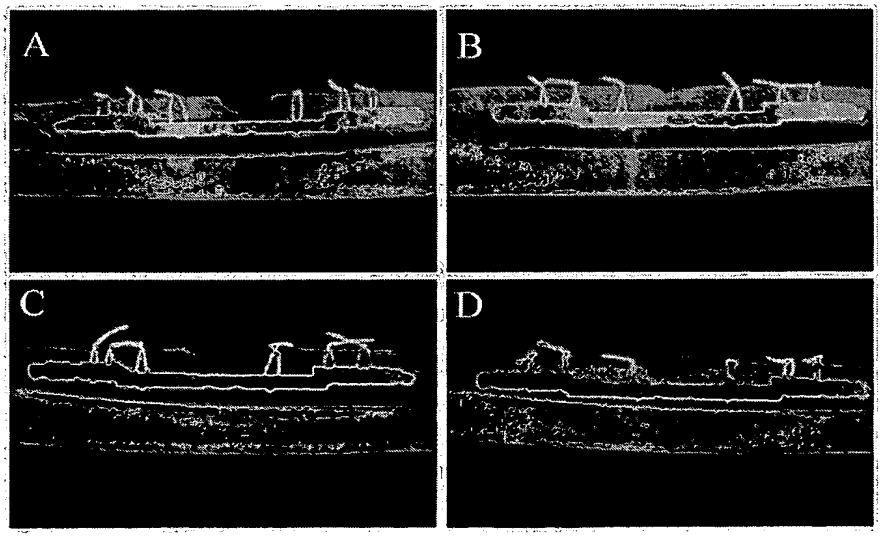

visional cortex with well-formed osteons (Figure 3). Three specimens had bilateral fusion, two unilateral fusion and four had discontinuous fusion masses that showed zones of fibrous or cartilaginous tissue at the level of the intervertebral disc. Higher magnification of the bone mass showed increased osteoblast activity and abundant marrow spaces with fatty haematopoietic marrow. There was no evidence of residual matrix in any specimens in this group. The histological fusion score for this group was 63 out of a possible 81, with an average score of 7. The matrix 1500 $\mu g/cm^3$ rhGDF-5 specimens generally showed less bone formation and appeared to undergo a more complex process of healing, both with respect to cellular constituents and the timing of bone formation and resorption. Modelling and remodelling activity appeared to have been more robust and at an earlier time point than in the other groups, resulting in a bone mass of lower volume at 20 weeks. This group consistently showed a hypercellular haematopoietic marrow with a decreased ratio of fat to marrow. No bilateral fusions and only one unilateral fusion were observed in this group and the average fusion score was 4.3 with a total score of 34 out of a possible 72 (one animal lost). No residual matrix was apparent in any of the specimens of this group. Autograft-treated specimens were seen to have large bony fusion masses consisting of irregular lamellar trabecular bone that contained normocellular haematopoietic marrow and well-developed provisional cortices. Overall cellularity and osteoblast numbers were decreased compared with the mat-

Figure 2

Reconstructed CT scans (dorsal view) at 20 weeks of excised primate L4–L5 motion segments

Segments were grafted with mineralized collagen matrix alone (**A**), autograft (**B**), matrix with 500 $\mu g/cm^3$ rhGDF-5 (**C**) and matrix with 1500 $\mu g/cm^3$ rhGDF-5 (**D**).

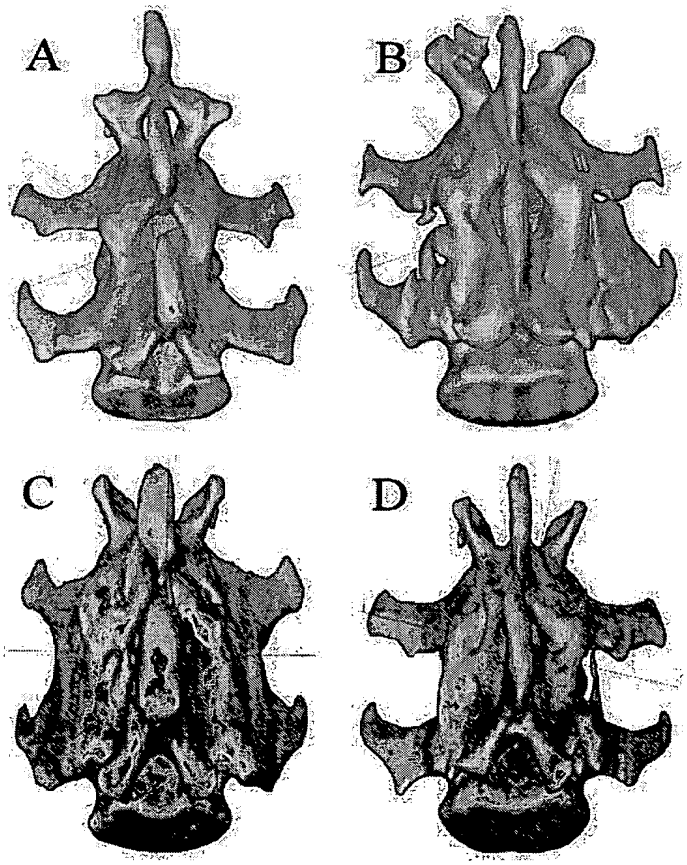

rix 500 $\mu g/cm^3$ rhGDF-5 group. Two bilateral and two unilateral fusions were observed in this group. Discontinuous fusions showed regions of dense hyalinized fibrocollagenous connective tissue. The average fusion score for this group was 6.5, with a total score of 59 out of a possible 81. Specimens treated with matrix alone showed only minimal evidence of new bone formation that was limited to the transverse process origins. The average fusion score for this group was 2.9, with a total score of 26 out of a possible 81. The rule of reasonable decision based on histological fusion scores demonstrated equivalence between the matrix 500 $\mu g/cm^3$ rhGDF-5 and autograft-treated groups. The null hypothesis test (Wilcoxon rank sum test) failed for all comparisons except autograft versus matrix with 500 $\mu g/cm^3$ rhGDF-5.

Figure 3

Photomicrograph of haematoxylin- and eosin-stained thin plastic histological section (coronal plane) through L4–L5 vertebral motion segment grafted with mineralized collagen matrix with 500 $\mu g/cm^3$ rhGDF-5

Arrows point to regions of teardrop-shaped fusion mass that bridge the motion segment.

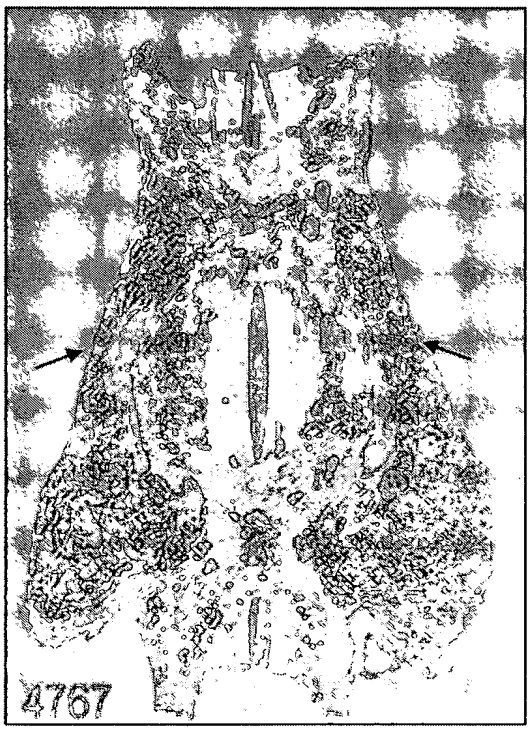

Discussion

As a subgroup-defining member of the BMP family of proteins, GDF-5 was initially distinguished from other family members based on a divergence of primary sequence, a unique expression pattern in developing skeletal systems and on the abnormalities that result from sequence mutations [1–6]. Subsequent studies that identified preferential receptor utilization, angiogenic activity, tendon and ligament induction, and neuronal-cell survival activity of GDF-5 added further distinctions [7–10]. The results presented in this current study have also extended the list of unique properties and activities of GDF-5.

The predominance of cartilaginous-like tissue observed in response to rhGDF-5 in the *in vitro* culture and *in vivo* implantation studies is consistent with the proposed role for GDF-5 in chondrogenesis and endochondral bone formation [14]. It has been suggested that the diverse biological functions documented for GDF-5 may relate to a more restricted utilization of signalling receptors compared with other BMP proteins [10]. The influence of specific ECM such as type-I collagen and hyaluronate on the *in vitro* response to rhGDF-5 observed here suggests an additional level of control over the function and activity of this growth factor. All of the described biological activities of GDF-5 (chondrogenesis, osteogenesis, angiogenesis, etc.) can also be influenced directly by components of the ECM [17]. The synergy demonstrated between components of the ECM and the response to rhGDF-5 can be expected to have a direct impact on the activity and efficacy of matrix/rhGDF-5 combinations in tissue-grafting indications.

An important factor in the design of a successful matrix/growth factor combination for tissue grafting is the optimization of the conductive properties of the matrix with the inductive activity of the growth factor. These attributes come 'ready-made' and 'pre-optimized' in an autogenous grafting material such as autograft. Incorporating them into an engineered substitute requires that the response to the inductive agent be balanced with the conductive activity and persistence of the matrix at the defect site. This can be accomplished through the manipulation of physical properties of the matrix that affect persistence or by tailoring the response to the growth factor by adjusting the loading concentration. Given the dependence of the cellular response to rhGDF-5 on an interaction with ECM components, matrix persistence and growth factor

concentration become even more important for the performance of a matrix/rhGDF-5 tissue graft. The primate bone studies described in this report have provided direct evidence for these concepts.

In the primate long-bone-defect model, a clear trend towards a dose-dependent response to mineralized collagen/rhGDF-5 was observed over a 2-log increase (10–1000 $\mu g/cm^3$) in rhGDF-5 concentration. The formation of radio-opaque tissue and the frequency of union and maturity of the reparative bone at 21 weeks all appeared to increase with higher rhGDF-5 concentrations (Figure 1). This was not the case, however, in the primate spinal fusion study. While equivalence to autograft was demonstrated at 500 μg rhGDF-5 per cm^3 of matrix (5-mg total dose per side; Figures 2 and 3), a 3-fold increase in rhGDF-5 (1500 $\mu g/cm^3$, 15 mg total dose per side) markedly decreased the efficacy of this matrix/growth factor combination (Figure 2). The exact mechanism underlying the poor performance at this dose level is not clear, but histological evidence at 20 weeks suggests a more complex healing process with respect to cellular constituents and the timing of bone formation and matrix resorption.

The mineralized collagen matrix (Healos®) used in the *in vivo* studies of this report was designed as an osteoconductive matrix to be used in conjunction with endogenous or exogenous osteogenic and osteoinductive components. It incorporates desirable physical attributes (continuous pore structure, high wet strength and radiolucency) with osteoconductive properties and resorption characteristics that allow it to be replaced completely by new bone [13]. It has performed equivalently to autograft in previous long-bone-defect and spinal-fusion studies when mixed with a bone marrow aspirate [13,18]. The performance of the mineralized collagen matrix in conjunction with an inductive growth factor clearly relies on a proper balance between matrix resorption and bone formation. This balance is even more critical in light of the enhanced activity observed with rhGDF-5 in combination with collagen-based matrices.

We thank Dr Larry Swain, Dr Neil Vail and Dr Casey Fox of BioMedical Enterprises (San Antonio, TX, U.S.A.) for their help with the *in vivo* studies and Dr Tom Aufdemorte of the University of Texas Health Science Center (San Antonio, TX, U. S. A.) for performing the histological processing and evaluations. In addition, we thank all of our collaborators at Nippon Hoechst Marion Roussel in Kawagoe, Saitama, Japan and Biopharm, Heidelberg, Germany, for providing the rhGDF-5 and activity data. This work was supported by funds from Orquest, Hoechst Marion Roussel and National Institutes of Health grant AR44153 to R.C.S.

References

1 Kingsley, D. M. (1994) Genes Dev. **8**, 133–146
2 King, J. A., Storm, E. E., Marker, P. C., Dileone, R. J. and Kingsley, D. M. (1996) Ann. N. Y. Acad. Sci. **785**, 70–79
3 Chang, S. C., Hoang, B., Thomas, J. T., Vukicevic, S., Luyten, F. P., Ryba, N. J. P., Kozak, C. A., Reddi, A. H. and Moos, M. (1994) J. Biol. Chem. **269**, 28227–28234
4 Hötten, G., Neidhardt, H., Jacobowsky, B. and Pohl, J. (1994) Biochem. Biophys. Res. Commun. **204**, 646–652
5 Storm, E. E., Huynh, T. V., Copeland, N. G., Jenkins, N. A., Kingsley, D. M. and Lee, S.-J. (1994) Nature (London) **369**, 639–643
6 Brunet, L. J., McMahon, J. A., McMahon, A. P. and Harland, R. M. (1998) Science **280**, 1455–1457
7 Yamashita, H., Shimizu, A., Kato, M., Nishitoh, H. Ichijo, H., Hanyu, A., Morita, I., Kimura, M., Makishima, F. and Miyazono, K. (1997) Exp. Cell Res. **235**, 218–226
8 Sullivan, A. M., Pohl, J. and Blunt, S. B. (1998) Eur. J. Neurosci. **10**, 3681–3688
9 Wolfman, N. M., Hattersley, G., Cox, K., Celeste, A. J., Nelson, R., Yamaji, N., Dube, J. L., DiBlasio-Smith, E., Nove, J., Song, J. J., Wozney, J. M. and Rosen, V. J. (1997) Clin. Invest. **100**, 321–330
10 Nishitoh, H., Ichijo, H., Kimura, M., Matsumoto, T., Makishima, F., Yamaguchi,A., Yamashita, H., Enomoto, S. and Miyazono, K. (1996) J. Biol. Chem. **271**, 21345–21352
11 Seyedin, S. M., Thomas, T. C., Thompson, A. Y., Rosen, D. M., Piez, K. A. (1985) Proc. Natl. Acad. Sci. U.S.A. **82**, 2267–2271
12 Liu, L.-S., Thompson, A. Y., Heidaran, M. A., Poser, J. W. and Spiro, R. C. (1999) Biomaterials **20**, 1097–1108
13 Spiro, R. C., Pacetti, S., Thompson, A. Y., Lotz, J. C., Aufdemorte, T. B. and Poser, J. W. (1997) Trans. Orthop. Res. Soc. **22**, 753
14 Hötten, G. C., Matsumoto, T., Kimura, T., Bechtold, R. F., Kron, R., Ohara, T., Tanaka, H., Satoh, Y., Okazaki, M., Shirai, T. et al. (1996) Growth Factors **13**, 65–74
15 McCarthy, T. L., Centrella, M. and Canalis, E. (1988) J. Bone Miner. Res. **3**, 401–408
16 Basic, N., Basic, V., Bulic, K., Grgic, M., Kleinman, H. K., Luyten, F. P. and Vukicevic, S. (1996) J. Bone Miner. Res. **11**, 384–391
17 Boudreau, N. and Bissell, M. J. (1998) Curr. Opin. Cell Biol. **10**, 640–646
18 Tay, B. K.-B., Le, A. X., Heilman, M., Lotz, J. and Bradford, D. S. (1998) Spine **23**, 2276–2281

Received 1 March 2000